Measurements of the magnetic anisotropy of gadolinium

Roe, W. C.

M E A S U R E M E N T S O F T H E M A G N E T I C A N I S O T R O P Y O F G A D O L I N I U M.

by

W.C. ROE, B.Sc.

Presented in candidature for the degree of Doctor of Philosophy.

October, 1961.

P.136

ABSTRACT.

Measurements of the magnetocrystalline anisotropy constants of gadolinium have been made using a torque method. Torque observations were made on a single crystal oblate spheroid of the material which contained the hexagonal axis in its plane. The system for measuring torque was null-reading and a counter - torque was provided by passing currents through a small coil running in an instrument magnet. Balancing was done automatically with a photocell feed-back amplifier system.

Values of the anisotropy constants have been derived from observed torque curves by a least - squares fit to the theoretical curves. The process was carried out on the Ferranti Pegasus computer.

The anisotropy constants were obtained over the temperature range from the Curie point ($\sim 289^{\circ}K$) to $20^{\circ}K$ and they are presented graphically. K_1 is found to be negative below $\sim 235^{\circ}K$ indicating an easy direction in the basal plane and the crystal only exhibits a uniaxial character above this temperature. The change in sign of K_1 prevents any comparison with the Zener theory.

CONTENTS.

CHAPTER ONE.

INTRODUCTION.

CHAPTER ONE.

INTRODUCTION.

1.1. Ferromagnetism.

William Gilbert (1540 - 1603), a physician, made the first attempt to study magnetism in a scientific manner, although his work on the properties of lodestone largely involved separating superstition from fact. Little progress towards a fundamental understanding of the phenomenon was then made until Weber (1854), using the idea of circulating atomic currents postulated by Ampére (1823), suggested an interaction between the elementary magnets. In 1900, Ewing assumed, with Weber, that each atom was a permanent magnet free to turn in any direction. He calculated I,H. curves for small bar magnets situated at points of a plane square lattice and, in general, they resembled the actual curves for iron. However, it was not until 1905 that Langevin formulated his well-known theory of paramagnetism, using the recently discovered Boltzmann statistics.

Shortly after this in 1907, Weiss put forward the theory which describes the basic phenomena of ferromagnetism. In this theory, he extended Langevin's work on paramagnetism to ferromagnetic substances by postulating the existence of an internal field, often called the Weiss molecular field, which tends to produce parallel alignment of the atomic dipoles. Secondly, he proposed that a ferromagnetic specimen of macroscopic dimensions contains a number of small regions

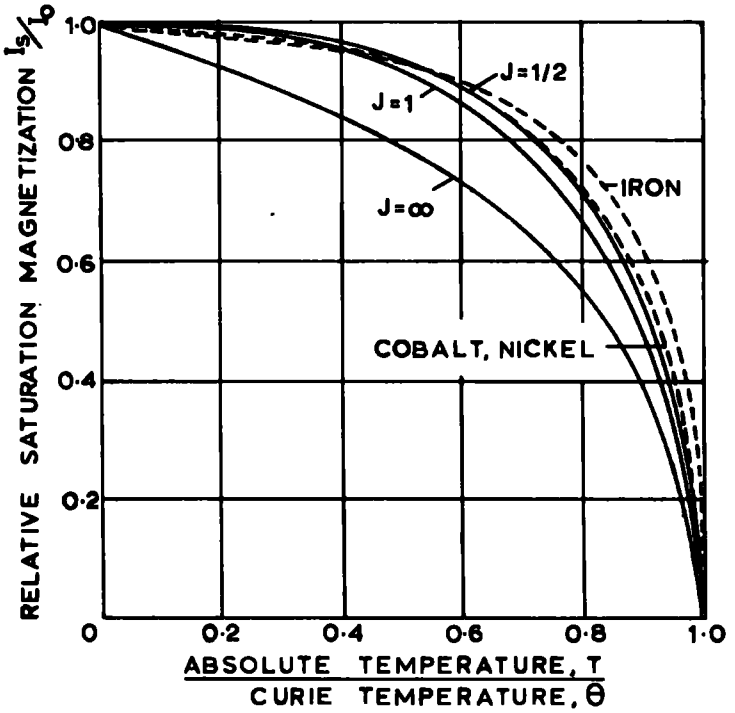

FIG. 1.1 TEMPERATURE DEPENDENCE OF THE SATURATION MAGNETIZATION OF Fe, Co AND Ni

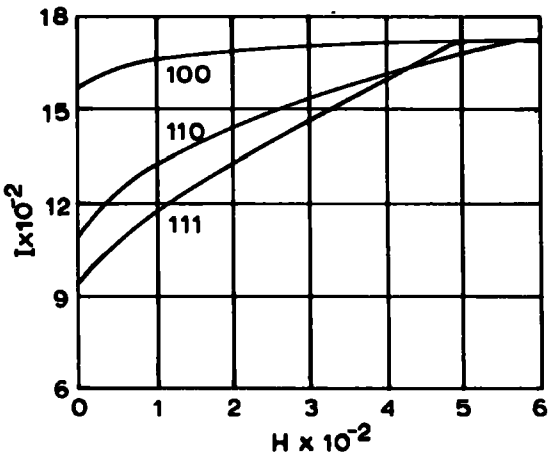

FIG. 1.2 MAGNETIZATION CURVES AT 18°C FOR A SINGLE CRYSTAL OF IRON (PIETY, 1936)

(domains) which are each spontaneously magnetized and the net magnetization of the whole specimen is obtained from the vector sum of the magnetization of each domain.

These two hypotheses provide a general explanation of most of the phenomena connected with ferromagnetics. Above a certain temperature Θ_f, known as the ferromagnetic Curie point, all spontaneous magnetization disappears. Well above this temperature there exists a linear relationship between the reciprocal of the susceptibility and the temperature:-

$$\frac{1}{\chi} = \frac{T - \Theta}{C}$$

where Θ is known as the paramagnetic Curie temperature, different from Θ_f because the relation deviates from linearity at temperatures near this point. Below the Curie temperature the Weiss theory also predicts a unique relationship between the saturation magnetization and temperature, when reduced units are employed. This postulate is known as the law of corresponding states. The curve representing Weiss's classical approach, $J=\infty$, is shown in Fig. 1:1 and it is seen not to be a good fit with the experimental data. The domain concept also gave an immediate way of accounting for hysteresis effects.

The origin of the large molecular field ($\sim 10^7$ oersteds) postulated in the Weiss theory was not understood until Heisenberg (1928) formulated his theory of quantum mechanical exchange forces between electrons. These forces arise essentially from overlapping orbital wave functions, but owing

to constraints imposed by the Pauli exclusion principle they appear as a strong spin-spin coupling between atoms which is independent of the magnetic moment of the electron.

Quantum mechanics was also used to modify the molecular field theory such that only discreet orientations of the magnetic carriers were allowed rather than a continuous distribution. This gives a much better agreement with the law of corresponding states. In Fig. 1.1. it is seen that the points for Fe, Ni, and Co are best fitted to the curve $J = \frac{1}{2}$ indicating that the magnetic carriers are probably electron spins. This fact has been confirmed by gyromagnetic experiments which give a 'g' value of ~ 2; however, since g is not exactly 2 orbital contributions cannot be entirely neglected.

Heisenberg has shown that the energy of interation of atoms i, j containing spins Si, Sj is given by:-

$$E = \text{const.} - 2\, Jij\, Si.\, Sj$$

where Jij is the exchange integral for the two atoms. For spontaneous magnetization the exchange integral Jij must be positive, although a positive Jij does not automatically mean a ferromagnetic state. In general, Jij. is negative, but Bethe has shown that it is likely to be positive, when the interatomic spacing is large compared to the orbital radii of the electrons involved. Slater (1930) has also shown that ferromagnetism can result if the ratio of the interatomic distance to orbital radius is larger than 3, but not much larger

e.g.

	Fe	Co	Ni	Cr	Mn	Gd
r_{ab}/r_o	3.26	3.64	3.94	2.6	2.94	3.1

The problem of the ferromagnetic lattice is very complicated and the Heisenberg model, in which the electrons responsible for ferromagnetism are associated with one particular atom, does not altogether provide a satisfactory solution. The collective electron theory put forward by Stoner (1933) is based on a band model of the metal where the electrons are circulating through the periodic potential field in the lattice. This theory is particularly successful in explaining why the saturation intensity of magnetization corresponds to a non-integral number of spins. In both theories successes are achieved and the truth lies somewhere intermediate between the two and in the limiting cases results do not differ by much.

1.2. Ferromagnetic Crystalline Phenomena

1.21. Anisotropy. - Qualitative Description.

The theoretical treatments outlined above generally provide satisfactory explanations of the phenomena of ferromagnetism. However, two important exceptions to this exist of which there is, as yet, no satisfactory quantitative explanation, namely magnetocrystalline anisotropy and magnetostriction. Kittel (1949) has shown that the two phenomena are inter-related and a satisfactory theory for one will explain the other.

A ferromagnetic crystal which, exhibits magnetocrystalline anisotropy has directions of 'easy' magnetization within the lattice such that the energy required to saturate the crystal in this direction is a minimum. The 'easy' directions usually conform to the crystallographic axes and directions away from these axes are conversely known as 'hard' directions. The anisotropy energy is then considered to be the difference in energy required to saturate the crystal in these two directions.

In iron the easy directions lie along the cube edges, and for nickel the cube diagonals, while cobalt has the hexagonal axis as its easy direction.

1.22. Magnetostriction.

When a ferromagnetic body is magnetized a change in length occurs known as the Joule magnetostriction. A saturation fractional change in length of the order of 10^{-5} is observed with the common ferromagnetics. The effect may be described if it is assumed that the crystal lattice is spontaneously deformed as a result of its instrinsic magnetization. Changes in the magnetization will therefore cause a change in the state of strain within the lattice which then deforms to its new state of minimum energy.

Magnetostriction is dependent on the temperature and also the applied field. Generally magnetostriction decreases with increasing temperature; in the case of nickel $\lambda_s \propto I_s^2$ approximately. The variation with field may be correlated with domain processes. In the case of iron agreement is good;

initially, in field up to a few oersteds, an expansion occurs corresponding to domain boundary movements. A contraction occurs when domain vector rotations take place and saturation magnetostriction results when rotations are complete.

A volume magnetostriction also exists, but it is very much smaller than the linear magnetostriction e.g. for nickel the fractional decrease in length is $\sim 30 \times 10^{-6}$ in a field of 25 oersteds, while the fractional change in volume is only $\sim 0.1 \times 10^{-6}$ in a field of 1000 oersteds.

1.3. Anisotropy - Phenomenological Theory.

For quantitative evaluation of the magnetocrystalline anisotropy energy it is found convenient to make use of the crystal anisotropy constants K_1, K_2 ..... These constants are defined by expressing the magnetocrystalline anisotropy energy as a function of the angular position of the magnetization vector with respect to some preferred direction in the crystal lattice. It would be expected that the energy E_k might be represented, using these constants, by some form of series.

In the case of iron, a cubic crystal, it is seen from the magnetization curves in Fig. 1.2. that the cube edges, [100], are the directions of easy magnetization. In forming an expression for the anisotropy energy in a cubic crystal, such as iron (for an arbitrary direction in the crystal defined by direction cosines α_1, α_2, α_3) the cubic symmetry applies constraints on the terms used. For example, the energy must be an even power of α_1, α_2, α_3, and also it must be invariant

with interchanges of $\alpha_1, \alpha_2, \alpha_3$, among themselves.

Thus, in a cubic crystal the energy can be written:-

$$E_k = K_o + K_1(\alpha_1^2\alpha_2^2 + \alpha_2^2\alpha_3^2 + \alpha_3^2\alpha_1^2) + K_2\alpha_1^2\alpha_2^2\alpha_3^2 + \ldots\ldots$$

the quadratic term is absent because,

$$\alpha_1^2 + \alpha_2^2 + \alpha_3^2 = 1$$

and therefore does not describe any anisotropic effects. Also, no term in $(\alpha_1, \alpha_2, \alpha_3)^4$ appears because,

$$(\alpha_1^2 + \alpha_2^2 + \alpha_3^2)^2 = 1 = \alpha_1^4 + \alpha_2^4 + \alpha_3^4 + 2(\alpha_1^2\alpha_2^2 + \alpha_2^2\alpha_3^2 + \alpha_3^2\alpha_1^2)$$

It has been found experimentally that it is unnecessary to take the series to higher terms in order to explain the data obtained.

For a hexagonal crystal, such as cobalt, it is found more convenient to express the anisotropy energy density in a sine series rather than one involving cosines. Here, the energy needed to magnetize the crystal in a direction making an angle Θ with the hexagonal axis is given by:-

$$E_K = \sum_n K_n \sin^{2n}\Theta$$

Crystal symmetry again imposes certain constraints on the series such that odd powers of $\sin\Theta$ are omitted, since the '$-\Theta$' direction is magnetically and crystallographically equivalent to the '$+\Theta$' direction. Thus the energy expression usually takes the form,

$$E_K = K_0 + K_1\sin^2\Theta + K_2\sin^4\Theta + \ldots\ldots$$

Experimentally, in the case of cobalt, this expression is sufficient to describe the anisotropy energy and it is seen that the hexagonal nature of the crystal does not emerge but only its uniaxial character.

Mason (1954) has shown that for a two constant expression, as above, obtained from fourth rank tensors results are the same as those for circular symmetry. However, when sixth rank tensors are employed the characteristic hexagonal symmetry appears and four constants are needed to describe the anisotropy energy. The expression he obtains is given by:-

$$E_K = K_0 + K_1 \sin^2\Theta + K_2 \sin^4\Theta + K_3 \sin^6\Theta + K_4 \sin^6\Theta \cos 6\Phi$$

where Θ is the polar and Φ is the azimuthal angle.

The magnetocrystalline anisotropy energy has also been studied in tetragonal crystals by Guillaud (1943). He obtains an expression for this lattice.

$$E_K = K_0 + K_1 \sin^2\Phi + K_2 \sin^4\Phi + K_3 \cos^2\alpha \cos^2\beta$$

Φ being the angle between the magnetization vector and the tetragonal axis, and α, β are the angles made with the other two axes.

The treatment of magnetocrystalline anisotropy in this manner is purely empirical and no question as to the origins or explanation of the processes causing the effect are involved. The method does, however, provide a starting point from which the phenomenon can be studied experimentally in an attempt to provide

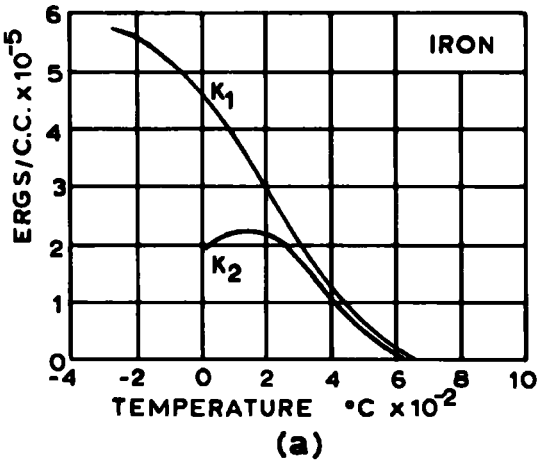

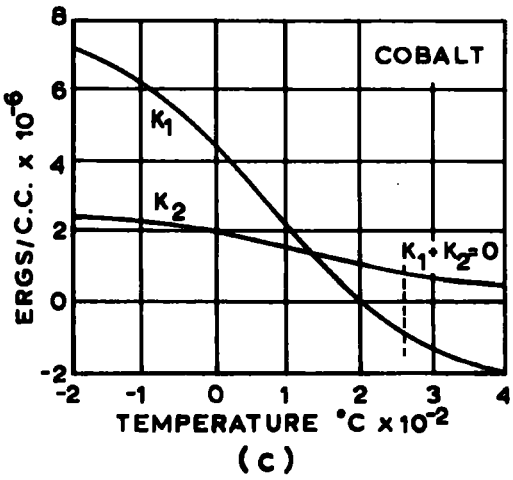

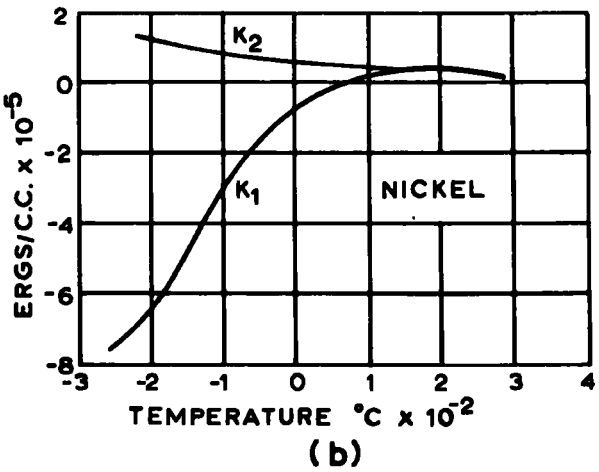

FIG. 1.3 TEMPERATURE VARIATION OF THE CRYSTAL ANISOTROPY CONSTANTS OF Fe, Ni AND Co

data which might be of assistance in the development of a satisfactory theoretical approach to the problem.

1.4. The Temperature Dependence of Anisotropy.

The magnetocrystalline anisotropy constants which represent the anisotropy of the ferromagnetic material are extremely sensitive to temperature changes. The constants are found to vary greatly in magnitude, and sometimes in sign, over a wide range of temperature.

In Fig. 1.3. is shown the temperature variation of the anisotropy constants for (a) iron (b) nickel and (c) cobalt.

The values of the anisotropy constants for the three common ferromagnetics (at room temperature) are shown in Table 1.1.

Table 1.1.

	K_1(ergs/cc)	K_2(ergs/cc)
Iron (Tarasov 1939)	$+ 4.7 \times 10^5$	$+ 1.5 \times 10^5$
Nickel (Mckeehan 1937)	$- 0.34 \times 10^5$	$+ 0.5 \times 10^5$
Cobalt (Bozorth 1954)	$+ 4.3 \times 10^6$	$+ 1.2 \times 10^6$

Obviously any theory of anisotropy must be capable of providing a satisfactory explanation of the temperature dependence of the anisotropy constants. It can be seen that the variation with temperature is quite irregular, and no simple interpretation is obvious.

1.5. Origins of Anisotropy and Present Theories.

The fact that in general the direction of magnetization in a crystal does not coincide with the direction of an applied field is perhaps the most interesting aspect of the study of

ferromagnetism. This occurs even in crystals with cubic symmetry which were erroneously supposed by Faraday and Tyndall to be magnetically isotropic. Introduction of the Weiss Molecular field theory provided no answer to this problem although magnetic phenomena generally were well explained by this theory.

In the early attempts to provide a solution to the problem, Mahajani (1929) studied the interaction of magnetic elements of various types situated at lattice points within the crystal. He considered the possibilities of simple dipoles, small bar magnets and electronic orbits constituting flat disc-shaped magnets. He found that the dipole case does not give rise to any anisotropy, since there is no quadrupole or higher power in the expression for the mutual potential energy and that the case of cubic iron is qualitatively described if the magnets are assumed to be flat discs; this gives an easy direction in the [100].

This could be interpreted by saying that the direction of the easy magnetization is determined by the distribution, about the atom, of the electron spins which are associated with the ferromagnetism. For iron the distribution is nearer a circular plate while for nickel (Mckeehan 1937) a qualitative explanation is obtained if the distribution is more nearly a prolate ellipsoid.

Purely magnetic interactions have, however, been shown to be too small in predicting the correct order of magnitude for the observed results by a factor of ~ 1000. Obviously there is need

of some much stronger form of interatomic interaction. No anisotropy can arise from the exchange energy, since the exchange interaction refers only to the angle between spins in different atoms and not to the angular position of the spins in relation to the lattice.

Powell (1930) formulated a theory in which the anisotropy is derived from an anisotropic Weiss molecular field which arises from some form of spin-orbit interaction of the electrons. A somewhat similar approach has been made by Bloch and Gentile (1931), but a much more complete investigation of the spin-orbit interaction theory has been made by Van Vleck (1937).

The theory as developed by Van Vleck is very complex. Briefly, the anisotropic character of the magnetization in crystals derives basically from a spin - orbit interaction. The spin - orbit coupling has the effect of making the spin vectors, responsible for the ferromagnetism, sensitive to the anistropic electrostatic forces that exist within the lattice. This occurs because the spin interacts with the orbital motion and the orbital motion is controlled by the lattice due to electrostatic fields and overlapping orbital wave functions of neighbouring atoms.

Van Vleck considers two particular models, namely a dipole-dipole and quadrupole - quadrupole coupling between spins of different atoms. In the dipolar model anisotropy exists only when the second approximation of perturbation theory is used, in which case the elementary magnets need not be perfectly

parallel. The quadrupolar model gives anisotropy in all cases. Both models give values of K_1 of the right order of magnitude . in the cubic case but the temperature variation is given only roughly in that K_1 vanishes much more rapidly than I. However, the calculations do not explain the different behaviour of nickel and iron. Values of K_2 could not be calculated satisfactorily.

A calculation for the case of a hexagonal crystal was also carried out by Van Vleck. Here dipole - dipole interaction can occur as the cubic symmetry no longer exists. In cobalt, values of the right order of magnitude can be obtained, if it is realised that the cobalt lattice is only slightly different from cubic, but here again temperature dependence is found to be far too slow.

Brooks (1940) has tried another approach using the 'collective electron' model of Stoner instead of the Heisenberg stationary conception as did Van Vleck. He treats the exchange energy as a Weiss internal field and the spin - orbit coupling is introduced as a perturbation. Anisotropy of the right magnitude and sign for iron and nickel appears in the fourth approximation. However, observations on the Fe Ni alloy systems show no sharp change in anisotropy as the lattice passes from face - to body-centred cubic which would be expected with this model. Also, the temperature dependence of the anisotropy is not described at all by this model. Fletcher (1954) has made a similar calculation, using the revised earlier model of Brooks, for K_1 in nickel. K_1 in this case is further from the measured

value than in Brooks' earlier estimate.

A classical approach to the problem has been made by Zener (1954) in which he considers the effects of random deviations of the direction of magnetization, caused by temperature, in localized regions. Anisotropy is then a function of the magnetization in each region and the temperature dependence arises from the fluctuations in the magnetization. He arrives at a power law relationship for K associated with the n.th order harmonic,

$$K_{(T)} \propto \left[\frac{I_{s(T)}}{I_{s(0)}}\right]^{\frac{n(n+1)}{2}}$$

This is in good agreement with the results for iron with $n = 4$ for K_1 and $n = 6$ for K_2. In the case of K for nickel this is much too slow. Later, Keffer (1955) showed that Zener's classical approach was really the same as Van Vleck's quantum mechanical argument, the former being a low temperature and the latter a high temperature approximation to the same physical picture - decreasing anisotropy with increasing temperature.

Vonsovski et al (1956), from quantum mechanical considerations have determined a very approximate expression for the anisotropy of a hexagonal crystal near the Curie point. However, the approximations involved are so extensive that little significance can be attributed to the result.

Thus it can be seen from the preceding brief description of the various hypotheses, there is as yet no satisfactory unified theory that can correctly explain the phenomenon of

magnetocrystalline anisotropy. However, it is apparent that some form of spin coupling must be invoked in order to realise anisotropies of the observed magnitudes. Anisotropy is extremely temperature sensitive and it is in attempting to explain this variation that the theories all fall short.

1.6. Objects of the Present Investigation.

The following investigation on gadolinium has been carried out in the hope of providing more data, on the variation of magnetocrystalline anisotropy with temperature, which will possibly allow a better insight into the phenomenon as a whole. Gadolinium, as emphasized by Van Vleck, is a very interesting ferromagnetic and at first sight should be comparatively simple in behaviour. The metal is reported by Trombe (1937) to have a ferromagnetic Curie point of 16°C. Its apparent simplicity derives from the fact that it exhibits a saturation magnetization corresponding closely to the value expected for an ^8S state, where the magnetic moment per atom is due to the parallel alignment of the 7 electrons in the incomplete 4f shell, which is situated deep in the atom. The spins responsible for the ferromagnetism are thus effectively screened and are not subject to interatomic interactions, which is the case with the common ferromagnetics. Hence, gadolinium is a good representative of the localized model of a ferromagnetic., and theoretical treatment of its properties should be appropriately simpler.

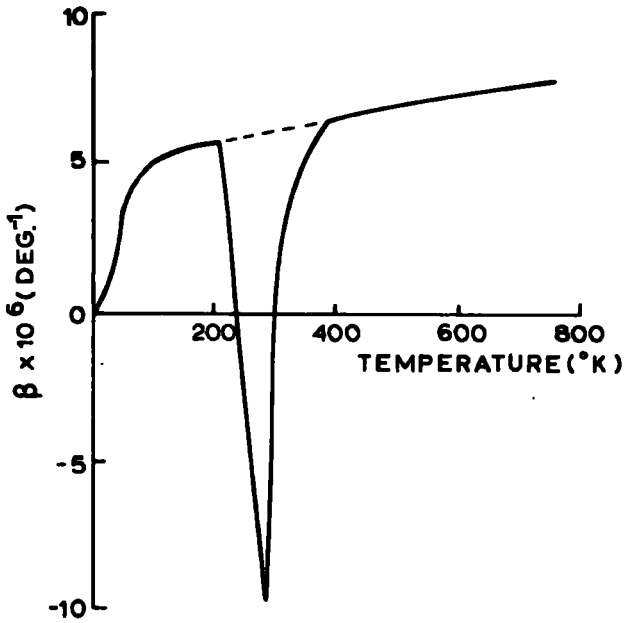

FIG. 1.4 TEMPERATURE VARIATION OF THE COEFFICIENT OF THERMAL EXPANSION FOR GADOLINIUM (BIRSS 1960)

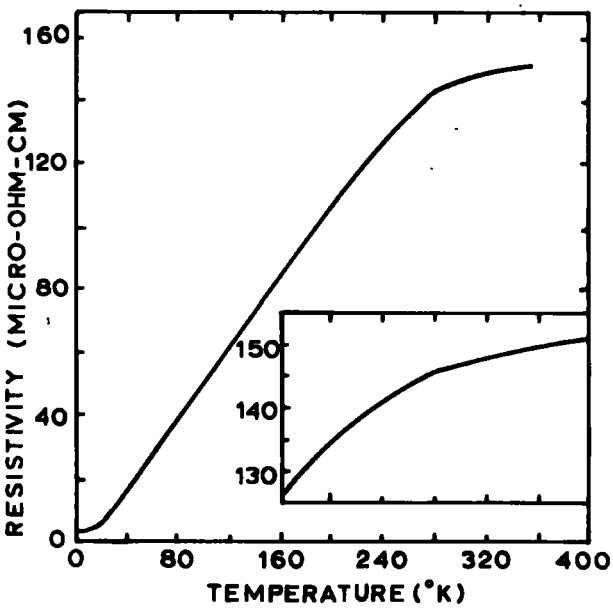

FIG. 1.5 TEMPERATURE VARIATION OF THE RESISTIVITY FOR GADOLINIUM (LEGVOLD ET AL 1953)

1.7. Gadolinium - some Physical and Magnetic Properties.

Gadolinium is a metal of the rare earth group, atomic number 64, and it crystalizes in a hexagonal close - packed structure having undergone a phase change from a cubic system just below the melting point of 1320°C. X-ray measurements of Bannister et al (1954) have shown the hexagonal structure to be stable over the range from 300°K to 4.2°K, with a thermal expansion of -2×10^{-6} / °K below the Curie point and 10×10^{-6} / °K above the Curie point. The small change in the region below the Curie point is attributed to an expansion of the C - axis when the temperature decreases. However, Birss (1960) has measured the temperature dependence of the thermal expansion and his results, shown in Fig. 1.4. are not in agreement with those of Bannister. The density of the metal is ~ 7.8 gms/cc.

The electrical resistivity is shown in Fig. 1.5 and there is seen to be a knee in the curve in the region of the Curie point. More striking perhaps is the λ- type anomaly in the heat capacity which is shown in Fig. 1.6. The anomaly occurs at T = 291.8°K.

Following the work of Trombe, Elliot et al (1953) have made extensive studies of the magnetic properties of polycrystalline gadolinium. Using a sample with slight rare earth impurities, but no ferromagnetic materials, they have measured the saturation magnetization over the whole ferromagnetic range and found the data to be well represented by:-

$$\sigma_{\infty,T} = \sigma_{\infty,0}(1 - bT^{3/2})$$

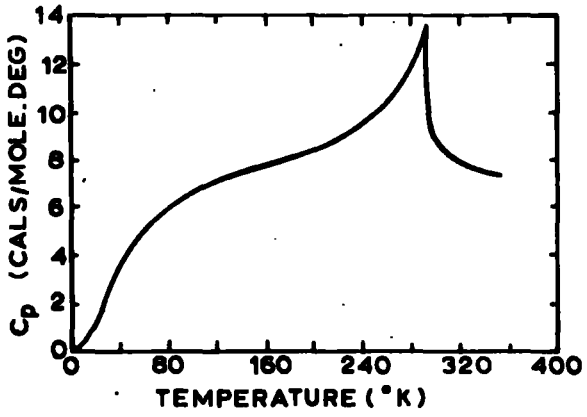

FIG.1.6 TEMPERATURE VARIATION OF THE HEAT CAPACITY OF GADOLINIUM (GRIFFEL ET AL 1954)

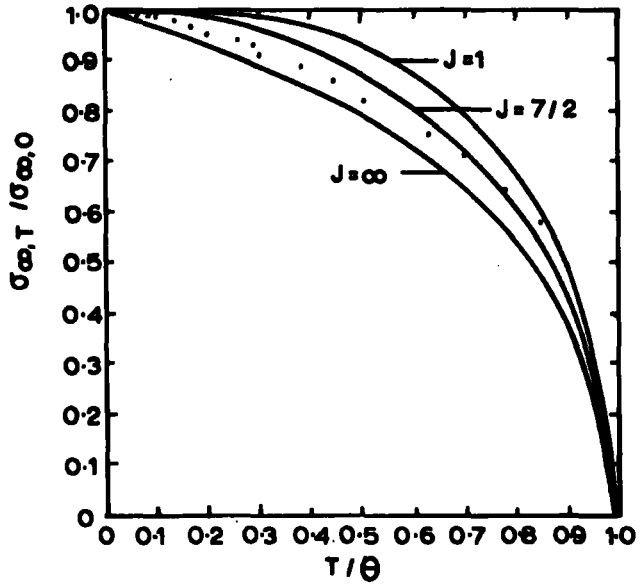

FIG.1.7 REDUCED MAGNETIZATION CURVE FOR GADOLINIUM AND THEORETICAL CURVES FROM THE WEISS (QUANTUM) THEORY (ELLIOTT ET AL 1953)

where $\sigma_{\infty,0}$ = absolute saturation magnetization, b = a constant and T = absolute temperature. The saturation magnetization at absolute zero was found to be 253.6 ± 0.6 c.g.s. units. This saturation moment corresponds to 7.12 Bohr magnetons/atom which is some 2% higher than would be expected if the 7 spins in the 4f shell were solely responsible. It is of interest to note that the saturation magnetization follows a $T^{3/2}$ law over nearly its entire ferromagnetic range, whereas this can only be applied to the other ferromagnetics over the low temperature region.

An estimate of the magnetic hardness was also obtained from the isothermal variation of the magnetic moment as a function of 1/H, using the expression:-

$$\sigma_{H,T} = \sigma_{\infty,T}(1 - aH)$$

where the constant 'a' is an indication of the hardness. Elliot obtained a value of 170, while Trombe had earlier given a = 1250. Corner and Hutchinson (1960) more recently, have obtained a value, intermediate between the two, of ~700. The large differences can probably be attributed to the purity of the samples examined.

The reduced magnetization curve for gadolinium is shown plotted in Fig. 1.7. It is evident that the agreement expected for $J = 7/2$ is disappointingly poor, with $\sigma_{\infty,T}/\sigma_{\infty,0}$ lying well above the curve up to $T/\Theta \simeq .75$ and then subsequently below. The difference is due to the apparent large value of the intrinsic magnetization in the region of the Curie point. Fig 1.8. (Hutchinson 1958) shows a plot of I v T for a constant internal

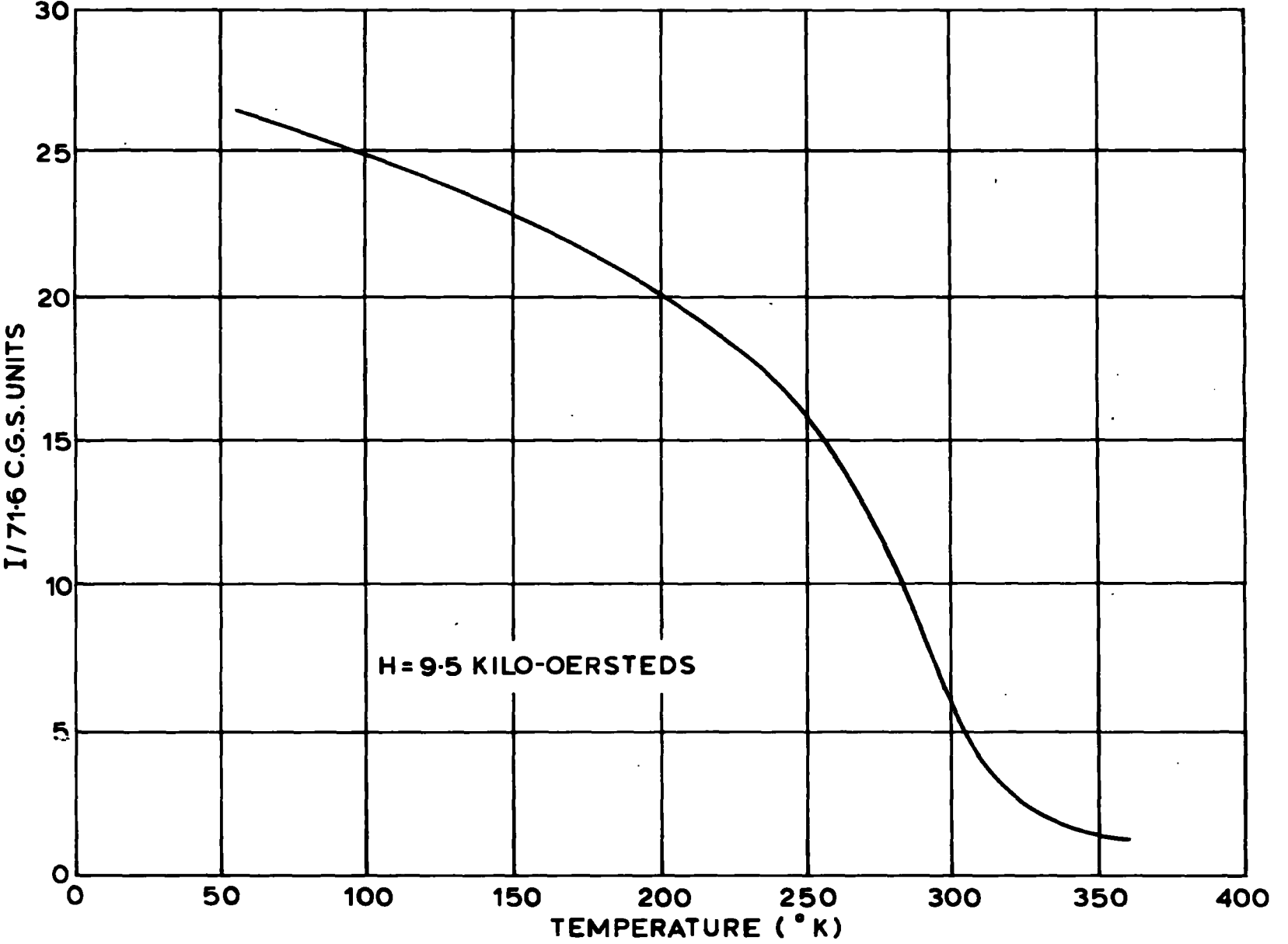

FIG. 1.8 TEMPERATURE DEPENDENCE OF THE INTENSITY OF MAGNETIZATION

field of 9,500 oersteds. The comparatively large value of I still existing at temperatures above the Curie point is attributed to a paramagnetic contribution which is much more noticeable with gadolinium than with the other ferromagnetics.

1.8. Methods Available for Measuring Anisotropy Constants.

By definition it is obvious that the crystal anisotropy energy density can be determined by directly measuring the difference in energy required to magnetize the crystal in two different directions.

The work done to magnetize a specimen to saturation in the direction (h, k, l) is,

$$A(h,k,l) = \int_0^{I_s} H.d\ I$$

i.e. the area beneath the magnetization curve. Thus in the case of a cubic crystal K_1 may be evaluated by considering the area beneath the magnetization curves in the [100] and [110] directions. Then the direction cosines are (1,0,0) and $(1/\sqrt{2}, 1/\sqrt{2}, 0)$ and therefore:-

$$A_{110} - A_{100} = K_1/4$$

Similar relations exist between other crystallographic directions from which K_2 may be derived.

Several disadvantages exist with this method. Demagnetization factors are critical unless 'picture frame' shaped specimens are used, but of course this is impossible with hexagonal structures. Separate specimens are also required for

the magnetization measurements in each direction.

A method of obtaining magnetocrystalline anisotropy measurement has been described by Kip and Arnold (1949) using a microwave resonance absorption technique. In this method resonance absorption is observed at 24,000 or 9,000 Mcs/sec. using an external magnetic field applied perpendicular to the R.F. magnetic field in the plane of the crystal. The resonance field is found to vary with the angular position of the crystal with respect to the applied field and Kittel (1948) has shown that this is a result of crystal anisotropy. For resonance absorption the conditions are given by:-

$$W_o = \gamma (B H)^{\frac{1}{2}}$$

where W_o = resonance frequency, $\gamma = ge/2mc$ = magneto - mechanical ratio for the electron, H = static field and B = induction in the specimen.

By considering the crystalline anisotropy energy in terms of an equivalent magnetic field on effective demagnetization factor is obtained which adds to the demagnetization factor used in calculating the Larmour frequency. For an infinite plane cubic system Kittel obtained for resonance in the (100) plane,

$$W_0 = \gamma \left[(H_2 + 4\pi I_S + 2K_1/I_S)(H_2 - 2K_1/I_S \cos 4\Theta) \right]^{\frac{1}{2}}$$

where H_2 is the applied magnetic field and Θ is the angle,

between the magnetization and the [100] direction.

It appears that only the first order constants can be easily obtained from this method and therefore a really complete description of the crystal anisotropy cannot be obtained.

Magnetocrystalline anisotropy constants have been evaluated by various workers from measurements of the torque acting on a single crystal specimen suspended in a strong magnetic field. Williams (1937) first described a torque magnetometer for ferromagnetic anisotropy work. In his method, the crystal specimen in the form of a thin disc of known orientation, is suspended in the pole gap of an electromagnet by a torsion fibre and the torque applied at the crystal, for various orientations of the magnetic field, is measured by the angular twist of the torsional suspension. A curve of torque versus field orientation, with respect to some reference direction, is then drawn and the relevant anisotropy constants can be obtained from simple measurements on the shape of the curve.

Thus the torque method provides a very simple means of deducing directly the anisotropy constants and it would also seem that no undue difficulty should be encountered in adapting the method so that measurements may be made over a wide range of temperatures.

For the present investigation on gadolinium we require the energy density for a hexagonal crystal:-

$$E_k = K_o + K_1 \sin^2\Theta + K_2 \sin^4\Theta + K_3 \sin^6\Theta + K_4 \sin^6\Theta \cos 6\Phi$$

CHAPTER TWO

THE GADOLINIUM SINGLE CRYSTAL SPECIMEN.

CHAPTER TWO.

THE GADOLINIUM SINGLE CRYSTAL SPECIMEN.

2.1. Attempts to grow a single crystal of gadolinium.

All the three familiar methods of growing single crystals, namely zone refining, strain and anneal and slow cooling from the melt, were tried in an attempt to produce a single crystal of gadolinium from pure polycrystalline material. The polycrystalline material obtained from Johnson, Matthey and Co. Ltd., was 99.99% pure gadolinium and was supplied in the form of a rod of 1/4" diameter.

At all temperatures and especially near its melting point, gadolinium is extremely reactive, readily forming oxides and nitrides when in contact with the atmosphere. For this reason all experiments must be conducted either in an inert atmosphere or a vacuum.

211. The Method of Zone Refining.

Most of the earlier work, attempting to grow a single crystal of gadolinium was carried out by Hutchinson (1958) using the method of zone refining described by Davis et al (1956). Only a brief review of the apparatus and its operation will be given here as a full account is available in Hutchinson's thesis.

In operation a floating molten zone of the material is formed by localised electron bombardment. By repeated traversal of the rod by the molten zone, purification of the material is obtained with resulting increase in grain size and possible

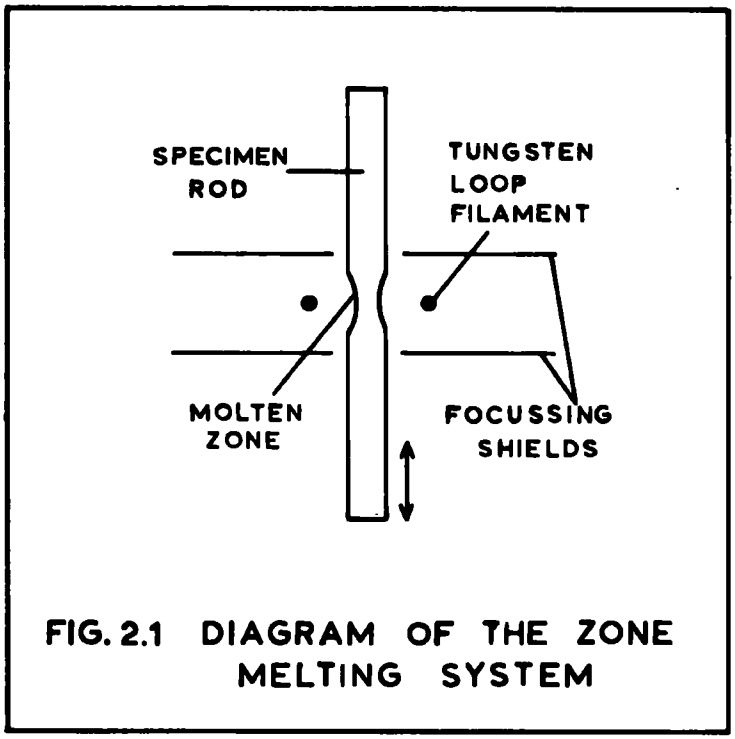

FIG. 2.1 DIAGRAM OF THE ZONE MELTING SYSTEM

formation of a large single crystal.

The cathode arrangement and its associated parts are shown in Fig. 2.1. The rod is supported by springs on a frame which is mounted in a glass bell - jar continuously evacuated and maintained at a pressure of 10^{-5} millimetres Hg. Electrons from a pure tungsten loop filament are accelarated toward the rod by a potential of a few kilovolts, until a molten zone is formed. Two focussing shields, at cathode potential, control the length of the molten zone. Traversal of the rod by the molten zone is attained by moving the frame up and down with respect to the loop filament system. This is done with a small gramophone motor which gives a traversal speed of 1 cm/minute. The system is surrounded by an earthed shield $\sim$ 7" in diameter which acts as a radiation shield and prevents deposition of the melted material on the walls of the vacuum chamber.

The H.T. power pack is a conventional full wave rectifier giving 300 milliamps at 1800 volts. An emission control system is incorporated in the apparatus because of the difficulty of manual adjustment during initial outgassing from the specimen. This simply compares the voltage $I_e \times R$, see Fig. 2.2, which is of the order of a few hundred volts with a variable 0-300 volt D.C. supply. The difference in these voltages is then used to adjust a thyratron firing time such that power supplied to the cathode maintains the bombardment current at the desired value.

Hutchinson initially tested the apparatus using Nickel

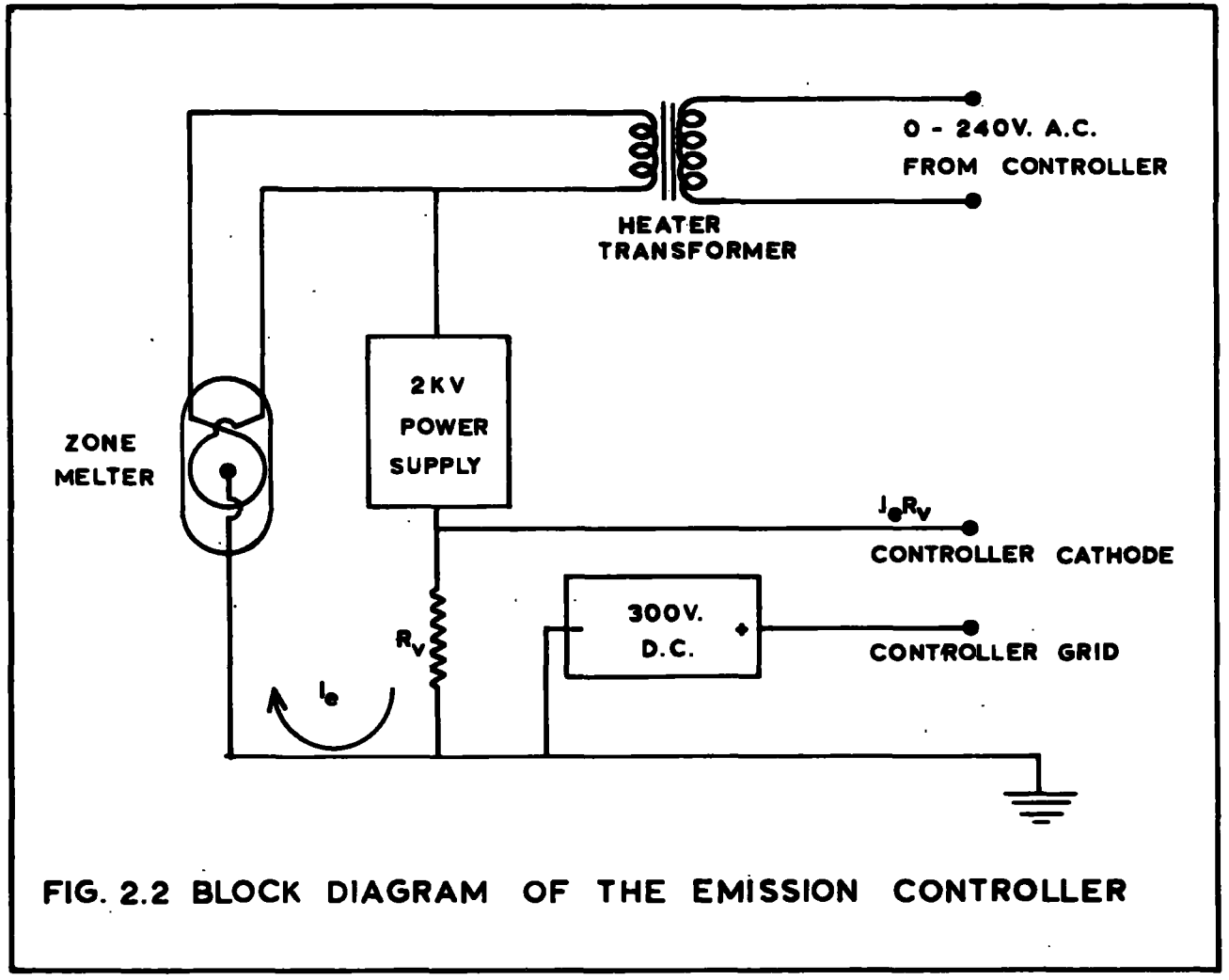

FIG. 2.2 BLOCK DIAGRAM OF THE EMISSION CONTROLLER

specimens. In this case little outgassing was observed and single crystals were produced after only a few traversals of the rod.

Only a short piece of 98.5% gadolinium, 1.1/4" long, was available at this time. However, with a possible length of 1" available for zone refining several traversals were carried out. Copious outgassing occurred which caused the rod to buckle and become non-uniform in diameter. Examination of the specimen after four traversals revealed some small grains $\sim$ 1 m.m., but deterioration in the shape of the rod prevented further runs.

This experiment was continued on the arrival of a new sample of 99.99% pure gadolinium. Initially it was decided to test whether this pure metal could be melted without introducing contamination. To this end a small piece was cut off and placed upright in a tantalum crucible, previously outgassed at 2000^{o}C for 3 hours. In all cases, melting of the gadolinium was carried out using crucibles of tantalum, this being the only material with a suffieiently high melting point which does not react chemically with the gadolinium.

Prior to melting, the specimen was examined under a microscope, having been polished down to 1/4μ diamond paste and then electropolished. After melting in the zone refining apparatus it was re-examined under the same conditions. The specimen was estimated to be 20% contaminated with compounds or other elements. Under polarizing light at least five different phases were recognisable. This was much too high to be accounted

for by residual gas in the apparatus ($\sim 10^{-5}$m.m. Hg). Repeated similar experiments always yielded the same result.

It seemed probable that, since the crucible was thoroughly outgassed and also the residual gas present in the system was negligible, contamination of the gadolinium resulted from reaction with its own occluded gas. At room temperature this is inactive but violent reaction occurs when heated. Another possible source of contamination may have been tungsten which was shot off from the hot filament. This was checked using chemical tests but results were inconclusive.

With these facts in mind it was decided to abandon attempts at growing a single crystal by the zone - refining method.

2.12. The Method of Strain and Anneal.

The following experiments were carried out jointly with Hutchinson to ascertain whether single crystals could be produced by the method of strain and anneal, which can be used very successfully for producing single crystals of iron.

Tests were initially made on a small amount of 98.5% gadolinium. The specimens, which were cut into small discs 2.3 m.m. thick, were strained to varying degrees by rolling. After straining they were annealed in a thermostatically controlled resistance furnace at 1000°C and then cooled from this temperature at a rate of 75°C/hour. To prevent contamination, a stream of argon was passed through the furnace during the period of anneal. The argon was previously purified by passing over heated magnesium turnings at 500°C and then through a

mixture of 25% sodium / 75% potassium, to remove nitrogen and oxygen respectively.

Straining was varied from 0.9% to 3.6% and periods of anneal varied from 6 hours to 140 hours. Generally results were poor, with little or no increase in grain size and in some cases, with the longer anneal times, the gadolinium had entirely transformed to a compound. However, some little success was obtained when the grain size increased ~ 6 x for a strain of 3.6% and an anneal of 140 hours.

With this in mind samples of the very pure 99.99% gadolinium were tried. Four discs of the material were cut and rolled to 1.6%, 2%, 2.2% and 3.5% and then annealed for a period of 113 hours. No change was observed and all the discs were 30% - 50% decomposed. Obviously a very high purity atmosphere is required to maintain the 99.99% gadolinium uncontaminated. The material, in fact, seemed to be more highly reactive than the less pure 98.5% metal.

This method was therefore found to be unsuitable, except for the limited increase in grain size which was noted in one case with the 98.5% metal. The difficulties of maintaining the very pure gadolinium uncontaminated at a temperature of 1000°C for long periods of time were considerable with the apparatus available.

2.13. The Method of Slow Cooling from the Melt.

At this time, using X-ray methods of examination,

Spedding (1959) confirmed the existence of a phase change in gadolinium. This phase change, consisting of a change from body centred cubic to close pack hexagonal crystal structure, occurred at 1263°C which is about 50°C below the melting point.

It seems very probable that this is the reason why zone refining did not meet with any success quite apart from purity problems. Also annealing at 1000°C would not have created the optimum conditions for the strain and anneal method.

Considering this fact it was decided to try the method of slow cooling from the melt. In this method the crystal temperature is lowered very slowly through the temperature of the crystalline phase change so that the change can take place without rupturing the crystal lattice. This method works very effectively for cobalt (Myers and Sucksmith 1951). In their method slow cooling was obtained by lowering the crucible containing the cobalt at varying rates through a resistance furnace, which consisted of molybdenum resistance wire wound on an Alumina tube and dissipating 2 K.W. at a temperature $\sim$ 1600°C.

To this end, the vacuum system, previously used for the zone refining apparatus, was redesigned with a view to obtaining lower pressures in an attempt to reduce contamination. The system uses an Edwards 2M2 mercury diffusion pump, with a liquid air trap, which is backed by the usual rotary pump operating at $\sim$ .05 m.m. Hg. With this arrangement pressures of 10^{-5} m.m. Hg. could be reached and maintained while being

continuously pumped.

The vacuum chamber was of steel construction with copper pipes brazed on the outer surface to provide water cooling:- this actually being connected in series with the water - cooling of the diffusion pump. The top plate had a small window through which an optical pyrometer could be used to assess temperatures in the furnace. This instrument was kindly loaned by the I.C.I. Research Dept. Billingham. The chamber was mounted on the steel base used for the zone refining apparatus and vacuum seals were again made with L - shaped rubber gaskets, one at the base and one at the top plate.

Initially a small furnace was constructed to investigate whether the gadolinium could be melted and maintained at high temperatures for long periods of time without suffering undue contamination. If this was possible a larger more sophisticated furnace would be constructed to carry out the actual slow cooling.

The melting was to be carried out in small Tantalum crucibles 5 cms. x 0.6 cms. diameter with a surface area of $\sim$ 10 cm.^{2} The energy dissipated at a temperature $\sim 1500^{o}$K, assuming radiation loss only and using Stefan's law is $\sim$ 30 Watts/cm^2 i.e. a total of 300 watts. Therefore a small furnace was constructed giving a maximum power of $\sim$ 1 Kilowatt.

A heater element with low vapour pressure and low reactivity with gadolinium was required. Tantalum was tried at first, but little success was achieved. There was a chemical

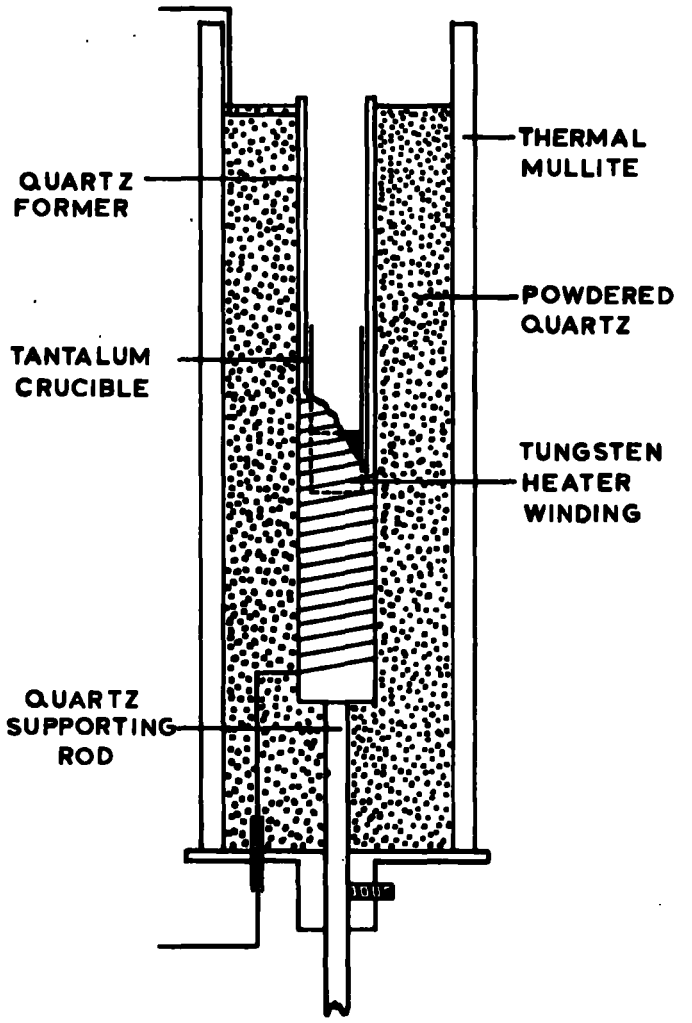

FIG. 2.3 DIAGRAM OF THE RESISTANCE FURNACE

reaction between the quartz former and the Tantalum wire at high temperatures and repeated failures of the heater occurred.

Tungsten was then substituted for the heater, this time quite successfully and the final form of the furnace used is shown in Fig. 2.3. The element is wound on a spirally grooved quartz tube which is surrounded by a sheath of powdered quartz, held in by an outer tube of Thermal Mullite. The unit is supported on a small steel platform which is mounted on a quartz stalk fixed to the base of the chamber. Power is carried in and out of the chamber via the same vacuum sealed electrodes (Edwards Type 7A) as used for the zone refining system.

Several experiments were carried out melting gadolinium specimens of 99.99%. In each case a sharp rise in pressure occurred in the system when the specimens were at temperatures near to the melting point and, since the furnace and crucible were thoroughly outgassed before melting, it was apparent that the gas was coming from the gadolinium. Examination of the melted specimens under a reflecting microscope, after the usual polishing procedure, showed contamination of various types; particularly evident in the matrix were greyish needle-shaped inclusions. A run on a weighed specimen was also carried out to determine whether any loss in weight occurred. A loss of $\sim$ 0.1% was detected suggesting that some metal must have evaporated. This figure of 0.1% should be larger as the specimen gained weight during the weighing ($\sim$ .000025 gms/min) due to the formation of compounds from the atmosphere and this

would offset the loss of metal.

These experiments showed that in every case a very high percentage of the gadolinium had been contaminated, and single crystal growth was impossible under such conditions.

2.14. Conclusion of Crystal Growing Experiments.

Several facts became obvious in summarizing these experiments. When it was known that there was a cubic to hexagonal phase change just below the melting point, the method of zone refining was immediately ruled out because of the too rapid rate of change of temperature connected with the molten zone arrangement.

In all three methods contamination was evident, and, since gadolinium is so reactive acting like a 'getter' at high temperatures, some form of very good vacuum apparatus was needed capable of maintaining pressures below 10^{-5} m.m. Hg.

It is doubtful whether this would be the whole answer, since it appeared that the metal reacted with its own occluded gas on being raised to temperatures near the melting point. Evaporation of the metal when molten was also apparent, suggesting the necessity of conducting the operation in a sealed crucible; however, this would present problems with respect to loading in an inert atmosphere or vacuum.

It was evident that gadolinium could not be melted and maintained in a pure state with the apparatus then available and attempts to grow a single crystal were abandoned when a crystal became available from other sources.

2.2. The Gadolinium Single Crystal.

A visit to the Research Dept. of Johnson Matthey and Co. Ltd., (Wembley) designed to learn more of the methods used in handling pure gadolinium in the molten state, resulted in the acquisition of a single crystal piece of the metal.

In the research department at Wembley the apparatus used for melting the gadolinium consisted of a high vacuum system working at pressures of $\sim 10^{-6}$ m.m. Hg. while being continuously pumped and having a leak rate of less than 20 microns Hg./hour. Melting was done inside a water-cooled steel bell jar in tantalum crucibles capable of carrying up to 2 kilograms of metal at a time. Tantalum sheets surrounding the crucible formed the heaters and power was delivered at 1000 amps and 7 volts. This system was then surrounded by a complex set of tantalum radiation shields extending almost to the walls of the chamber. Absolutely no refractory material was allowed in the chamber.

Owing to the extremely good vacuum and insulation of the system, the mass of molten metal cooled quite slowly and single crystals were formed all round the sides of the kilogram melt.

A small crystal, cut from one such melt, was kindly given by Dr. J.C. Chaston for the purposes of this experiment. The crystal piece was in the form of a wedge - shaped slab $\sim$ 7 m.m. x 3 m.m. x 6 m.m. and weighing just over 1 gm. A chemical analysis of the gadolinium crystal is given in Appendix 1.

2.3. Orientation of the Gadolinium Single Crystal.

Orientation of the single crystal was carried out with X-rays using the Laue back-reflection method.

Before mounting in the X-ray diffraction camera the crystal was well etched with a solution of 50% Alcohol/50% Concentrated Nitric Acid to remove the strained surface layers.

Exposures were made using tungsten radiation, as this has a wide spread of wavelengths necessary for the Laue type of picture. A large number of exposures were made and the position of the hexagonal axis, and orientation of the basal plane were obtained to within $\pm\frac{1}{2}^{o}$.

To ensure that the piece was a single crystal, an exposure was made after rotating the crystal through an angle of 180^{o} from the hexagonal axis which was located on the first side. A similar pattern with three-fold symmetry was obtained confirming that the piece was a single crystal.

The orientation of the crystal was very fortunate in that the hexagonal axis was lying nearly in the largest plane of the piece, thus allowing a maximum possible disc of $\sim$ 0.55 cms. diameter x 0.15 cms. thick which would contain the hexagonal axis and one of the symmetry axes lying in the basal plane.

2.4. Cutting the Single Crystal.

Normal methods of mechanical cutting are undesirable for single crystals because of the strain which such methods cause.

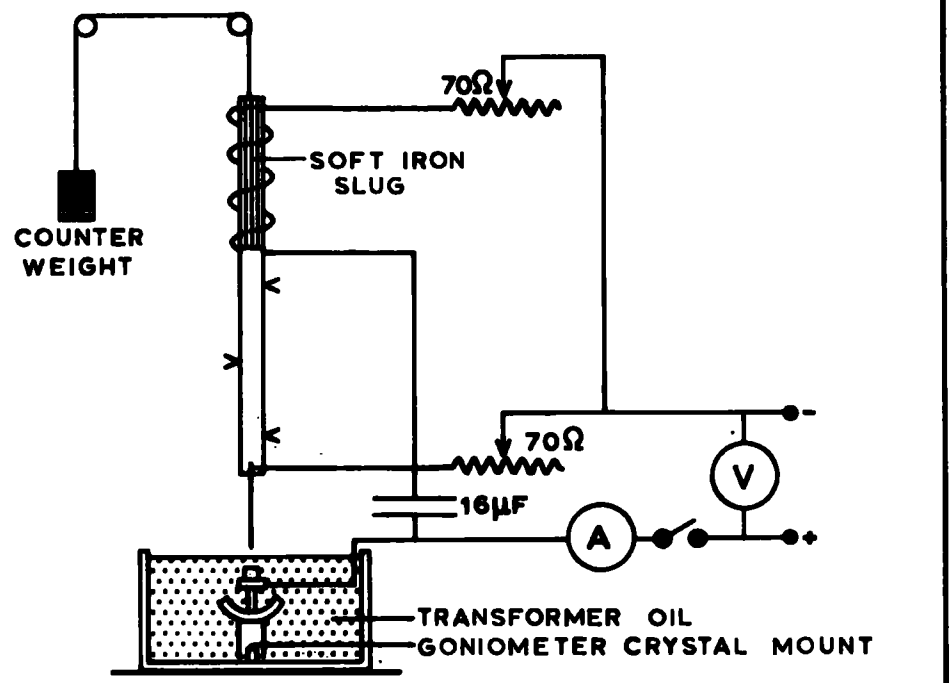

FIG. 2.4 DIAGRAM OF THE ELECTRO-SPARK MACHINE

A strain - free method of working metals by electro-sparking has been described by Nosov and Bykov (1956). In this method material is removed from the surface of the metal being worked by the passage of an electric spark between it and the working tool. The discharge releases heat energy which causes a momentary fusion and vaporization of a small volume of metal at the point where the discharge occurred. The specimen being worked is made the anode and the tool the cathode. Repeated successive discharges then slowly remove the metal and any shape of cut can be made with the appropriate tool used as the cathode. Very little strain is introduced by removing metal in this way.

The apparatus used actually takes the form shown in Fig. 2.4. The crystal being worked is mounted on a goniometer head to allow cuts to be taken at any desired angle. The system works quite simply:- with open electrodes there is no current through the energising coil on the tool feed and this then begins to fall under its own weight and makes contact with the specimen. On making contact, current immediately flows drawing the tool away as the coil is energised, and at the optimum separation the condenser, charged to the operating potential, then discharges across the gap between the tool and the specimen. The system is then in its initial state and the process is repeated. By suitable adjustment of the counter-balancing weights and rheostats the system can be made to run continuously, the counter weight system allowing the tool to feed on as metal

is eroded from the specimen and tool.

Several trial cuts were carried out on the machine with pieces of polycrystalline gadolinium, to test whether the system could be used satisfactorily with this metal. No difficulty was experienced using a tool of brass shim .015 cms. thick which was found to give the best results - maximum rate of cutting for minimum erosion of the tool.

The crystal was mounted on the goniometer head with Durofix and a cut was made through the crystal forming a thin slab, the surface of which was a plane containing the hexagonal axis. This reference surface was then cleaned with grade 4/0 emery paper to remove the slight pitting from the electro-sparking and mounted horizontal on the goniometer head. A circular tool was then used to cut a disc of maximum diameter from this slab. The disc so obtained was slightly wedge shaped having dimensions ~0.54 cms diameter x 0.10 cms. thick and having one reference face containing the hexagonal axis.

2.5. Forming the Oblate Spheroid.

In forming the single crystal into an oblate spheroid, mechanical working was again ruled out because the total volume of the crystal specimen would be small and the percentage of strained material will therefore be relatively large.

For this reason it was decided to develop a process of removing the metal electrolytically. Earlier this had been partially used in a method whereby the correct shape plus a small

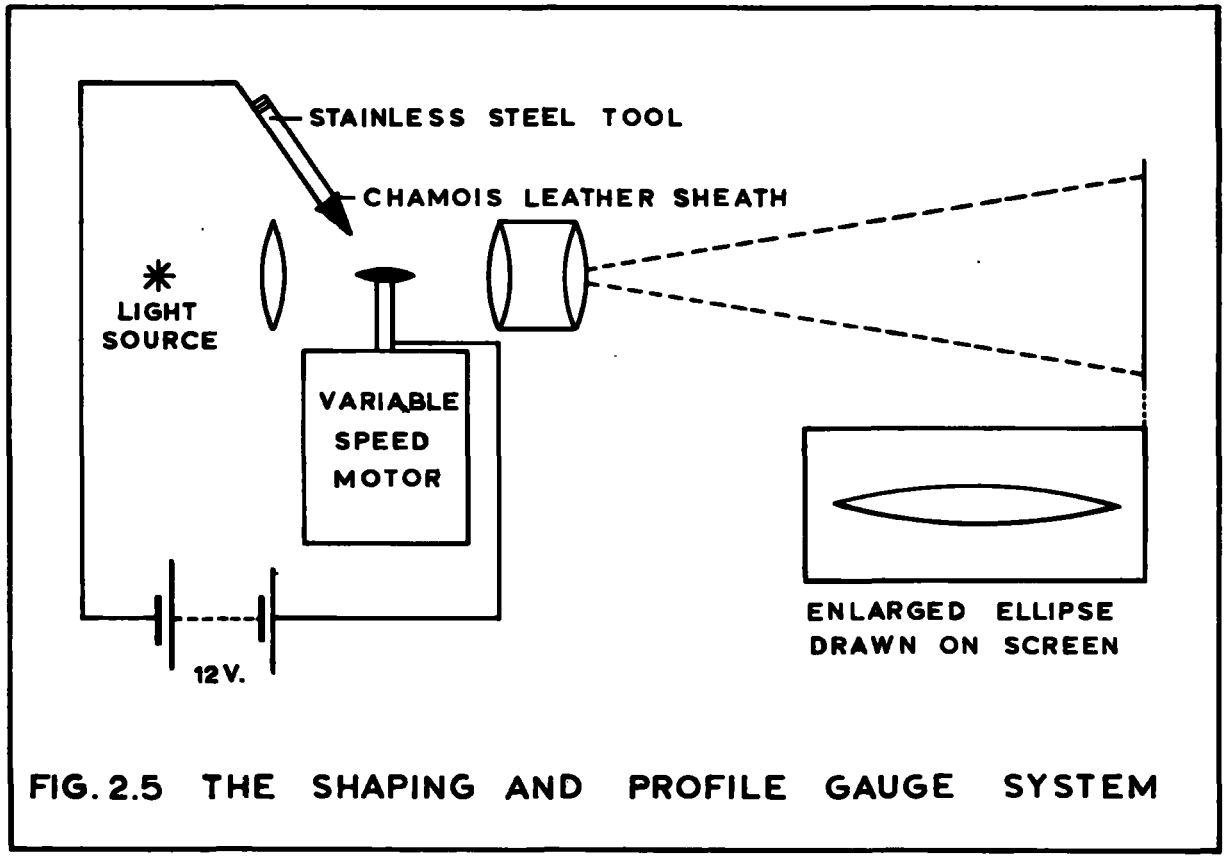

FIG. 2.5 THE SHAPING AND PROFILE GAUGE SYSTEM

thickness, equal to the depth of strain, is formed mechanically and then this thin layer is removed in an electrolytic bath. The method is not entirely satisfactory because the electrolytic removal is not uniform but dependent on the radius of curvature of the surface being removed.

Other ideas have been tried with limited success. Farmer and Glaysher (1953) have used a method in which a jet of electrolyte is directed at a rotating specimen, but here removal of metal is not very precise, and the method can only be applied to relatively large specimens. An attempt (Hunt, 1954) to form prolate ellipsoids by lowering a rod specimen in a bath of electrolyte at a predetermined rate such that an ellipsoid is produced, has also been tried. In this case difficulties arose due to pitting, non - uniform removal and also surface tension in the electrolyte.

In the present method metal is removed electrolytically with a pointed stainless steel tool having a chamois leather sheath dipped in electrolyte surrounding the tip. The system is shown diagrammatically in Fig. 2.5. To obtain the correct ellipsoidal shape, a "profile gauge" arrangement is used similar to that suggested by Mckeehan (1934). The specimen is mounted on the shaft of a variable speed electric motor using Durofix glue, which is mixed with silver dust to provide a contact between the specimen and the shaft. A strong light shines on the specimen and an enlarged silhouette is thrown onto the screen behind by an enlarger lens system of low distortion. Cold air

is blown at the specimen, while it is rotating to keep it cool when the electrolytic action is occurring. The outline of the rotating specimen was actually magnified 40 X at the screen on which is drawn an ellipsoid of the required type. Shaping then consists simply of making the silhouette coincident with the drawn ellipsoid.

Experimentally, a solution of Orthophoshoric Acid of specific gravity 1.35 was found to be the most suitable electrolyte. Several ellipsoids were first produced from polycrystalline material in order to perfect the method. To begin with, accuracy was not particularly good, this being due to a tendency for metal to be removed preferentially from the edges of the disc rather than the middle. However, with care and practice this could be allowed for and it was possible to produce oblate spheroids from disc blanks of polycrystalline material with shape correct to better than 1%.

To shape the actual crystal specimen, the wedge shaped disc, so far obtained, was set up on the profile gauge with the reference surface running true and horizontal as seen by the shadow on the screen. The top was then worked with grade 4/0 emery paper to produce another face parallel with the reference surface giving a perfect square edged disc 0.538 cms. x 0.095 cms.

A cross - section of a disc with these dimensions was then drawn on graph paper enlarged 40 X and within this was drawn an ellipse with semi-axes 0.254 cms. and 0.021 cms. also enlarged 40 X.

The disc was mounted on the motor shaft and made to run coincident with the drawn cross-section, on the screen. The top surface was then worked down to the correct ellipsoidal profile, initially using grade 4/0 emery paper and then the remaining .02/cms. of metal using the electrolytic process. With one surface shaped the specimen was removed from the shaft, inverted and replaced, after the top of the shaft had been slightly machined out to fit the ellipsoidal profile. The specimen was again made to run with the lower ellipsoidal surface coincident with the appropriate surface drawn on the screen and the shaping process repeated for the new top surface. This was accomplished successfully and the specimen was removed from the shaft, now in the shape of an oblate spheroid.

2.6. The Final Shape of the Specimen.

The final shape of the specimen was that of an oblate spheroid with a cross-section which is a true ellipsoid to better than 1%. The diameter of the spheroid was 0.5075 ± .0005cms. and the maximum thickness was .0425 ± .0005 cms. The demagnetizing factor for the specimen was calculated to be $N = 0.76$.

The volume of the specimen was also calculated from the above measurements, giving a value of 5.73×10^{-3} c.c. On checking this figure by using the published value of density, a value some 5% lower than this, was obtained. To remove the discrepancy, the density of the crystal was determined

independently using Archimedes principle. The crystal was weighed in air and then in water of known temperature. The density of the water was obtained from reference tables and the value of density for the crystal was found to be 7.619 ± .012 gms/cc. This gives the volume of the crystal as 5.640 ± .009 cc. The slight difference still existing is caused by the oblate spheroid not having a perfectly ellipsoidal cross-section. In all future measurements, the value of 5.640×10^{-3} cc. will be used as the volume of the specimen.

CHAPTER THREE.

APPARATUS.

CHAPTER THREE.

APPARATUS.

3.1. The Electromagnet.

3.11 Design Considerations.

For the purposes of the present experiment a magnet was required which would be capable of giving fields of the order of 10,000 oersteds which must be uniform over a volume greater than 10^{-2}ccs. at the centre of a pole-gap of 5 cms. The large pole separation is necessary to allow for a Dewar vessel to surround the specimen and apparatus in the gap. The magnet was also required to be freely rotateable and able to be set at any orientation.

These two requirements were most easily satisfied with a small iron - cored electromagnet using high - power excitation coils, the field from which directly augments the flux across the pole - gap. A small magnet was also favoured because of the consequent ease of mobility, both in rotation and in moving the magnet in and out of the experimental position, which was necessary to allow access to the instrument.

The source of power available in the laboratory consisted of two Lister Diesel generators running in series and capable of producing a total power of 44 Kilowatts at 220 amperes. The magnet had therefore to be capable of operating from this supply and dissipating the resultant heat.

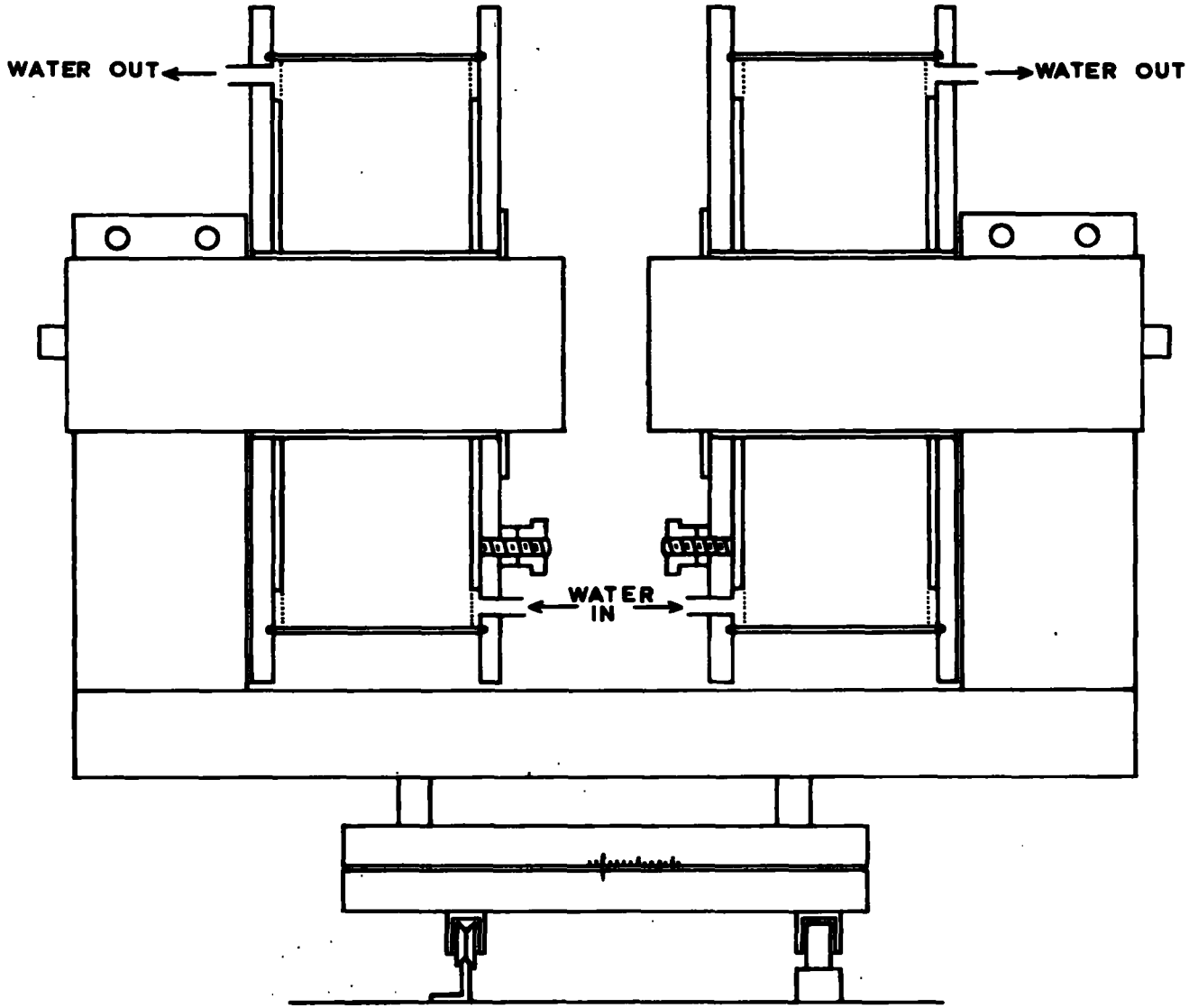

FIG. 3.1 THE ELECTROMAGNET (1/4 SCALE)

3.12. Constructional Details.

The electromagnet finally decided upon was based on a design for a small Weiss - type electromagnet described by Hudson (1949). The general layout of the electromagnet is shown in Fig. 3.1. The yoke and cores are constructed from mild steel throughout. The two end - blocks 6" x 4" x 11" are bolted to the base, 25" x 12" x 2" by four mild steel bolts. The cores, of 10 cms. diameter, are made a running fit in the end - blocks and are clamped in the appropriate position by closing the split top of each block with two heavy bolts.

The coil cases were rolled from 1/8" sheet brass and the end plates were turned from 5/8" Tufnol sheet. Each coil contains about 580 turns of 0.25" x 0.08" resin insulated copper strip which is wound on in 34 layers with 17 turns/layer. The layers are separated by strips of 1/4" x 1/16" Tufnol and these are spaced out at intervals of about 1" around the circumference of each layer. In winding, the spacers were held in place against the preceding layer by a piece of curtain wire which was unhooked when sufficient turns were on to support the spacers independently. The last layer, as well as having the normal spacers, is insulated from the brass case by Melinex polyester film. The layers are spaced off from the end plates by 16.1/4" x 1/4" strips of Tufnol, fixed radially to each endplate, and extending from the central Tufnol drum to within 1" of the brass casing. The endplates of each coil are held together by six bolts, spaced at 60^{o} intervals round their circumference.

These are tightened, drawing the rims of the brass case on to an 'O' ring seated in a groove in each plate. Another smaller 'O' ring is located at the join between the endplates and the central Tufnol cylinder, and an external Dural plate is drawn onto it to form a seal.

The coils are water cooled, the water being led into each coil at the bottom of the inner endplate and out at the top of the outer endplate. The water is thus distributed round the annular channel formed between the outer layers of the windings and the ends of the 1/4" x 1/4" strips; these then guide the water down to the centre of the coil producing what can be imagined as a sheet of water which then moves horizontally through the network of layers and spacers. On reaching the outer endplate the water collects in the reverse manner and is withdrawn from the top of the annular channel.

The layer winding has the advantage of giving a high space factor ($\sim$ 0.5) and therefore a small size, which is impossible with the tubular type of winding using internal cooling. This method also has the advantage of giving a low resistance to coolant flow.

Rotation of the magnet was achieved by mounting on a ring of ball-bearings, which run in a groove cut in two similar circular plates of steel. A scale of 360^{o} is engraved on the edge of the rotating plate and this moves against a marker fixed to the statuary plate. The magnet moves in and out of the experimental position on a short piece of railway track.

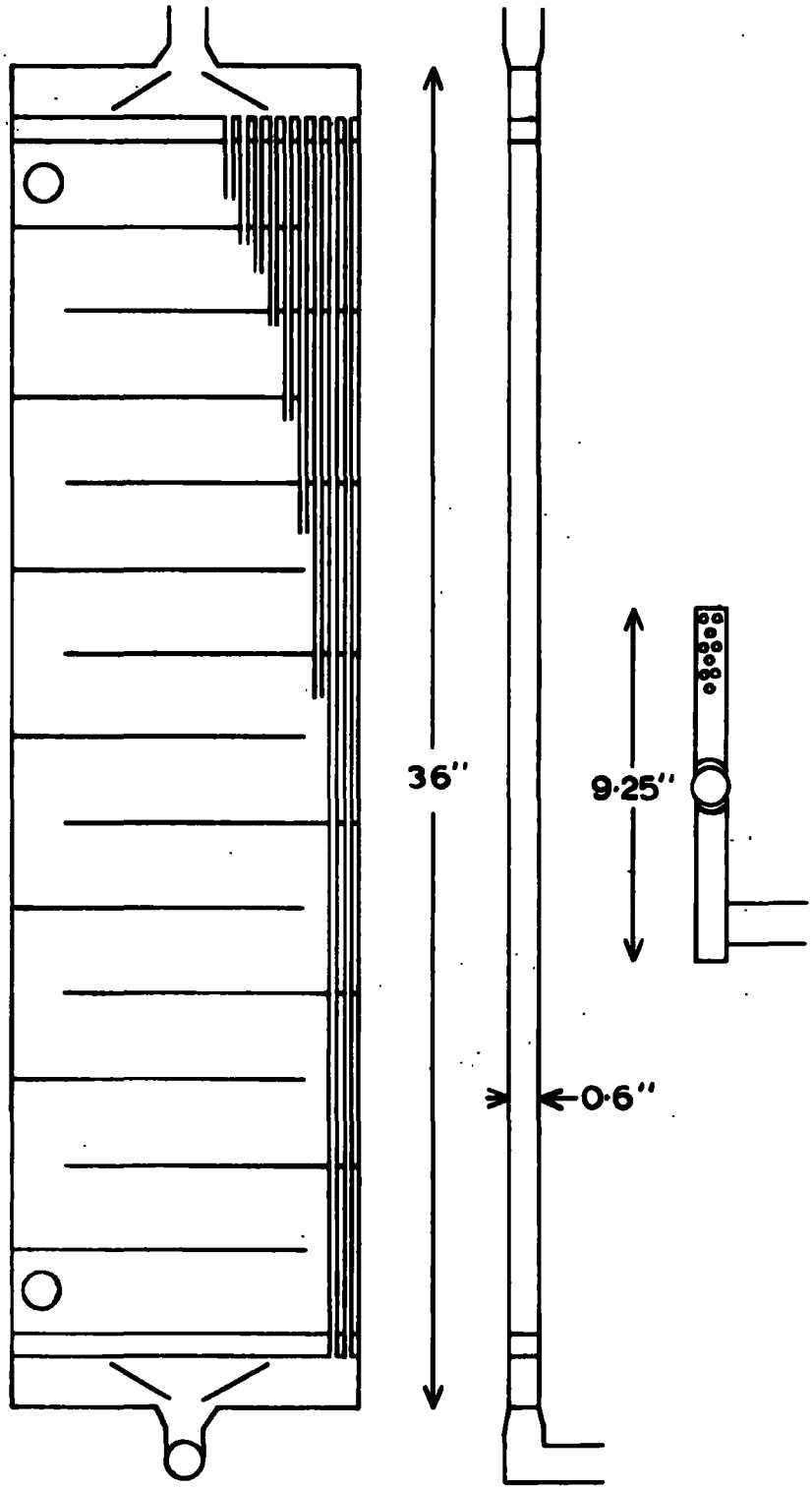

FIG. 3.2 THE HEAT EXCHANGER

It is mounted on three rollers, two of these being grooved while the third is flat. The grooved rollers run on a knife - edge rail and thus provide lateral location for the magnet. With a stop set on the rails, the magnet can be accurately moved out and returned to the experimental position, when access is required to the lower suspension and specimen holder.

3.13. The Heat Exchanger.

Since, by virtue of the method of winding, there are existing high potential differences between points which are only separated by thin layers of insulation and coolant, it was considered necessary to use circulating distilled water for the coolant. Ordinary tap water has a relatively high electrical conductivity and thus electrolysis and subsequent corrosion would be caused if this were used.

The surface area of winding exposed to the coolant, in each coil, is 5.7×10^4 sq. cms. On maximum power this is dissipating 22 Kilowatts and hence the heat transferred will be 0.4 Watts/ sq. cm.

The pump available in the laboratory was capable of giving 20 gallons/minute against a pressure of 1 atmosphere. A cross-section of the heat exchanger is shown diagrammatically in Fig. 3.2. It was designed with a view to compactness as well as efficiency. The system embodies both cross-flow and counter-flow principles to give a more efficient heat - transfer. There are 62 tubes running from top to bottom 3/16" O.D., 1/8" I.D. giving a total area of 8.4×10^3 sq. cms. exposed to

the cooling mains water. The total cross - sectional area available for flow of distilled water was made just less than the area of the delivery pipe to ensure that all pipes are completely filled, which is necessary for maximum heat - transfer. There are 13 baffles down the length of the exchanger which cause the cooling mains water to traverse the pipes 14 times in a state of great turbulence.

With the heat being transferred at 0.4 watts/sq. cm. and taking the thermal conductivity of the resinous insulation ($\sim$ .005") at .002 watts/sq. cm./^{o}C, the temperature drop across the insulation is $\sim$ 3^{o}C. When the magnet is dissipating the full 44 Kilowatts, the exchanger maintains the temperature of the distilled water, being fed into the magnet at 27^{o}C. The outlet is at 38^{o}C, giving a total rise of 11^{o}C. Estimating the temperature drop at the surface of the windings to be of the order of 10^{o}C, the temperature of the copper will be nowhere greater than 50^{o}C. These temperatures were maintained for a mains flow of 11 gallons/minute ($\sim$ 15^{o}C inlet and $\sim$27^{o}C outlet) through the exchanger.

3.14. Performance.

Each coil contains approximately 580 turns, thus at the maximum current of 220 amperes, there exists a Magneto - motive force of 320,000 ampere turns.

Field measurements were made using a search coil and fluxmeter. The fluxmeter was previously calibrated using a long solenoid of known turns / unit length and a sub - standard

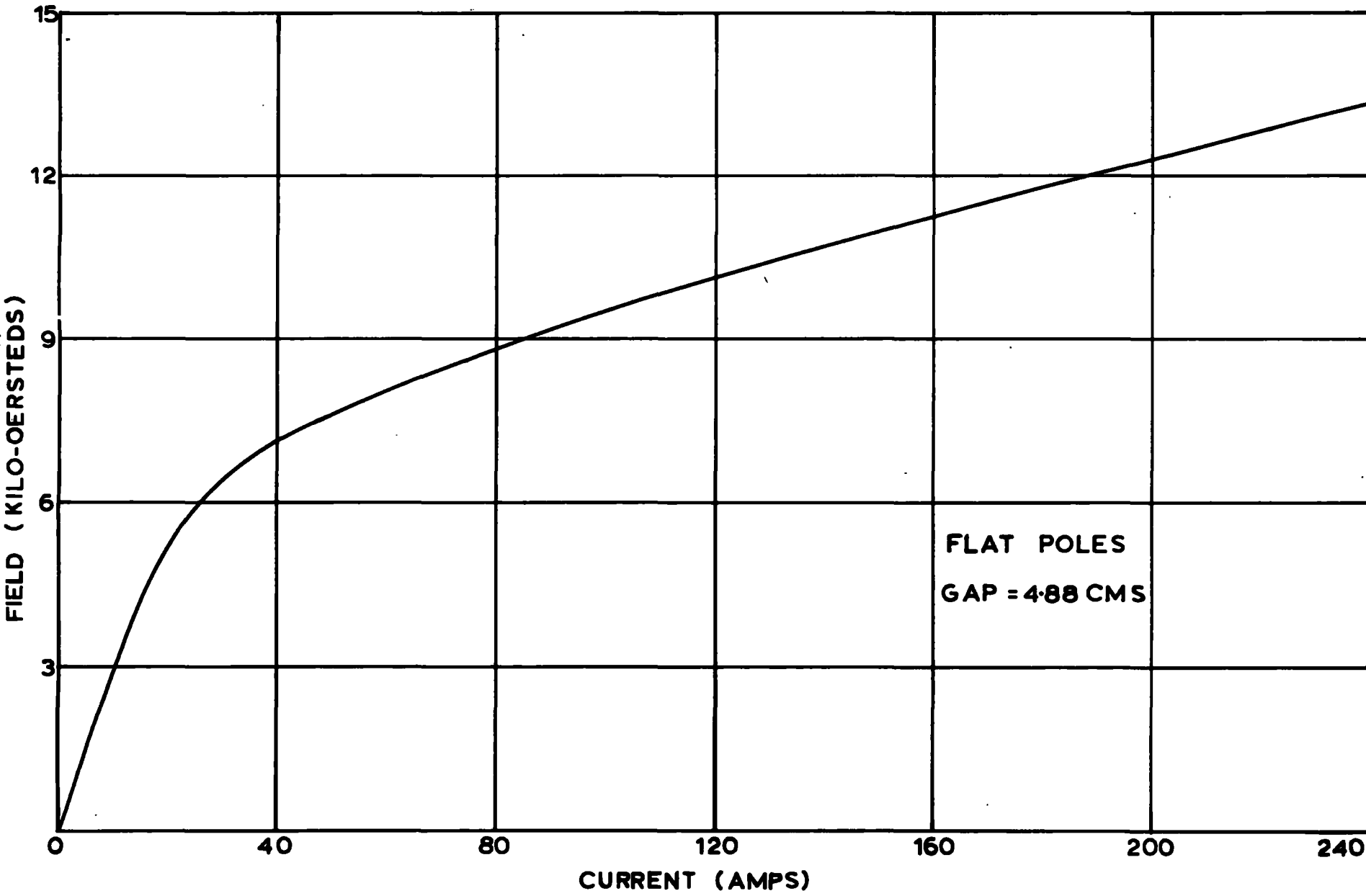

FIG. 3.3 VARIATION OF MAGNETIC FIELD WITH CURRENT

ammeter to read current values. The instrument was found to give 7098 Maxwell turns / cm. on a lamp and scale at 1 metre distant.

With the flat pole - tips of 10 cms. diameter at a gap of 4.88 cm. the maximum field obtainable at 220 amperes was 12,800 oersteds. Fig. 3.3. shows the complete calibration curve. This field was uniform to within $\pm \frac{1}{2}\%$ over a volume of more than 3 cubic cms. which was more than adequate for the purposes of this experiment.

3.2. The Torque Magnetometer.

3.21. Earlier Apparatus.

Designs of torque magnetometers have previously been described by Williams (1937), Tarasov (1939) and others. They consist simply of suspending the single crystal in a high magnetic field by means of a torsion wire and the torque acting on the crystal is then obtained from the angular twist induced in the wire. Values of the torque for different directions of magnetization in the crystal are obtained by either rotating the specimen or the magnet. Since the torsional constants of the wire are needed to convert to absolute units, the method is not readily adaptable when temperature variations are required, because of the temperature dependence of these constants. Also, it would seem extreme care would be necessary to obtain accurate results with such a system.

Croft, Donahoe and Love (1955) have described a torsional magnetic susceptibility balance, for study of the de Haas - van

Alphen effect, which is capable of measuring small values of torque accurately. In their apparatus, the specimen is suspended from the coil of an ordinary moving - coil galvanometer and values of torque are obtained from the amount of current fed back to the coil to maintain it in an equilibrium position. This current is directly proportional to the torque and the feed - back is done automatically with a photocell amplifier system. With this system the suspension does not move appreciably and thus torsional constants in the suspending wires can be neglected. Measurement of torque is also made considerably simpler since it is only necessary to calibrate the counter - torque coil appropriately.

This method was further developed by Penoyer (1956) and Pearson and Guildford (1957) for measuring much larger values of torque, as a function of crystal orientation rather than field strength. In this system the torque curves were plotted automatically with a pen recorder, which simultaneously recorded field orientation against feed - back current.

For the purposes of this experiment it was decided to build a torque magnetometer based on the designs of Penoyer and Pearson utilizing only a system of automatic balancing. It was considered unnecessary to introduce the extra complexity of automatic recording, when measurements on large numbers of different specimens were not required.

3.22. General Considerations.

Measurements were to be carried out on a single crystal

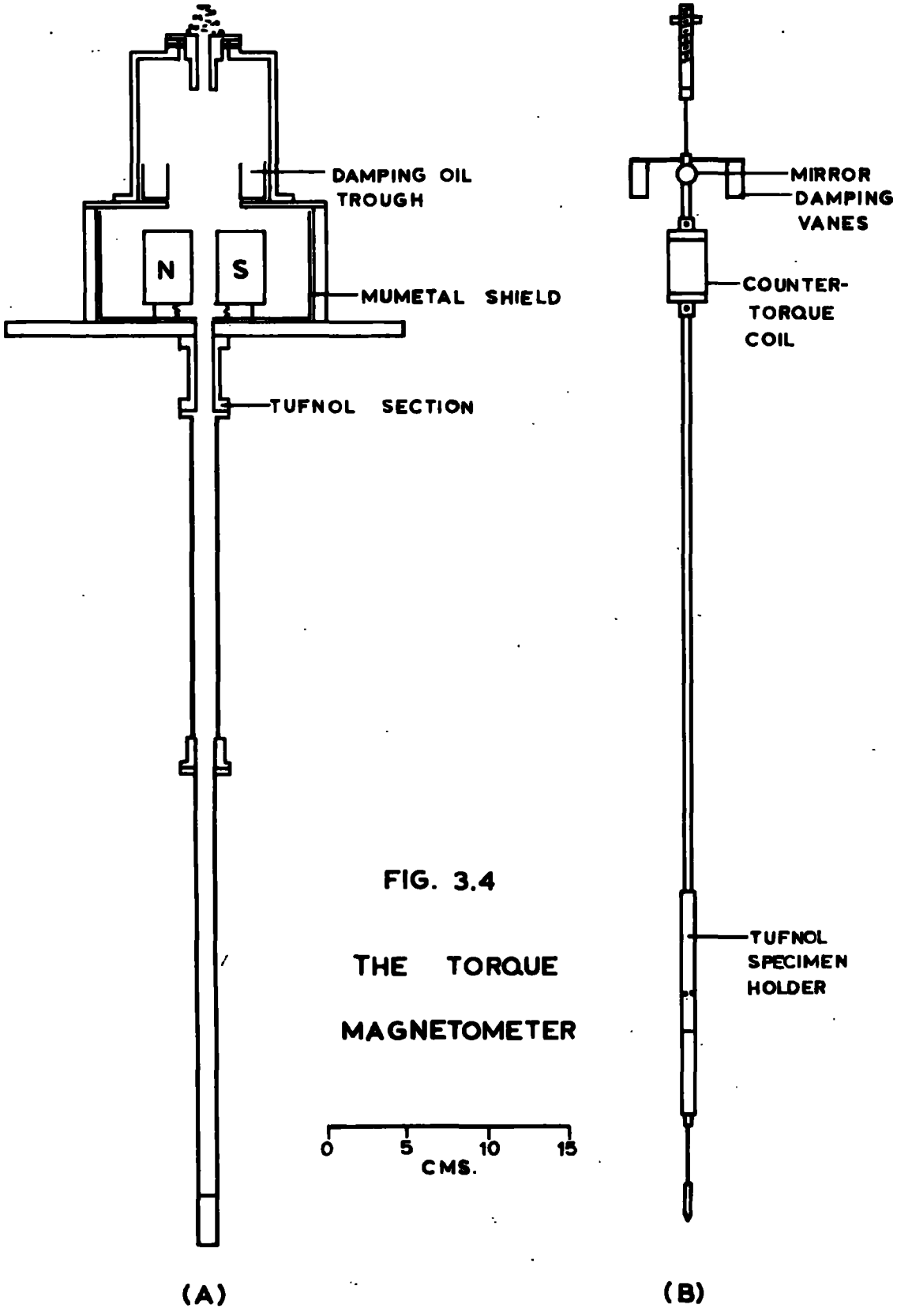

FIG. 3.4

THE TORQUE MAGNETOMETER

oblate spheroid of diameter .508 cms. and known orientation. The magnitude of the torque expected was not known. Using cobalt, also hexagonal in structure, as a possible indication of what might be expected, it was thought necessary to make the instrument initially capable of measuring torques of up to 10^7 ergs/cc.

The apparatus was also required to measure values of torque over the temperature range from 300°K to 20°K. As already stated, since the apparatus is a null reading instrument, movement of the suspension is negligible and therefore changes in the values of torsional constants of the suspending ligaments can be neglected.

The ultimate accuracy of the anisotropy constants, derived from measured torque curves, was aimed at being 5%.

3.23. Instrument Body.

A cross - sectional diagram of the instrument is shown in Fig. 3.4a. The small permanent magnet used for the basis of the counter - balancing system was adapted from a 6" G.E.C. portable moving coil ammeter. With a soft iron core fixed in the gap it produces a radial field of $\sim$ 300 oersteds.

The magnet is mounted on a 5/8" circular Dural plate of 12" diameter, which forms a base for the whole instrument. A box, built up from Dural sheet, surrounds the balancing magnet and also supports the brass casing which provides a support for the top ligament of the suspension. Inside this box is

another of Mumetal closed on five sides and with only four small holes drilled in it to permit entry of the suspension and location of the magnet. This provides a magnetic shield to prevent disturbance of the balancing system by the large stray field from the electromagnet.

Three adjustable studs, locating on three brass plates fixed to a massive teak board, form a mount for the base thus giving the instrument a means of levelling and of producing small changes of the position of the specimen in the gap.

The upper brass casing, 4" in diameter and 3.1/2" high, carries the upper ligament support. This support consists of a circular brass guide in which a steel rod slides smoothly. At the end of the steel rod a small brass cap enables the ligament to be attached with soft solder. The rod is held off from the guide by a spring, which induces a constant tension in the ligaments and absorbs the small changes in length of the lower support tube when undergoing changes in temperature. The guide itself floats freely on accurately machined shoulders, which rest on the lip of the large hole at the top of the brass case. Location of the guide is then obtained by four Allen grub screws which project through the lip and bear on the edge of the guide, thus acting rather like a four - jaw chuck. This system enables the suspension to be accurately centred in the gap of the balancing magnet.

In the lower part of the case a circular trough is fitted with a gap in one side opposite the window. This trough holds

the suspension damping oil and the gap allows for the passage of the light beam in and out.

The lower part of the instrument consists only of a tube which projects down into the electromagnet gap and carries the lower ligament of the suspension. It is constructed in three sections; the lower two sections are of straight 3/4" diameter thin wall brass tubing, the bottom section being removable for access to the specimen. Brass was particularly suitable for this as its relatively high heat capacity and thermal conductivity provide a uniform temperature jacket over a large region near the specimen. The top section is made of Tufnol and is designed to act as a thermal barrier between the upper part of the instrument and the lower tube, which is normally below room temperature.

A small brass slug, to which the lower ligament is attached, is held in place by a small grub screw. Small corrections in the vertical position of the suspension can be made by adjusting the position of this slug. The lower section is sealed by a small brass cap which seats onto an "O" ring.

Permanent joints in the body were made gas - tight with a non - setting form of jointing paste. Those which are removable for access to the suspension are sealed with either rubber or polythene gaskets in conjunction with Apiezon - L vacuum grease.

3.24. <u>The Suspension.</u>

The suspending ligaments are from 2.5 cm. lengths

of .005" diameter Beryllium - Copper wire supplied by Johnson Matthey Ltd. Attachment of the ligaments to the suspension and body was in all cases by soft soldering to brass which was extremely convenient. The major part of the suspension is made from 1/4" diameter aluminium rod, The short top section and the longer bottom section both push into the end - blocks of the counter - torque coil and are located with grub screws.

On the short top section are mounted the aluminised galvanometer mirror, 1.5 cm. diameter and 100 cms. focal length together with the two damping vanes.

The coil former is made up from brass. To enable it to be wound the end - blocks are removable. The soft iron core of the balancing magnet is inserted during construction and true alignment is obtained by carrying out the final assembly between centres on a lathe.

Prior to winding the former was given several coats of Shellac to form a layer of insulation on the brass. In the case of the 100 turn coil, the winding was from No. 40 gauge enamelled copper wire. This was wound on in a double strand to produce two coils as nearly identical as possible with respect to their electromagnetic properties. The method of calibration does not require that the cross - sectional area of the coil be known.

Current is led in and out of the coil when it is set up in the instrument via large loops of 40 gauge wire anchored close to the centre of the suspension. Since the instrument

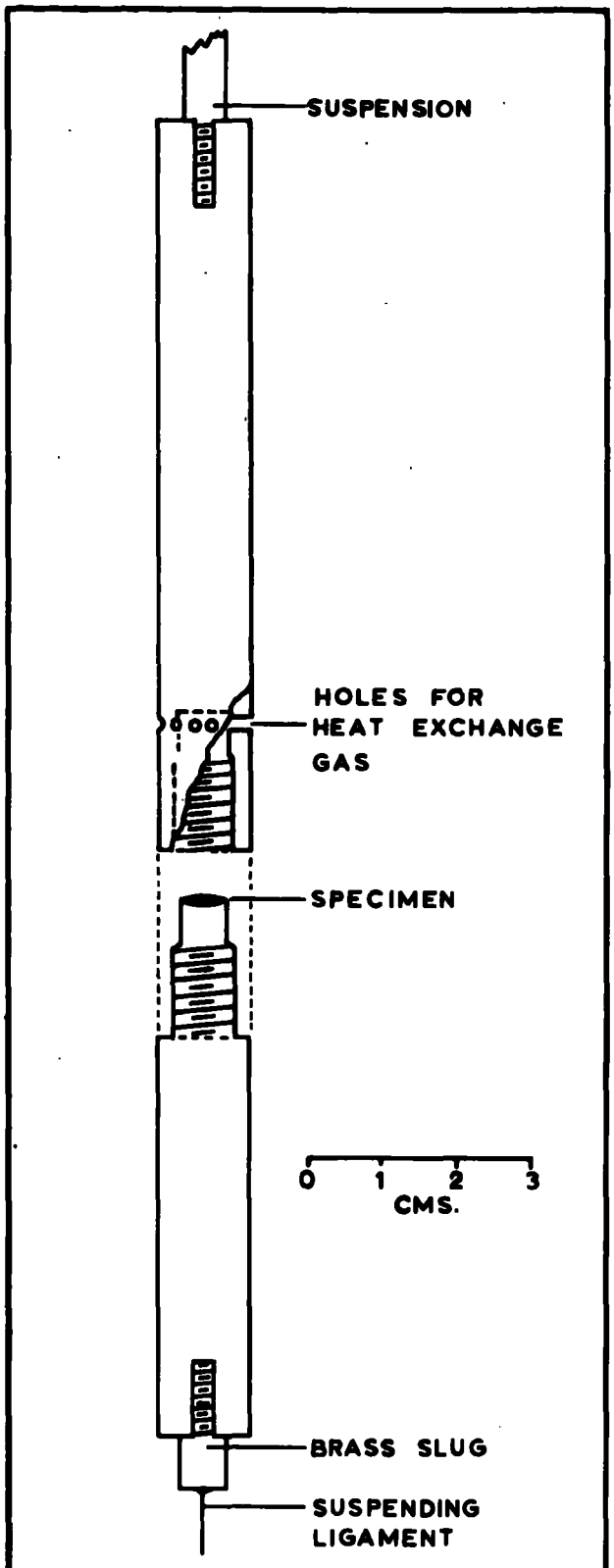

FIG. 3.5
THE SPECIMEN HOLDER

is null reading, the very small extra torques that these might apply to the suspension can be ignored.

The lowest section of the suspension is formed of the Tufnol specimen holder. The holder is screwed onto the lower aluminium rod and has a small brass stud at its bottom end for attachment to the lower ligament.

3.25. Specimen Holder and Mounting.

The specimen holder is turned from 1/2" diameter Tufnol rod, details of which are given in Fig. 3.5. Tufnol was chosen as it was considered preferable not to have anything metallic near the specimen which might give rise to spurious torques arising from ferromagnetic impurities and eddy currents. It is made in two halves, the lower half screwing into the upper, such that the specimen is situated in a small chamber with circular vent holes around the circumference. These allow free passage of gas around the specimen to produce an effective heat exchange.

Great difficulty was encountered in finding a satisfactory method of mounting the specimen in its holder. Four main problems existed: a) With the experiment to be performed over a wide range of temperature, the specimen changes size owing to thermal expansion: b) Similar changes in size will also result from a magnetostrictive effect: c) Gadolinium rapidly forms an oxide and nitride layer on its surface, therfore making it very difficult to obtain a reliable bond with any form of adhesive: d) The mount must have a high - torsional rigidity but must not constrain the crystal such as to introduce

undue strains.

Any type of mechanical location must necessarily introduce strain, therefore a form of adhesive would be preferred. The first idea was to have the specimen glued over a small region near the centre of the disc thus allowing free movement over most of its area. However, experiments with Durofix, Collodion, Araldite, Shellac and Bostik all proved unsatisfactory, in nearly every case the bond between the specimen and the glue failed when subjected to temperature changes. Bostik was found to be the most satisfactory, but this had the disadvantage of becoming plastic at $-15^{\circ}C/-20^{\circ}C$ and therefore did not positively locate the specimen.

The problem was finally solved by using Sellotape. A shallow depression was made in the top of the Tufnol mount to the same contour as the specimen. The specimen was placed in the depression and then covered with a piece of Sellotape which was stuck down all round the sides. This was then anchored with a further strip of Sellotape stuck round circumferentially. Tests showed that the mount was unaffected by repeated immersions in liquid air and also, the strain introduced by the Sellotape must be of negligible proportions because of the large difference in the rigidity moduli. There was possibly an extremely small amount of creep near the room - temperature, but it would be negligible because of the low torques in this region. Thus this seemingly unlikely method of mounting proved most satisfactory under working conditions.

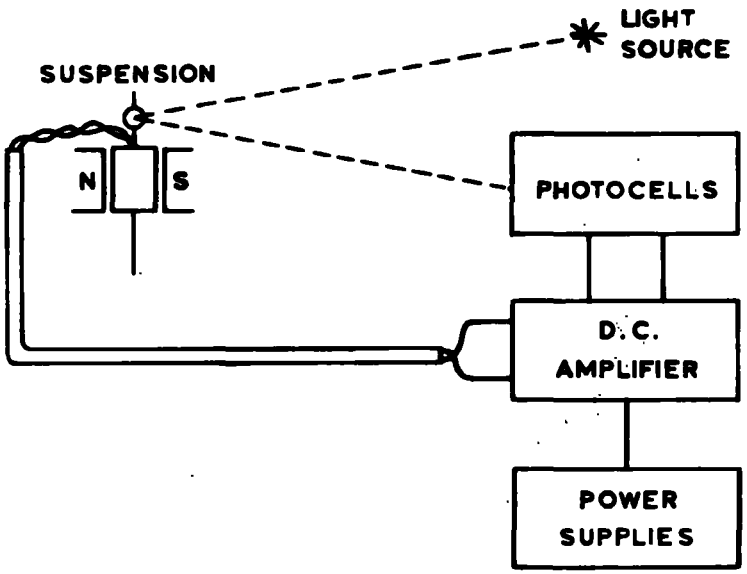

FIG. 3.6

BLOCK DIAGRAM OF THE AUTOMATIC BALANCING SYSTEM

3.3. The Automatic Balancing Equipment.

3.31. General Description.

The method of using a photocell amplifier feed back system for automatic balancing has become a somewhat standard technique. How the system works is shown diagrammatically in Fig. 3.6. A strong source of light is set up to shine on the galvonometer mirror and this then focuses the beam back on to a double photocell unit. When a torque acts on the specimen under test, the suspension, balancing coil and attached galvonometer mirror are caused to rotate. The mirror rotation then produces an unbalance in the amount of reflected light falling on each photocell, and consequently the photocell conduction currents are made unequal. This inequality is then amplified by means of a direct current amplifier and fed back degeneratively to the balancing coil, restoring it to its equilibrium position.

In actual fact the suspension must move in order to produce the signal, but for maximum counter - torque values this movement is less than 0.3^{o} and since this is proportional to the torque being applied a correction can be made.

Harrison (1955) has calculated that, under certain circumstances, magneto - torsional systems will become unstable unless:-

$$\tau > V \frac{dL}{d\theta}$$

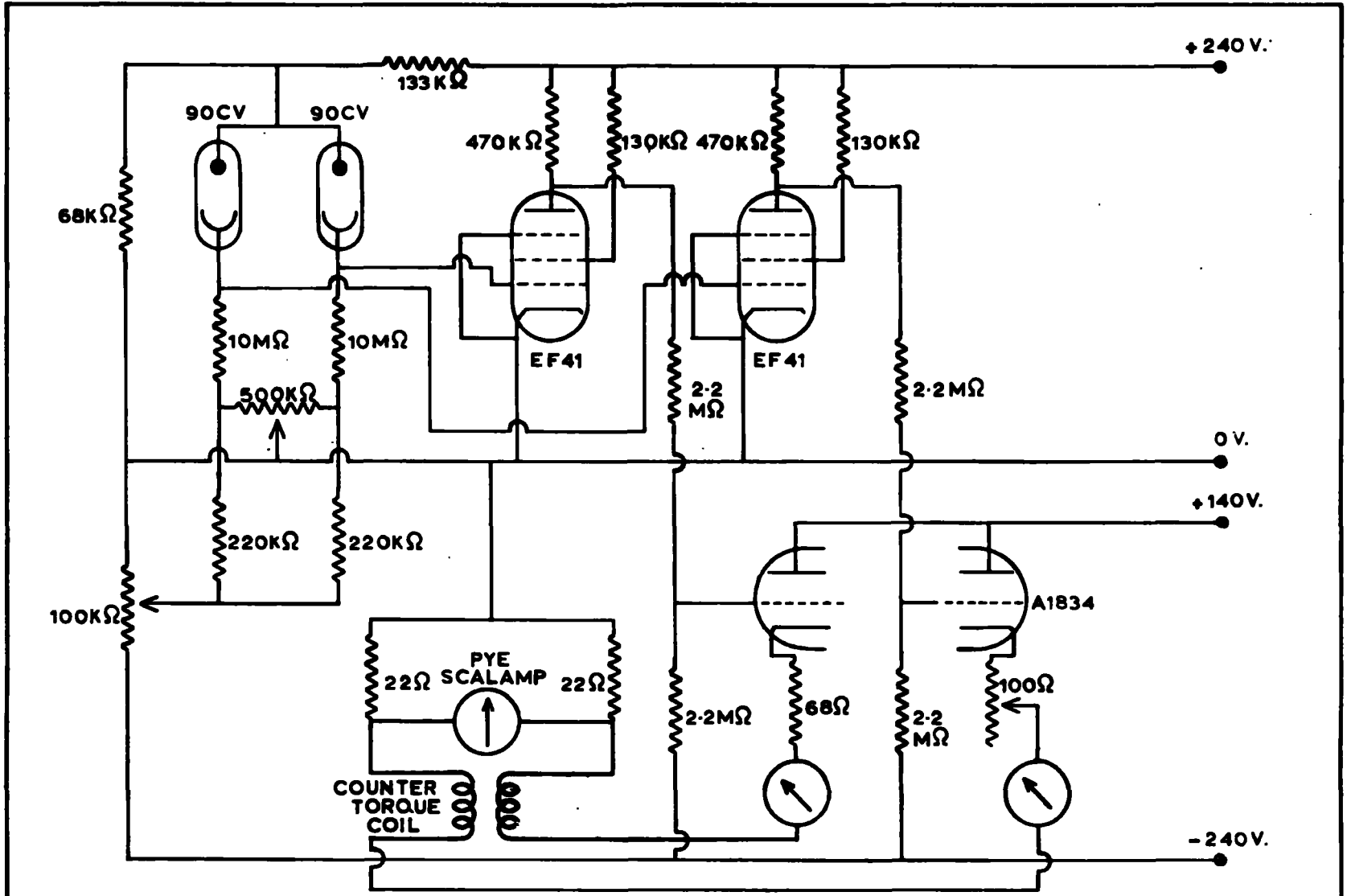

FIG. 3.7 CIRCUIT DIAGRAM OF THE PHOTOCELL AMPLIFIER

where τ = torsion constant of suspension

$\frac{dL}{d\theta}$ = maximum positive slope of torque curve

V = volume of the specimen.

These arguments do not apply to the present system, since the automatic balancing, with negligible movement of the suspension, effectively makes the torsional constant become very large.

3.32. The Photocell Amplifier.

A circuit diagram of the photocell amplifier is shown in Fig. 3.7. Several types of amplifier were initially tried but the one described below proved to be most satisfactory. It is capable of feeding back currents of up to 120 milliamps

The light source consists of a 150W. projector lamp (Atlas Truflector A1/184) housed in an adapted galvonometer lamp housing which is cooled with a small fan. The parallel light beam in them reflected and focussed by the suspension mirror onto a 90° mirror arrangement which splits the beam into two equal halves. Two Mullard 90 CV vacuum photocells, which constitute the basic unit, are situated either side of this mirror arrangement in a box which permits only light reflected from the suspension mirror to reach the photocells. A movement of the beam to either side then throws more or less light onto one of the photocells. (see Fig. 3.8).

An anode potential of 100 volts is applied to the photocells. A biasing system is incorporated which allows the EF 41's to be brought almost to cut - off, under conditions of

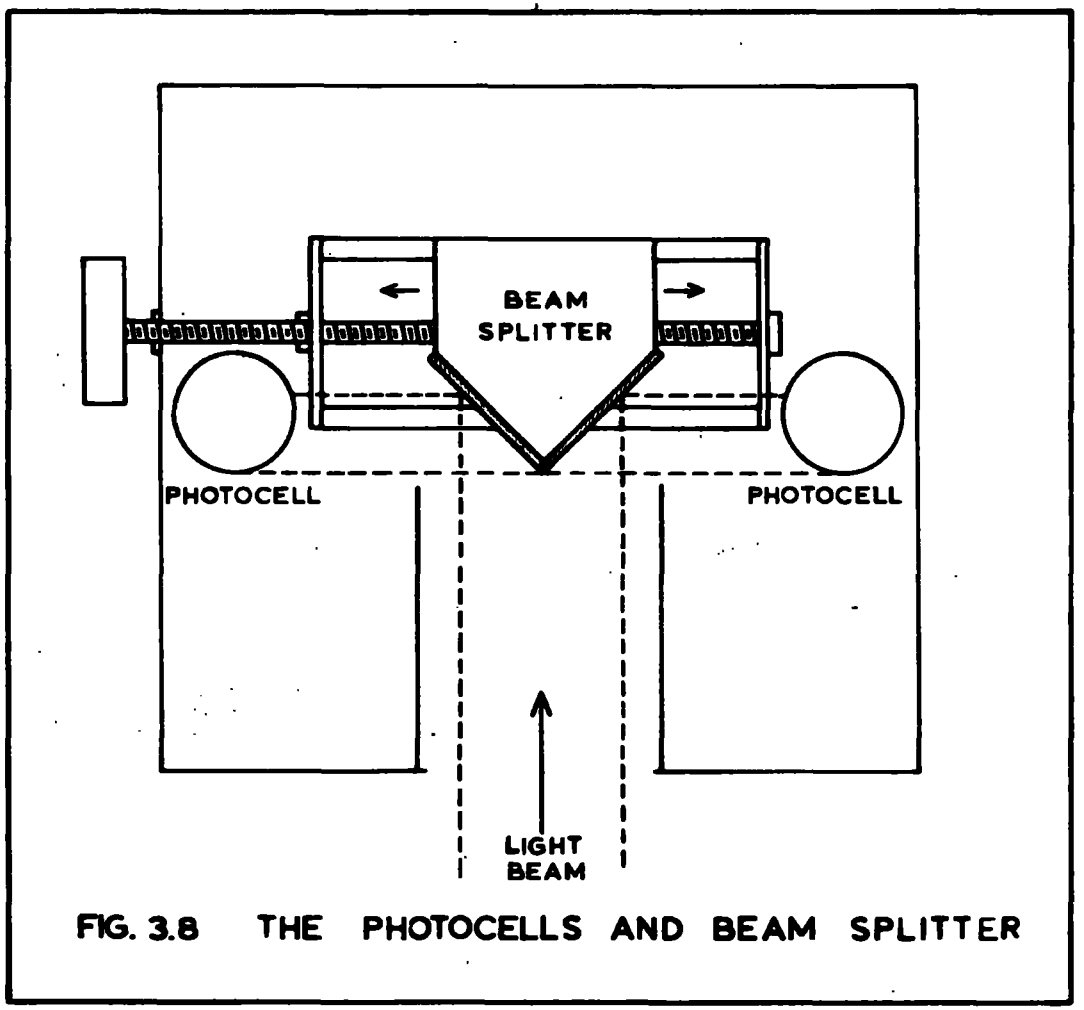

FIG. 3.8 THE PHOTOCELLS AND BEAM SPLITTER

no signal. When under operating conditions with the photocells conducting, the EF 41's are also both conducting.

To illustrate the working process, suppose a larger light signal is applied to one of the photocells, the conduction current in this photocell will rise. The voltage developed across the 10 megohms resistor then drives the grid of the appropriate EF 41 more positive. The pentode consequently begins to conduct more and, as a result, its anode potential drops. Therefore the grid of the A1834 goes more negative, by virtue of the potentiometer across the negative H.T. line, and begins to cut off more current. The opposite process will be occurring with the other photocell causing the appropriate half of the A1834 to conduct more. The counter - torque coil system, which has one coil in each cathode line of the double - triode, then deflects degeneratively according to the difference in currents so as to restore equilibrium conditions.

Precision resistors ($\pm \frac{1}{2}\%$) are used throughout the circuit. Two controls are incorporated for zeroing purposes. A 500 KΩ potentiometer dividing the cathode resistors of the photocells provides a coarse adjustment and a variable 100 ohm resistance in one side of the double - triode cathode lines gives a fine adjustment.

Currents in each of the coils are monitored by two 0 - 100 milliammeters. Actual recording of the difference current producing the counter - balancing torque is achieved by comparing the voltages produced across two standard 22 ohm

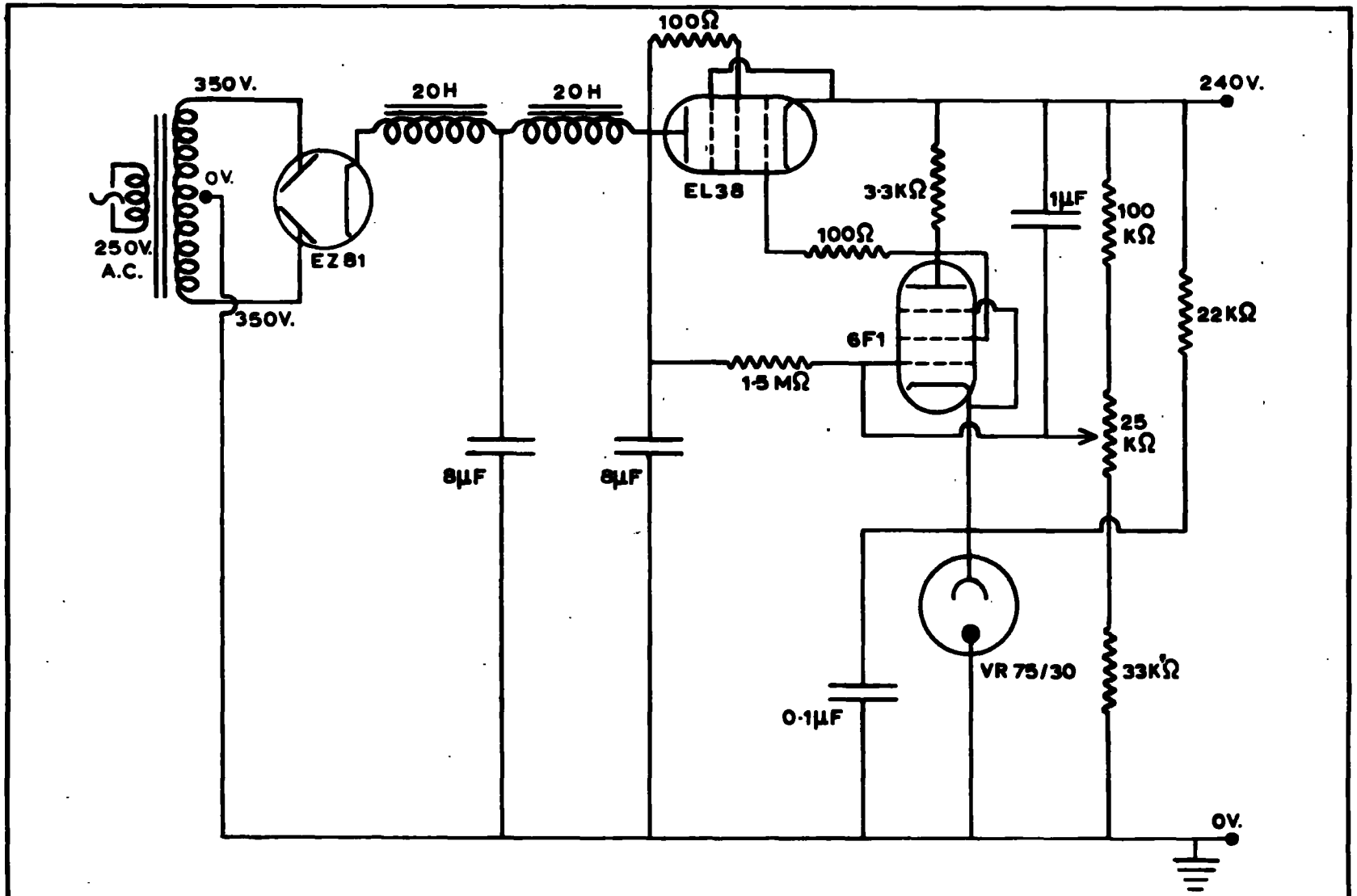

FIG. 3.9 CIRCUIT DIAGRAM OF THE STABILIZED POWER UNIT

resistors ($\pm \frac{1}{2}\%$). A Pye Scalamp galvanometer has been used to indicate the difference in potential. This was calibrated directly in terms of actual difference currents and three ranges of sensitivity were employed - 1.28, 0.80 and 0.20 milliamps/millimetre. Full scale deflection on either side for the highest range is equivalent to a torque of 7.3×10^4 dyne cms. for the 100 turn coil.

3.33. The Power Supplies.

A stabilized H.T. power unit was required to operate the amplifier stages of the photocell amplifier. The negative H.T. supply was obtained by strapping a similar unit to the earth - line of the positive side.

A circuit diagram of the stabilized H.T. unit is shown in Fig. 3.9. Rectification of the A.C. mains is performed by an EZ81, coupled in the usual manner as a full - wave rectifier, and followed by a conventional choke - capacity filter for good smoothing.

The stabilizing circuit is designed to compensate for changes in output voltage and also changes resulting from variations in the mains supply voltage. It is of the conventional series - parallel type, in which the impedance of a triode in series with the load is controlled by a high gain pentode, connected in parallel with the load. This operates as follows; the VR75/30 voltage stabilizer provides a reference voltage for the cathode of the 6F1. Variations of the output voltage are transmitted, via the 100KΩ - 25KΩ - 33KΩ resistor chain, to

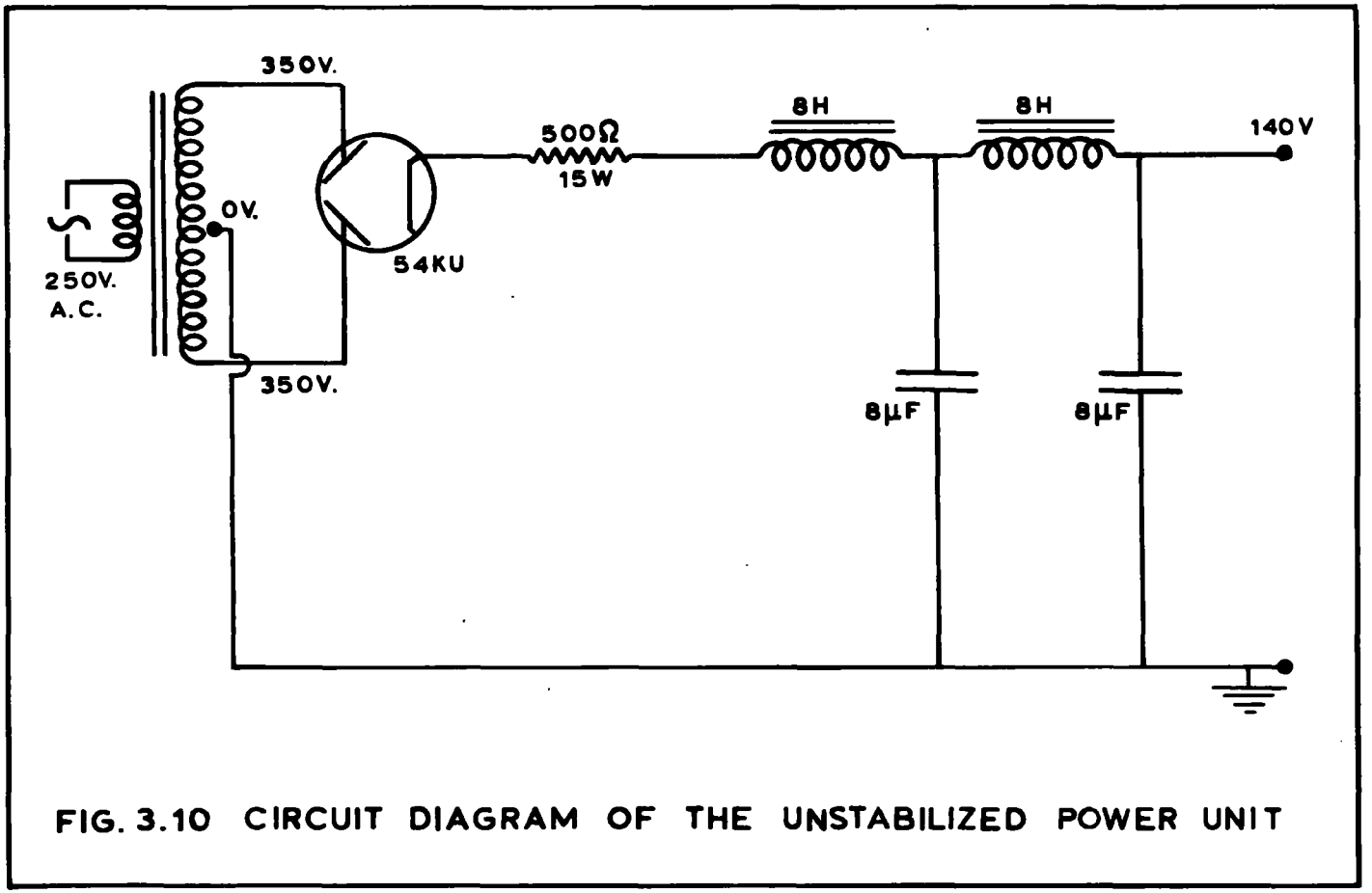

FIG. 3.10 CIRCUIT DIAGRAM OF THE UNSTABILIZED POWER UNIT

the grid of this valve, which then amplifies them. The resultant change in anode potential then appropriately biases the low impedance EL38 in such a way as to oppose the change in voltage. Changes in the input voltage are similarly corrected through the 1.5 MΩ -25KΩ - 33KΩ resistor chain, which makes the 6F1 grid fall in potential with drop in input voltage. The VR75/30 is actually designed to operate at about 10 milliamps and as this is much too large for the 6F1 (~ 1 milliamps) a 22K resistor is placed in parallel with the pentode. Values of the resistor chains, were determined by testing, with the circuit under operating conditions.

Testing showed that the unit had a stable output voltage of 240 volts to within ± 1 volt. for changes of output current between 5 and 15 milliamps, and for variations of applied mains input voltage from 225 volts to 275 volts.

Stabilization of the power unit supplying H.T. to the double - triode was not necessary since slight variations in H.T. voltage will not effect any unbalance in the system. The unit is therefore a straightforward full - wave rectifier (54 KU) followed by the normal choke - capacity filter unit for smoothing purposes. The circuit diagram is shown in Fig. 3.10. A 500Ω 15 Watt resistor is placed in series with the H.T. to bring the output to 140 volts at a current of 180 milliamps.

3.4. Temperature Control and Measurement.

3.41. General Considerations.

Values of the anisotropy constants were required for

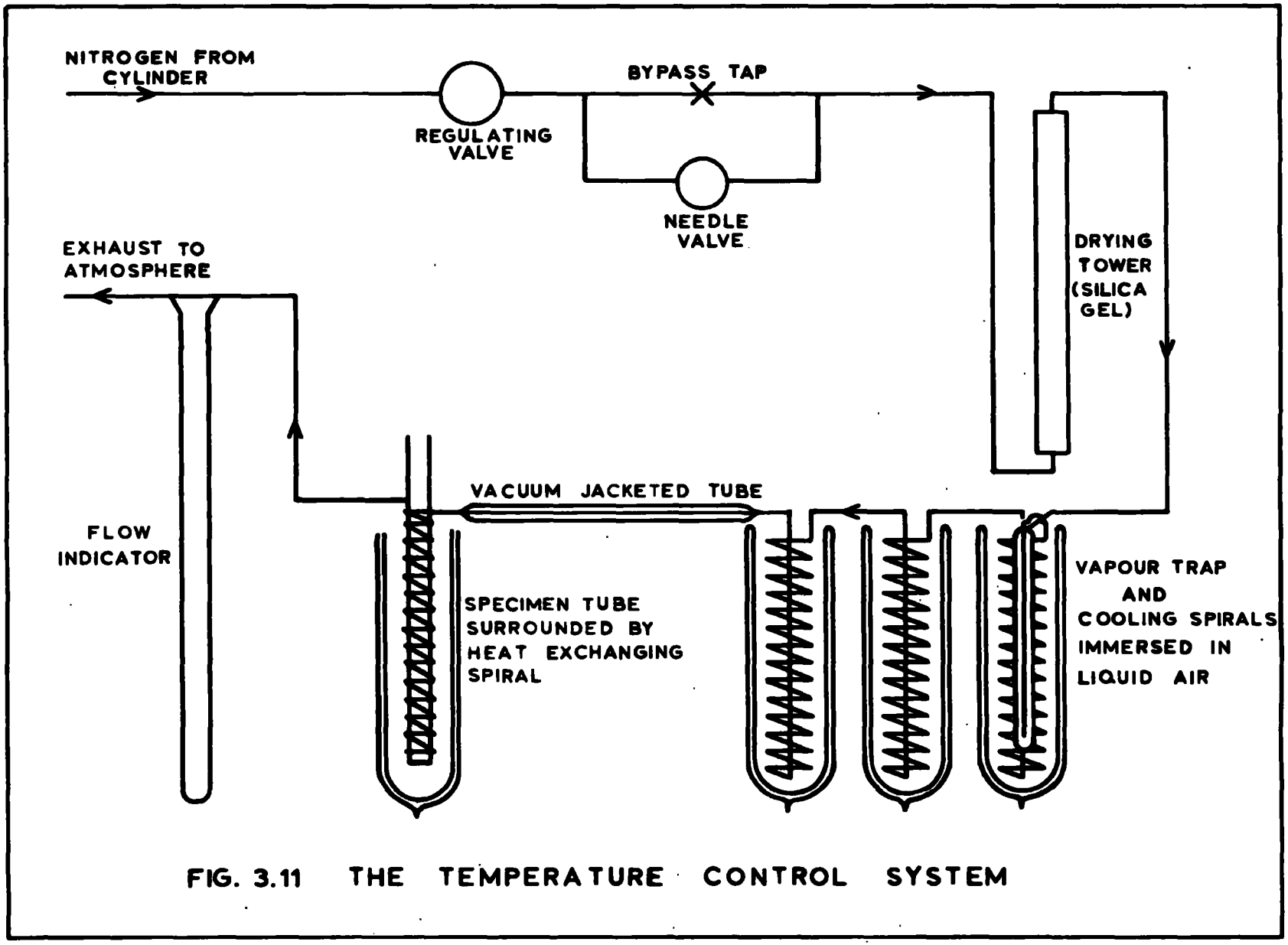

FIG. 3.11 THE TEMPERATURE CONTROL SYSTEM

a range of temperatures from 300°K down to 20°K. Temperatures were required to be constant for periods of about 10 minutes, the time necessary to take a set of measurements at a particular temperature. This comparatively long period of time prohibited use of the method by which readings are taken while the apparatus slowly warms up to room temperature, having been previously cooled with liquid nitrogen or hydrogen. The use of freezing mixtures was also considered but the total number of temperature points available with this system was rather limited, apart from the difficulty of obtaining some of the compounds.

For these reasons it was decided to use a system similar to that used by Pearson (1959). In this system, cooled gas is passed through a heat - exchanger surrounding the specimen and various temperatures are obtained by regulating the rate of flow of gas. The apparatus then simply arrives at an equilibrium temperature which is determined by the equalization of the heat leak into the apparatus and the amount of "cold" introduced by the gas.

Temperature measurement is accomplished with a copper constantan thermocouple placed close to the specimen.

3.42. The Temperature Control System.

The temperature control system is shown diagrammatically in Fig. 3.11. Nitrogen gas from a cylinder is expanded through a low pressure regulating valve which is followed by a needle valve for fine adjustment. The gas then passes through a drying tower containing silica gel and thence

to a vapour trap which removes the remaining water vapour and also carbon dioxide. Removal of these substances is imperative to prevent blockage of the system; even with the above precautions under operational conditions it was necessary to completely de - ice and dry the system after about three cylinders of gas (of 165 cubic feet each) had been passed through.

The gas passes through three cooling spirals immersed in Dewar vessels containing liquid air. The first two coils consist of 13 feet of 1/4" copper tubing each, while the third and last has 17 feet of 3/16" copper tubing. As the boil - off in this last Dewar vessel was not appreciably faster than that under storage conditions, it was assumed that the temperature of the gas leaving this spiral was close to the temperature of the liquid air. Most of the heat is extracted from the gas in the first Dewar vessel, partly through the vapour - trap and partly through the spiral, and for the low temperatures, i.e. high gas flow rates, the boil - off in this Dewar vessel was very rapid.

A vacuum jacketed tube takes the cold gas from the last cooling spiral to another copper spiral surrounding the specimen tube inside the instrument Dewar system. Here, it takes up heat from the system and therefore lowers the temperature. The gas is then exhausted to the atmosphere, after being monitored with a flow indicator.

Using this system, temperatures could be obtained anywhere in the range from 280°K to 100°K and could be maintained to

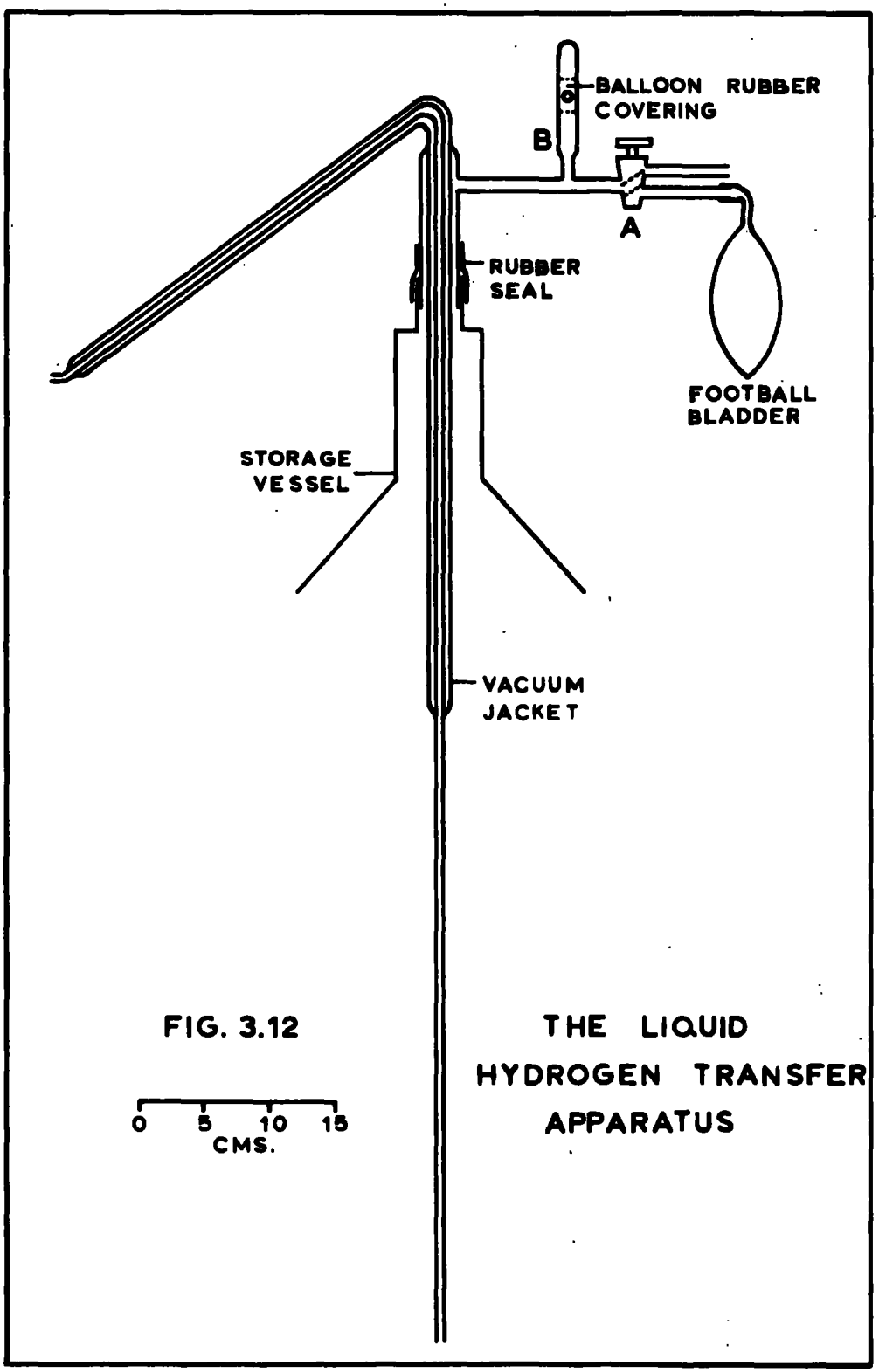

FIG. 3.12

THE LIQUID HYDROGEN TRANSFER APPARATUS

within $\pm$ 1°K over periods of more than 10 minutes by manual control of the flow rate.

For the few readings which were required at temperatures just above that of room - temperature, the system was used unaltered except for replacement of the liquid air in the Dewar vessels by water, which was maintained just below boiling point with thermostatically controlled heaters.

All parts of the instrument which were exposed and liable to be at temperatures greatly different from room - temperature were lagged with a 3 cm. thickness of foam plastic, which was found to be most efficient even with temperature gradients of $\sim 80°/cm$.

3.43. Temperatures below 100°K.

Readings below 100°K were taken at 90°K and 77°K by filling the instrument Dewar vessel with liquid oxygen and nitrogen respectively. A third reading in this low temperature region was taken at 20°K with a liquid hydrogen bath.

Special apparatus was constructed for handling the liquid hydrogen which was obtained from Liverpool University. The hydrogen was stored in a double - Dewar vessel containing liquid nitrogen in the outer container to act as a thermal barrier. Transference of the liquid hydrogen was effected using the Pyrex glass apparatus shown in Fig. 3.12. The vacuum - jacketed transfer apparatus is connected with a short piece of rubber tubing to the vacuum - jacketed tube leading into the instrument. To transfer the liquid hydrogen, the tap A is turned to connect

the storage vessel with the football bladder, which then inflates with hydrogen gas which has boiled off. On squeezing the bladder gas is forced back into the storage vessel and the pressure, caused by the warm gas boiling off more of the liquid, then forces liquid up through the central vacuum - jacketed tube. Since the boil - off is quite rapid a pressure is maintained inside the storage vessel and the process continues spontaneously. A safety valve at B prevents the pressure building up to a dangerous level. To cease transference, tap A is turned to release the pressure to the atmosphere.

When this was done precooling of the apparatus, with liquid nitrogen, was carried out immediately prior to transference of the hydrogen, thus lessening the initial boil - off. Even so, boil - off was quite large and the hydrogen gas from the instrument Dewar System was led outside through a 1" rubber pipe to avoid filling the laboratory with hydrogen gas.

To obtain good heat transfer between the specimen and the supporting tube, the inside of the instrument was filled with gas at atmospheric pressure. Over the range from room - temperature down to that of liquid nitrogen the instrument was simply filled with air which was kept dry with a small boat of phosphorous pentoxide. At liquid hydrogen temperature the instrument was filled with dry hydrogen gas also at atmospheric pressure.

3.44. Temperature Measurement.

Temperatures throughout the whole range were measured

using a copper - constantan thermocouple, the cold junction, of which, was maintained at $0^{o}C$ in a mixture of crushed ice and water. The recording junction was placed immediately adjacent to the specimen by insertion through a small hole in the support - tube which was then sealed with Bostik C adhesive.

The e.m.f.'s developed by the thermocouple were measured on a Pye Portable Potentiometer, which is simply a standard null - reading potentiometer where the e.m.f. is compared with that from a 2 volt cell previously calibrated with a standard Weston - Cadmium cell. A Pye Scalamp galvanometer was used as the null indicator.

Over the range from $20^{o}K$ to $90^{o}K$ the thermocouple had previously been calibrated at the N.P.L. Values of e.m.f.'s from $100^{o}K$ to above room - temperature were then taken from tables in the American Institute of Physics Handbook. A check on these values was carried out using the freezing - point of mercury ($-112^{o}C$) and the temperature of liquid nitrogen. Agreement was found to within 1%.

Using this arrangement, temperatures were measured to an accuracy corresponding to $\pm \frac{1}{2}^{o}K$.

3.5. General Arrangement of Apparatus.

The torque magnetometer and its massive teak base - board are supported above the electromagnet gap on a rigid framework, made up from lengths of Handy - Angle girders, which is bolted firmly to the floor of the laboratory.

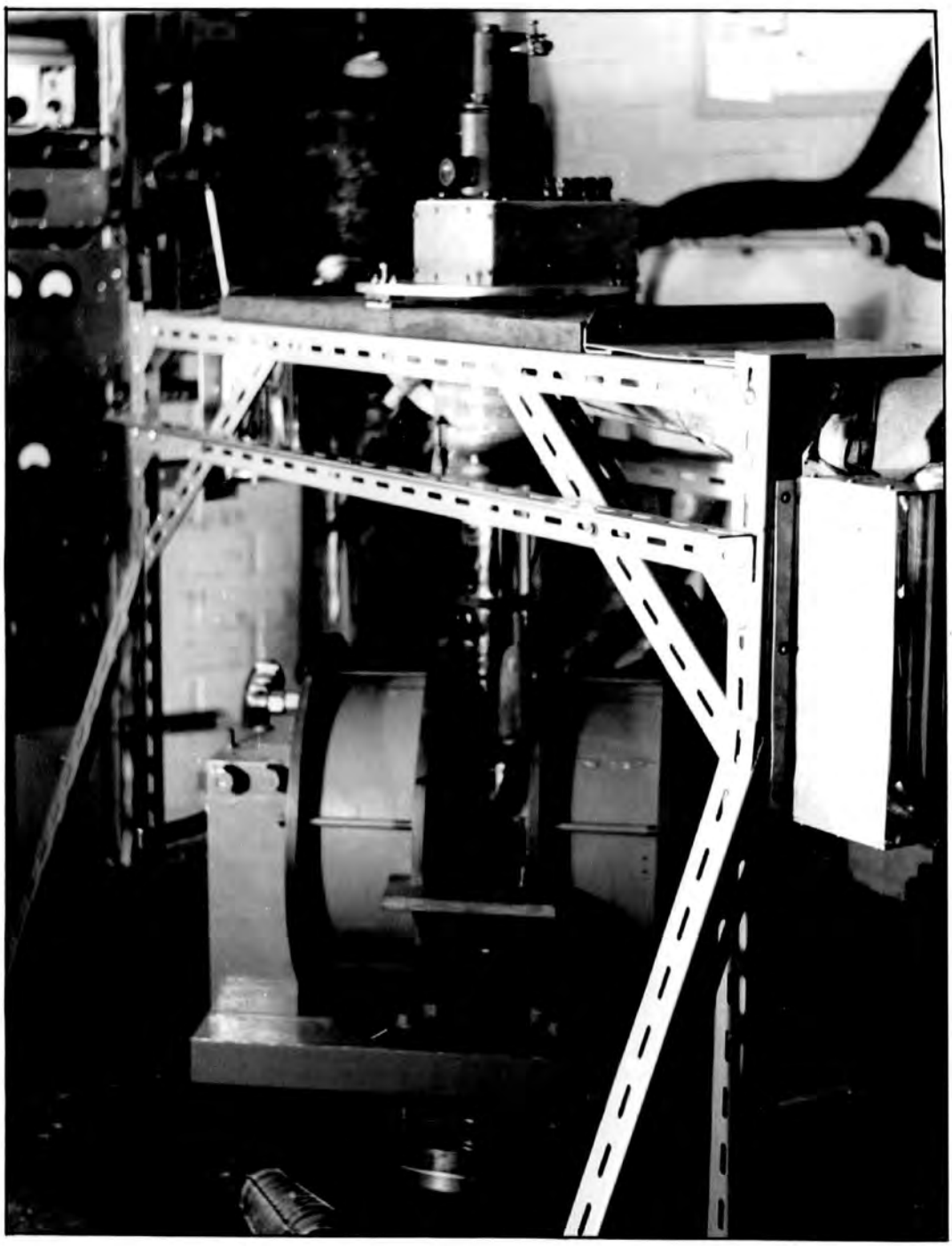

FIG. 3.13

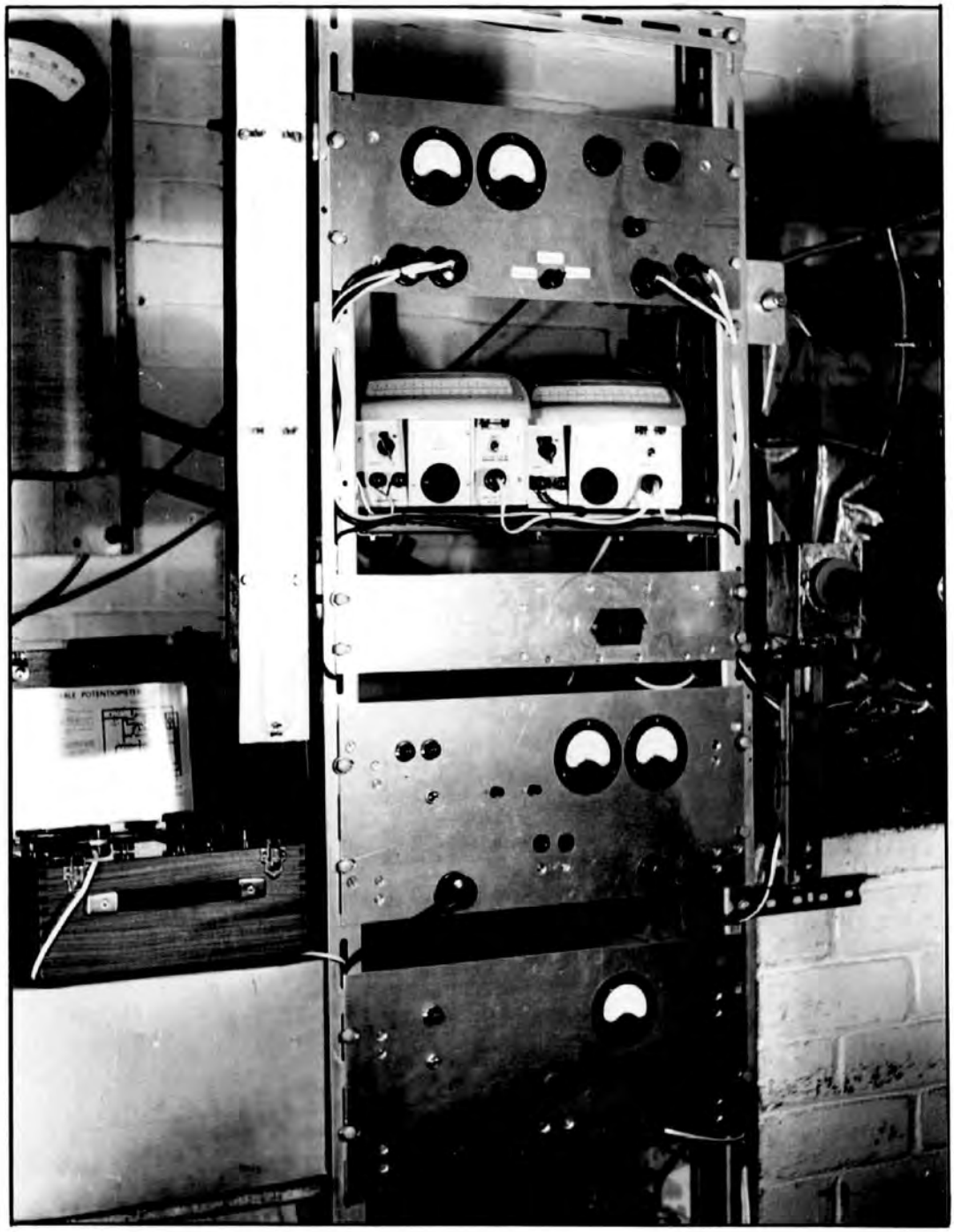

FIG. 3.14

The water cooling system for the electromagnet including the pump and heat exchanger are mounted on the wall immediately behind the apparatus. No trouble was experienced with vibrations, which could possibly have been introduced by the water pump while circulating the coolant.

The photocell unit, which is mounted on a rack containing all the electronic apparatus, is situated at a distance of 150 cms. from the suspension of the magnetometer. The light source is positioned just to the right of the electronics rack and is adjusted to focus on the photocell unit after having been reflected from the suspension mirror. The flow indicator for the cooling system is fixed to the left of the rack and further to the left on the wall are situated the generator governor controls and monitoring panel.

Two photographs of the apparatus are included. Fig. 3.13 shows the torque magnetometer set up in the gap of the electromagnet and Fig. 3.14 shows the rack holding the electronic circuits.

CHAPTER FOUR.

EXPERIMENTAL PROCEDURE AND ANALYSIS OF TORQUE CURVES.

CHAPTER FOUR.

EXPERIMENTAL PROCEDURE AND ANALYSIS OF TORQUE CURVES.

4. 1. Experimental Procedure.

4.11. Setting up the Instrument.

The magnetometer, and thus the gadolinium specimen when mounted on the suspension, was positioned accurately at the geometrical centre of the electromagnet pole - gap using a travelling microscope. Readings were taken with the microscope in two directions at right - angles. A coarse adjustment was obtained by moving the teak base - board relative to the Handy - Angle framework, and fine adjustments were made by slightly altering the setting of the three levelling screws on the instrument. Having set the instrument, the movable stop on the electromagnet railway was locked in position and it could then be moved in and out without disturbing the experimental conditions.

4.12. The Preliminary "Order of Magnitude" Experiments.

Initially nothing was known of the magnitude of the torque expected from a single crystal of gadolinium. In order to obtain a very rough estimate of this value, the instrument was set up with a single counter - torque coil of 20 turns, and having a sensitivity of $\sim$15 dyne cms/milliamp. A small thin piece of the crystal was then cut off with the electrospark apparatus and mounted in the instrument. It was not of uniform cross - section or circular and undoubtedly shape anisotropy would be present, but it was thought possible still to obtain an

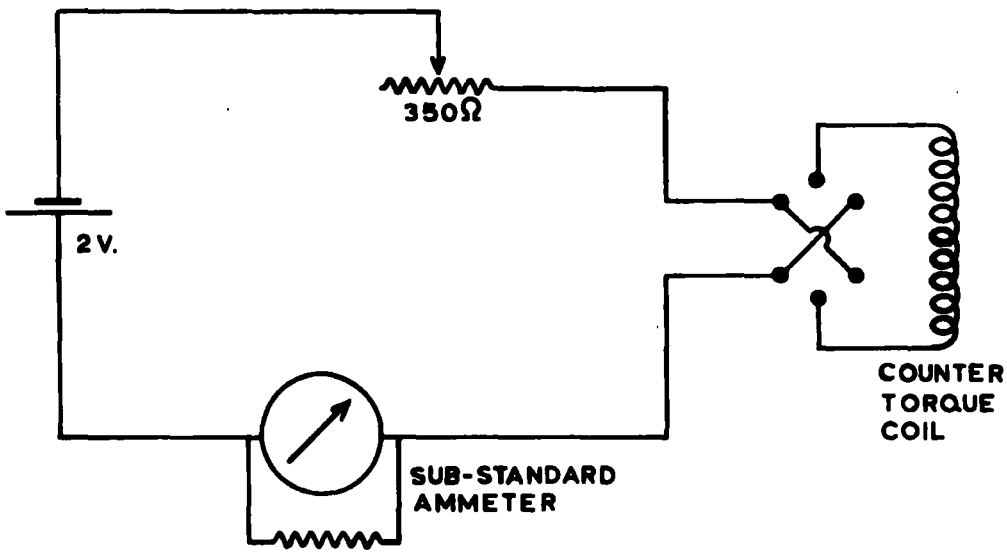

FIG. 4.1 THE MANUAL BALANCING CIRCUIT

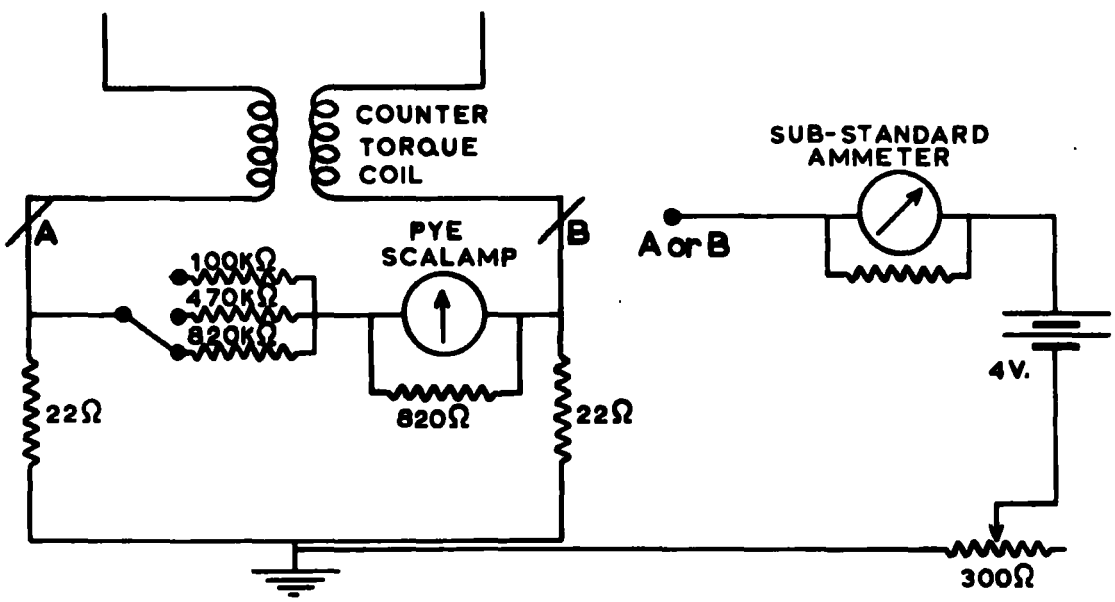

FIG. 4.2 THE GALVANOMETER CALIBRATION CIRCUIT

estimate of the order of magnitude. The volume of the single crystal piece used was $\sim 2 \times 10^{-3}$ c.c.

The electromagnet was rotated through 180^{o} about the specimen and balancing of the torque produced was done manually, using the circuit shown in Fig. 4.1. Balancing was difficult using this system, the zero position was easily over corrected and the suspension was liable to fly from one side to the other. This difficulty emphasized the need for some means of automatic balancing.

However, an order of magnitude measurement was obtained at liquid air temperature. Balancing currents of up to 400 milliamps were required, indicating that torques of the order of 10^{6} ergs/c.c. might be expected.

With this fact known it was possible to estimate the optimum size of specimen needed and also what torques the apparatus would have to measure for a crystal of this particular volume. A maximum balancing current $\sim$120 milliamps was available from the automatic balancing equipment and therefore a coil of $\sim$100 turns was needed over the range from room temperature down to 77^{o}K.

4.13. Calibration of the Torque Magnetometer.

Calibration of the torque magnetometer is carried out using the simple theory of the moving coil galvanometer.

The torque produced by a coil in a magnetic field and passing a current i is given by:-

$$L = AHi$$

where H = magnetic field strength, and A = a constant associated with the coil.

and thus:- AH = L/i = Torque / unit current.

Now, if the coil be deflected through an angle θ, the flux change through the coil will be given by:-

$$F = AH\theta$$

But θ is known and F can be measured, therefore AH, i.e. the Torque/unit current, can be calculated directly.

Experimentally, the suspension and coil were deflected through a small angle by mechanical means. The angular movement was measured by noting the deflection of a light spot, reflected from the mirror fixed to the suspension, on a centimetre scale at 1 metre from the mirror.

The flux change through the counter torque coil was measured using the Cambridge fluxmeter of sensitivity 7098 Maxwell turns/cm. with a lamp and scale at 1 metre distant.

A large number of readings were taken on each coil of the double counter - torque coil and a good estimate of the flux/radian twist for each was obtained. They were found to be identical to within 0.1%.

Calibration for the 100 turn coil gave the sensitivity as 57.0 dyne cms./milliamp. The 300 turn coil was equivalent to 166.6 dyne cms./milliamp. The 100 turn coil was used throughout the temperature range, except for the measurement at liquid Hydrogen temperature.

4.14. Calibration of the Recording Galvonometer.

A Pye Scalamp galvanometer of sensitivity .032 microamps/m.m. was used for recording the out-of-balance current being fed into the counter torque coil.

This instrument was calibrated directly using the circuit shown in Fig. 4.2. Varying currents were passed down each cathode line from the double triode by connecting in the calibrating circuit at A or B. The deflection of the Scalamp galvonometer was recorded and plotted graphically against different currents measured by a sub-standard ammeter. No difference was detectable for deflection left or right. This process was repeated for each of the three sensitivity ranges obtained by switching in the appropriate series resistance.

The results of the calibration gave the sensitivities on the three ranges as 0.200 milliamp/m.m; 0.797 milliamp/m.m. and 1.269 milliamp/m.m.

4.15. Recording Procedure.

(1) When the required temperature had been reached with the control system, the apparatus was allowed to remain at this temperature for a period of at least two hours. This period was necessary to obtain a stable temperature with the manual gas flow regulator and also to ensure complete thermal equilibrium of the specimen and apparatus.

(2) As soon as the required temperature was reached the automatic balancing equipment was switched on and it was allowed to warm up and stabilize during the 2 hour period. At the end

of this period during which the photocells had been kept dark the outputs from each side of the amplifier were balanced using the coarse and fine biasing controls.

(3) Next the projector lamp was switched on and the reflected light spot, from the mirror on the suspension, was locked in the zero position on the photocell compartment door. The door was then opened allowing the light to fall on the 90^{o} beam - splitter and thus onto the photocells. Generally an unbalance resulted from this and the outputs were then equalized by adjusting the position of the beam - splitter in a direction perpendicular to that of the beam, thus causing more light to fall on one of the photocells.

(4) The suspension was then released and any slight unbalance still existing was due to small torsional effects in the suspending ligaments and these were zeroed by small adjustments of the upper ligament mounting.

(5) At this point the apparatus was considered set up and ready for recording.

(6) The electromagnet was then switched on and the current adjusted to give the required field setting. It was then rotated to find the appropriate position of zero torque.

(7) To record a complete torque curve at this temperature the magnet was then moved round in steps of 5^{o} while the out of balance current was recorded, for each position, on the Scalamp galvanometer.

4.2. Analysis of the Torque Curves.

4.21. Recording Torque Curves.

Originally torque curves were obtained for a complete 360° rotation of the electromagnet. This was found to be unnecessary since all the required data needed to evaluate K_1 and K_2 can be obtained from one cycle of $\theta = 0^\circ - 90^\circ$ or $\theta = 90^\circ - 180^\circ$.

From the theory given in Chapter One, section (1.8) the torque is:-

$$L = -(K_1 + K_2) \sin 2\theta + {}^{K_2}/_2 \sin 4\theta$$

Thus $$\left[\frac{dL}{d\theta}\right]_{\theta=\pi/2} = 2K_1 + 4K_2$$

and $$\int_{\theta=0}^{\theta=\pi/2} L.d\theta = -(K_1 + K_2)$$

i.e. The slope of the curve at $\theta = 90^\circ$ is $(2K_1 + 4K_2)$ and the area beneath the curve from $\theta = 0$ to $\theta = 90^\circ$ is $-(K_1 + K_2)$. Hence the values of K_1 and K_2 can easily be calculated.

Experimentally it was found more convenient to record over the cycle $90^\circ - 180^\circ$, in which case the area beneath the curve becomes positive i.e. $(K_1 + K_2)$.

4.22. Analysis by the Slope and Area Method.

One or two preliminary points were recorded in the temperature region, near that of liquid air, and analysis of these by the method above was not very satisfactory.

The data was recorded and then plotted on millimetre graph paper from which the slope at $\theta = 90^\circ$ was obtained directly.

The area beneath the curves from $\Theta = 90^{o}$ to $\Theta = 180^{o}$ was measured using a planimeter. However, the values of K_1 and K_2 obtained from the analysis did not agree well when substituted back into the equation and re-plotted against the original experimental curve. A means of working out the constants by utilizing the position and magnitude of the torque maxima was also tried but similar poor agreement resulted. Even with trial and error methods, no possible fit was found for the experimental curves using just the constants K_1 and K_2.

Thus it seemed necessary to include the third anisotropy constant in order fully to describe the experimental data.

4.23. The Inclusion of K_3.

As seen earlier, the anisotropy energy may be represented by a series of the form:-

$$E_k = K_1 \sin^2\Theta + K_2 \sin^4\Theta + K_3 \sin^6\Theta + \text{------}$$

and the torque is given by $L = -\frac{dE_k}{d\Theta}$

$$\therefore L = -\left[K_1 + K_2 + \frac{27}{16} K_3\right] \sin 2\Theta + \left[\frac{K_2}{2} + \frac{3}{4} K_3\right] \sin 4\Theta - \frac{3}{16} K_3 \sin 6\Theta$$

With the torque curve now described by a three constant expression, it was necessary to have three different quantities read from the graph in order to evaluate K_1, K_2, and K_3 separately.

The slope at $\Theta = 90^{o}$ and the area from $\Theta = 0$ to $\Theta = 90^{o}$ were used as before and in addition the position of the torque maximum. In this case the three quantities are given by:-

$$\text{Slope} = \left[\frac{dL}{d\theta}\right]_{\theta=\pi/2} = 2K_1 + 4K_2 + \frac{15}{2}K_3$$

$$\text{Area} = \int_0^{\pi/2} L\,d\theta = -\left(K_1 + K_2 + \frac{7}{4}K_3\right)$$

$$L_{max} = -\left(K_1 + K_2 + \frac{27}{16}K_3\right)\sin 2\theta_{MAX} + \left(\frac{K_2}{2} + \frac{3}{4}K_3\right)\sin 4\theta_{MAX} - \frac{3}{16}K_3 \sin 6\theta_{MAX}$$

Analysis of the torque curves using these three equations was very slow and unwieldy, however it was evident from the analysis carried out with this method, that a better fit could be obtained with the K_3 included.

The accuracy with which the values of K_1, K_2, and K_3 were obtained was not very high because of the difficulties of reading off from the graph the appropriate quantities. This was particularly so in the case of the position of the torque maximum.

For this reason it was decided to use the Ferranti Pegasus computer to analyse the torque curves using a method which did not involve reading constants from a drawn graph.

4.24. Analysis by the Ferranti Pegasus Computer.

Initially the method used involved the solution of three simultaneous equations obtained by substituting three different values of L and θ into the general equation:-

$$L = -\left(K_1 + K_2 + \frac{27}{16}K_3\right)\sin 2\theta + \left(\frac{K_2}{2} + \frac{3}{4}K_3\right)\sin 4\theta - \frac{3}{16}K_3 \sin 6\theta$$

Ten sets of three readings of and L were taken from the graph between $\Theta = 90^{\circ}$ and $\Theta = 180^{\circ}$. The computer then solved the ten sets of simultaneous equations from which the mean solutions for K_1, K_2 and K_3 were taken.

In using the simultaneous equation programme the equation has to be set up in the form:-

$$aK_1 + bK_2 + cK_3 = L$$

where $a = -\sin 2\Theta$

$b = -\sin 2\Theta + \frac{1}{2}\sin 4\Theta$

$c = -\frac{27}{16}\sin 2\Theta + \frac{3}{4}\sin 4\Theta - \frac{3}{16}\sin 6\Theta$.

The computer then solves the equations:-

$$+a_1 K_1 + b_1 K_2 + c_1 K_3 = L_1$$

$$+a_2 K_1 + b_2 K_2 + c_2 K_3 = L_2$$

$$+a_3 K_1 + b_3 K_2 + c_3 K_3 = L_3$$

In operation, a short Autocode programme (Pegasus Library Specification R600) was written which set up the values of a, b and c for each given value of Θ, in a form that was acceptable to the simultaneous equation programme which already existed in the computer library.

Several torque curves at different temperature points were analysed in this way, but the results obtained were not

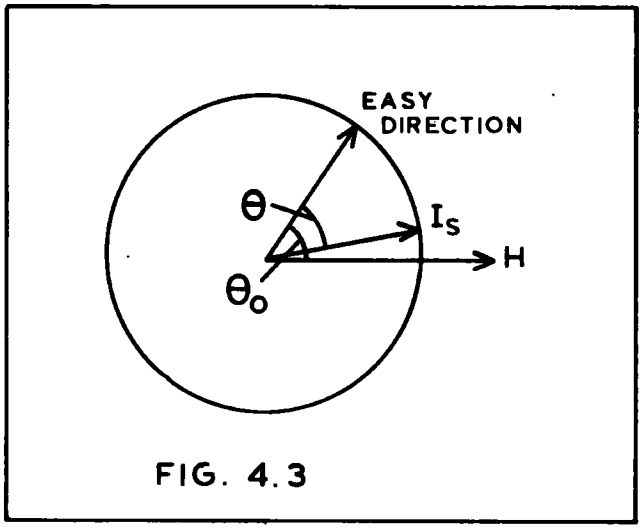

FIG. 4.3

particularly good. The ten sets of Θ and L were taken from the curve in groups e.g. $\Theta = 2^{o}, 32^{o}, 62^{o}; 5^{o}, 35^{o}, 65^{o}$ etc. The K values obtained in this manner were not consistent over the 10 sets, instead they all showed varying trends. For example; K_1 showed a maximum value, K_2 showed a decrease from the first to the tenth reading and K_3 tended to zero from the first to the tenth reading. This behaviour at first appeared to indicate that the curves obtained were not unique but had many values of K_1, K_2 and K_3 which would fit. This explanation however was realised to be impossible and the problem was resolved when a correction was applied to the experimental data, for lack of saturation. This correction was suggested by Williams and used by Bozorth (1954).

Consider the energy of the crystal disc shown in Fig. 4.3. In high fields all the magnetization may be considered to be lying along the direction of H.

If the field is not strong enough to completely draw Is into its own direction the energy of the system is given by:-

$$E = - HIs \cos (\theta_o - \Theta)$$

$$= - HIs \cos \alpha$$

where α is the angle between H and Is

Thus $$L = - \frac{dE}{d\Theta} = - HIs \sin \alpha$$

Now under experimental conditions a torque L is read as being associated with the measured angle Θ, but in actual fact this torque is being derived from the difference between the direction

of easy magnetization and Is i.e. $(\Theta - \alpha)$

But:-

$$\alpha = \sin^{-1}\left(\frac{-L}{HIs}\right)$$

and therefore a correction can be applied to the experimental data to allow for this. The correction term is proportional to L and has the effect of displacing each point, on the observed L versus Θ curve, along the Θ axis by an amount α.

When this correction was applied to the results previously analysed, the anomaly was resolved and consistent values of K_1, K_2 and K_3 were obtained over the 10 sets of readings from each curve.

4.25. Improved Computer Analysis.

The earlier method of analysis was still not considered to be entirely satisfactory, as it still involved drawing a graph from which experimental data was to be taken.

A programme of least - squares curve fitting was available in the computing library and examination showed that it could be used so that experimentally recorded data from this problem was fed directly into the computer.

The least - square curve fitting programme analyses results in the following manner. Suppose there are N pairs of values (x_i, y_i) and it is required to obtain an expression:-

$$y(x) = \sum_{1}^{m} c_s \Phi_s(x)$$

Such that it will fit the data so that

$$\sum_{i=1}^{N} \left[y(x_i) - y_i \right]^2$$

is a minimum for a particular choice C_1, C_2 ---- C_m.

The function $\Phi_s(x)$ may be anything and in this case it is

$$Y(x) = C_1 \sin 2x + C_2 \sin 4x + C_3 \sin 6x$$

In operation a short Autocode programme was first written which set up the data in a form acceptable to the R2500 Matrix Scheme. The Autocode programme then generates a single sequence of numbers in the order:-

$$\Phi_1(x_1)\ \Phi_2(x_1)\ ----\ \Phi_{m-1}(x_1)\ \Phi_m(x_1)\ \Phi_1(x_2)----\Phi_m(x_2)----\Phi_m(x_N)$$

This is in fact an (mXN) matrix. In this case m = 3 and N = 18, the number of readings between $\Theta = 90^\circ$ and $\Theta = 180^\circ$.

This is used with the matrix scheme R2500 which solves for the coefficients C_1, C_2 and C_3. If the matrix is represented by A^1, the elements C_1, C_2 and C_3 are given by:-

$$C_e = (A^1 . A)^{-1}\ y_e$$

where ye represents the elements $y_1\ y_2$ ---- y_N

The values $y_1\ y_2$ ---- y_N are output from the second part of the Autocode programme and represent in this case the values of L at the points $x_1 = \Theta_1$ $x_2 = \Theta_2$ etc.

The Autocode programme used in setting up the data is quite simple and its operation is shown below. A further correction is applied to the data, inside the computer, for the slight movement of the suspension which is again proportional to the

applied torque.

```
    J1.0                    - Autocode call
    STOP                    - pause to insert data tape.
    n1 = 0                  - clear counter 1
    n2 = 0                  - clear counter 2
1) v1 = TAPE 2              - read θ , L into v1 & v2
 → 2, n0 = 0                - go to instruction 2 when(L)read.
v (100 + n1) = v.2          - put L in v100, v101, etc.
v3 = v2 x 0.31.             - assess correction for suspension.
v4 = v1 + v3                - apply correction.
v5 = v2 / (HIs)             - assess lack of saturation correction
v5 = ARCSINv5               - find α (radians)
v4 = v4 x 0.01 74532925     - convert θ to radians
v6 = v4 + v5                - apply correction
v7 = v6 x 2                 - 2θ
XPv7 = SINv7                - print sin 2θ
v8 = v6 x 4                 - 4θ
XPv8 = SINv8                - print sin 4θ
v9 = v6 x 6                 - 6θ
XPv9 = SINv9                - print sin 6θ
n1 = n1 + 1                 - counter
 → 1                        - repeat programme
2) n0 = TAPE B*             - add CRLF * CRLF
3) XPv0 = v(100 + n2)       - print L from v100, v101 etc.,
n2 = n2 + 1                 - counter
→ 3, n2 ≠ n1                - repeat loop
```

n0 = TAPE B ✱ - . add CRLF ✱ CRLF

(⟶ 0) - enter programme.

The output tape from this programme has on it a sequence of numbers:-

(sin $2\theta_1$), (sin $4\theta_1$) (sin $6\theta_1$) (sin $2\theta_2$) (sin $4\theta_2$)------(sin $6\theta_N$)

and this is followed by a second sequence of:-

L_1, L_2, L_3 --------- L_N

A CRLF ✱ CRLF is inserted between the two sets of numbers and also at the end, its function is purely mechanical to allow the data to be fed into the computer.

To operate the programme the matrix scheme is first fed into the computer and this is followed by a short parameter tape of the form:-

T 1600	-	machine order.
m	-	in this case 3
N	-	in this case ~ 18
P	-	always 1
Z		

which indicates to the computer the form of matrix being used. The least - square curve fitting programme is then fed in and the computer arrives at an optional stop which allows the output tape from the Autocode programme to be fed in with a further optional stop separating the two number sequences.

The resulting output from the computer is printed out with first a column of 3 numbers which are the coefficients C_1, C_2

and C_3 and then a column of N numbers which are the residuals at each of the points on the original curve.

Values of K_1, K_2 and K_3 are then obtained by solving the three simple simultaneous equations:-

$$C_1 = -(K_1 + K_2 + \frac{27}{16} K_3)$$

$$C_2 = K_{2/2} + \frac{3}{4} K_3$$

$$C_3 = -\frac{3}{16} K_3$$

Inspection of the residuals also gives an immediate check on how well the curve has been fitted with the experimental data.

CHAPTER FIVE.

RESULTS AND DISCUSSION.

CHAPTER FIVE.

RESULTS AND DISCUSSION.

5.1. Results.

Values of the magnetocrystalline anisotropy constants of gadolinium K_1, K_2, and K_3 have been obtained over the temperature range from 320°K to 77°K. A further measurement has also been obtained at a temperature of 20°K. The results are shown graphically in Fig. 5.1a. (referred to H = ∞).

To indicate the torque variation over the range of temperature, representative curves for 270°K, 210°K, 150°K, 90°K and 20°K and at H = 12,500 oersteds, are shown in Figs. 5.2, 5.3, 5.4, 5.5 and 5.6. respectively. The curves are given corrected for lack of saturation. The effect of this correction is shown in Figs. 5.5. and 5.6. where the dotted line represents the experimentally recorded values.

Final values of K_1, K_2 and K_3 were referred to H = ∞ by the following method. Torque curves for various field values were recorded for a number of temperatures and, for each of these, graphs of K_1, K_2, and K_3 versus $1/H$ were drawn and extrapolated to $1/H = 0$. Values of ΔK_1, ΔK_2 and ΔK_3, the corrections to be added to the results for H = 12,500 oersteds, were then obtained and, when plotted against temperature, found to be a smooth function. It was therefore possible to obtain ΔK_1, ΔK_2 and ΔK_3 for intermediate temperatures from this graph. A typical K_1, K_2, and K_3 versus $1/H$ graph is shown

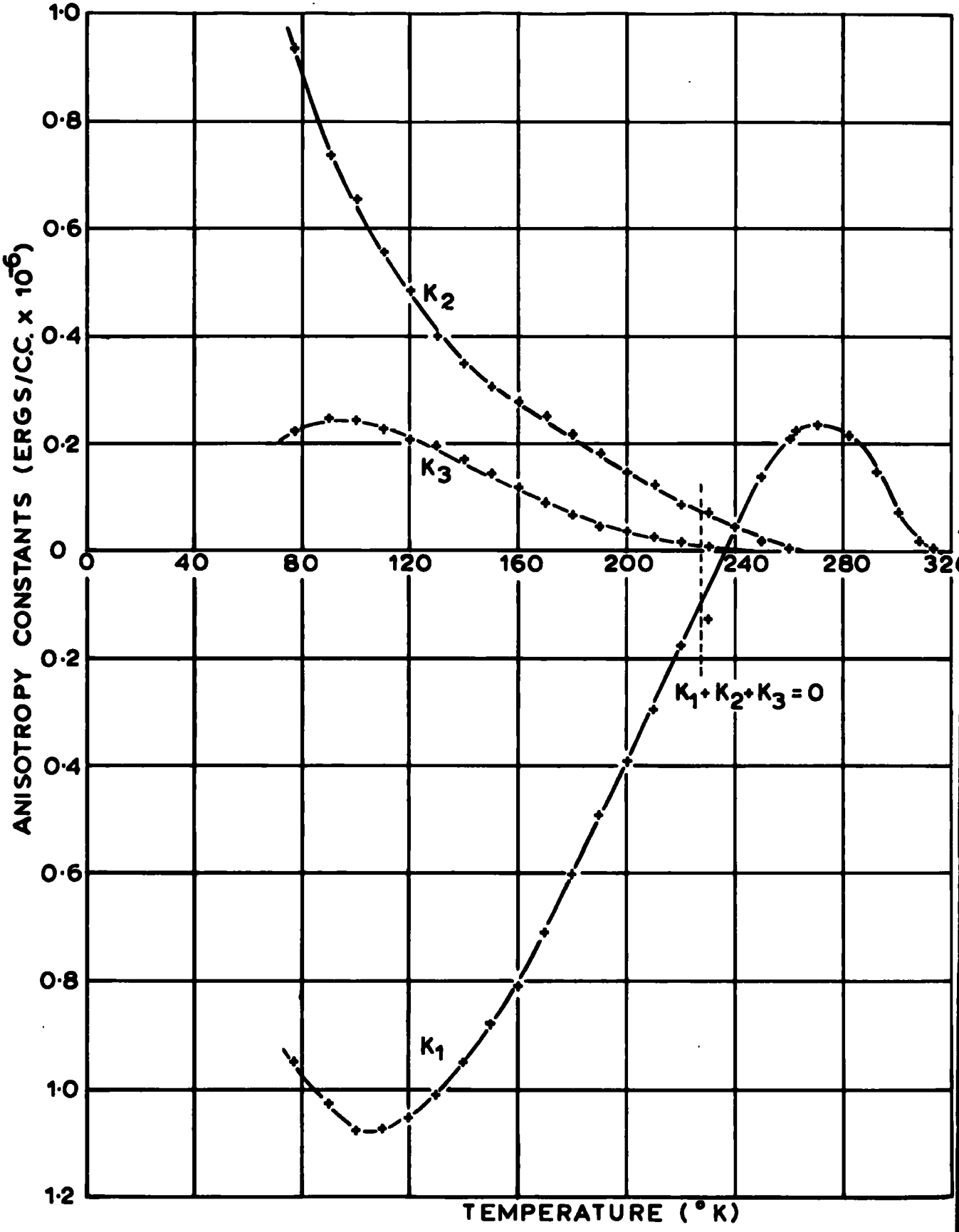

FIG. 5.1a THE TEMPERATURE VARIATION OF THE ANISOTROPY CONSTANTS OF GADOLINIUM

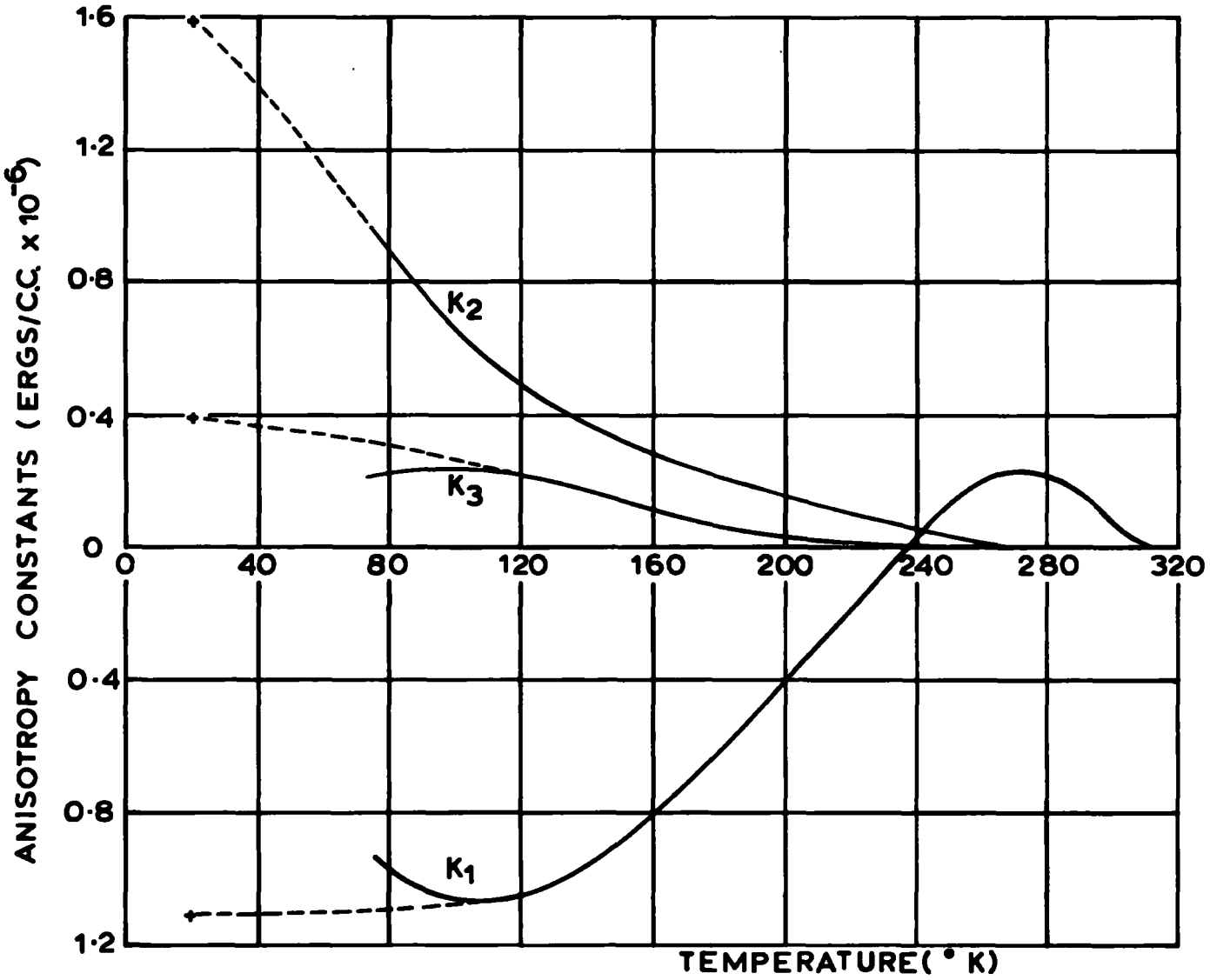

FIG. 5.1 b THE INCLUSION OF THE MEASUREMENTS AT 20°K

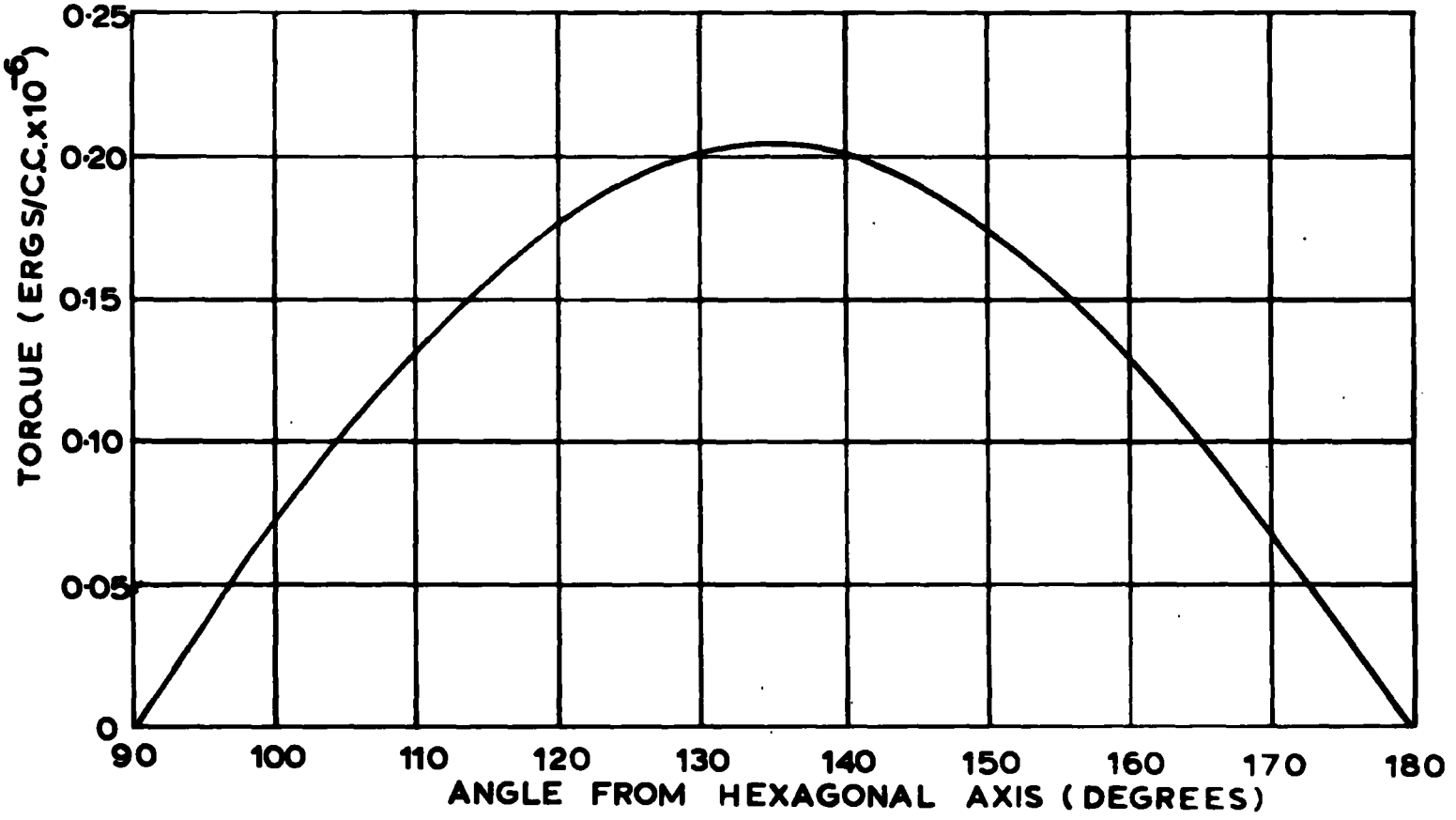

FIG. 5.2 TORQUE CURVE AT 270°K

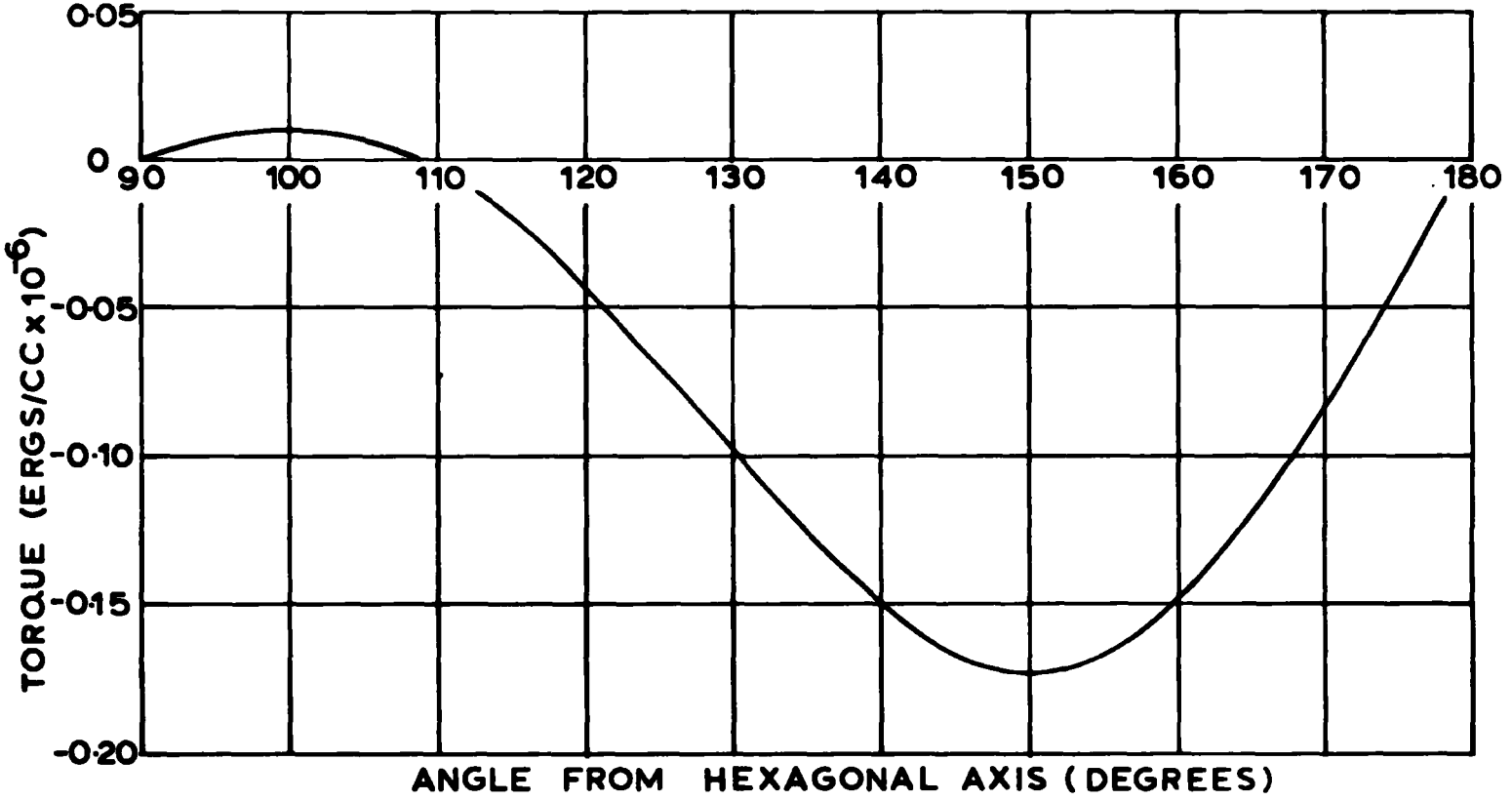

FIG. 5.3 TORQUE CURVE AT 210°K

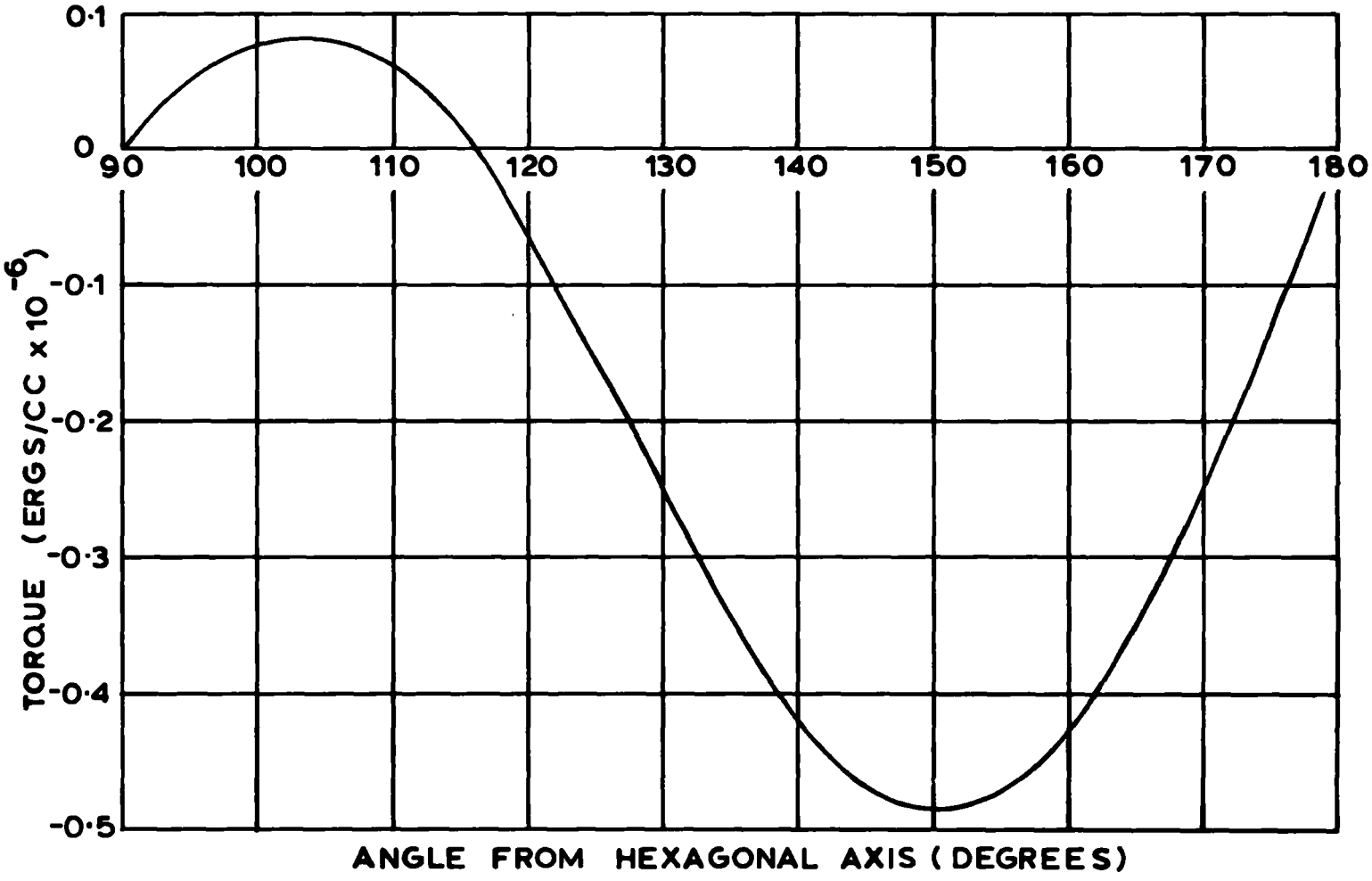

FIG. 5.4 TORQUE CURVE AT 150°K

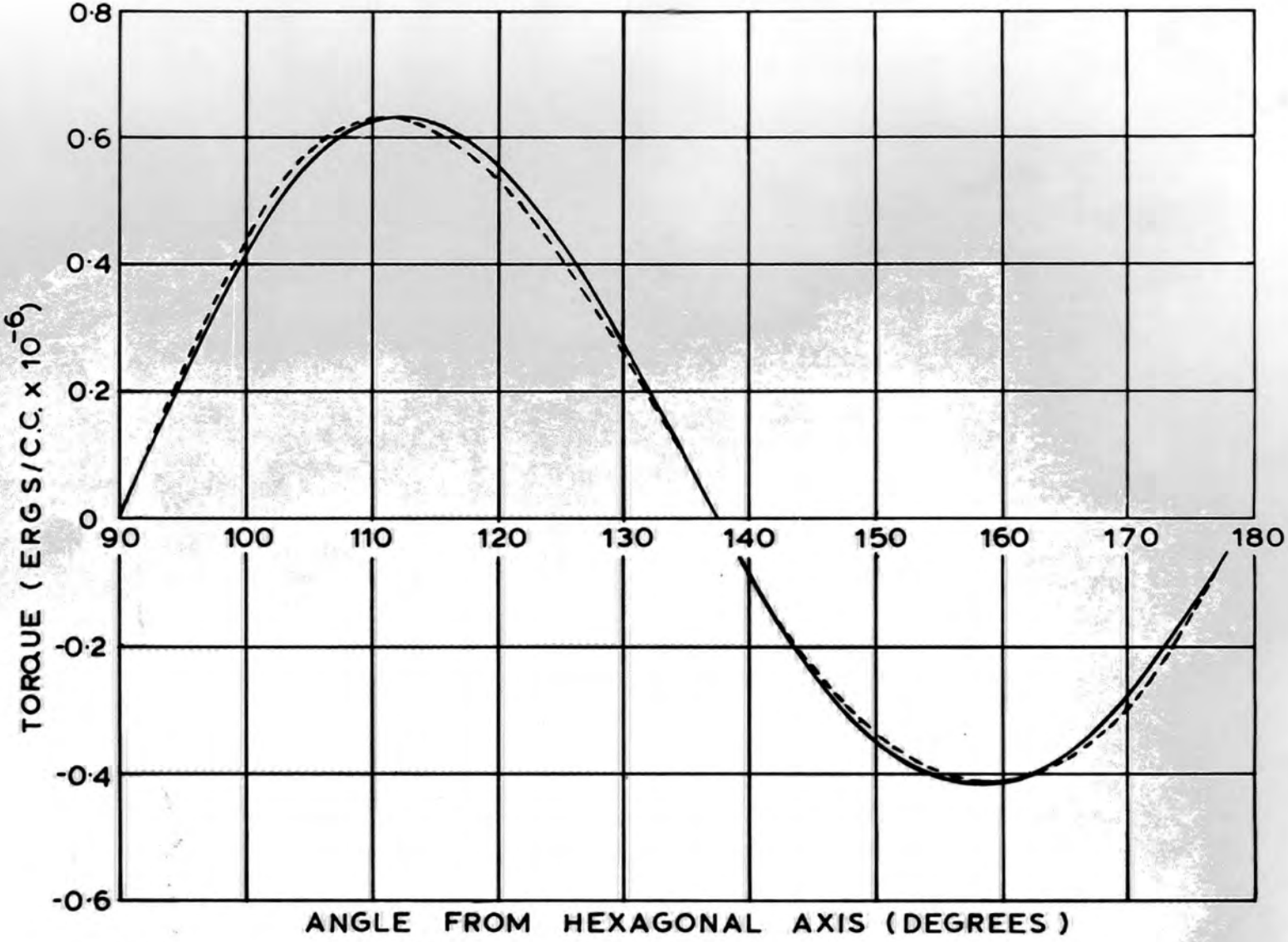

FIG. 5.5 TORQUE CURVE AT 90°K

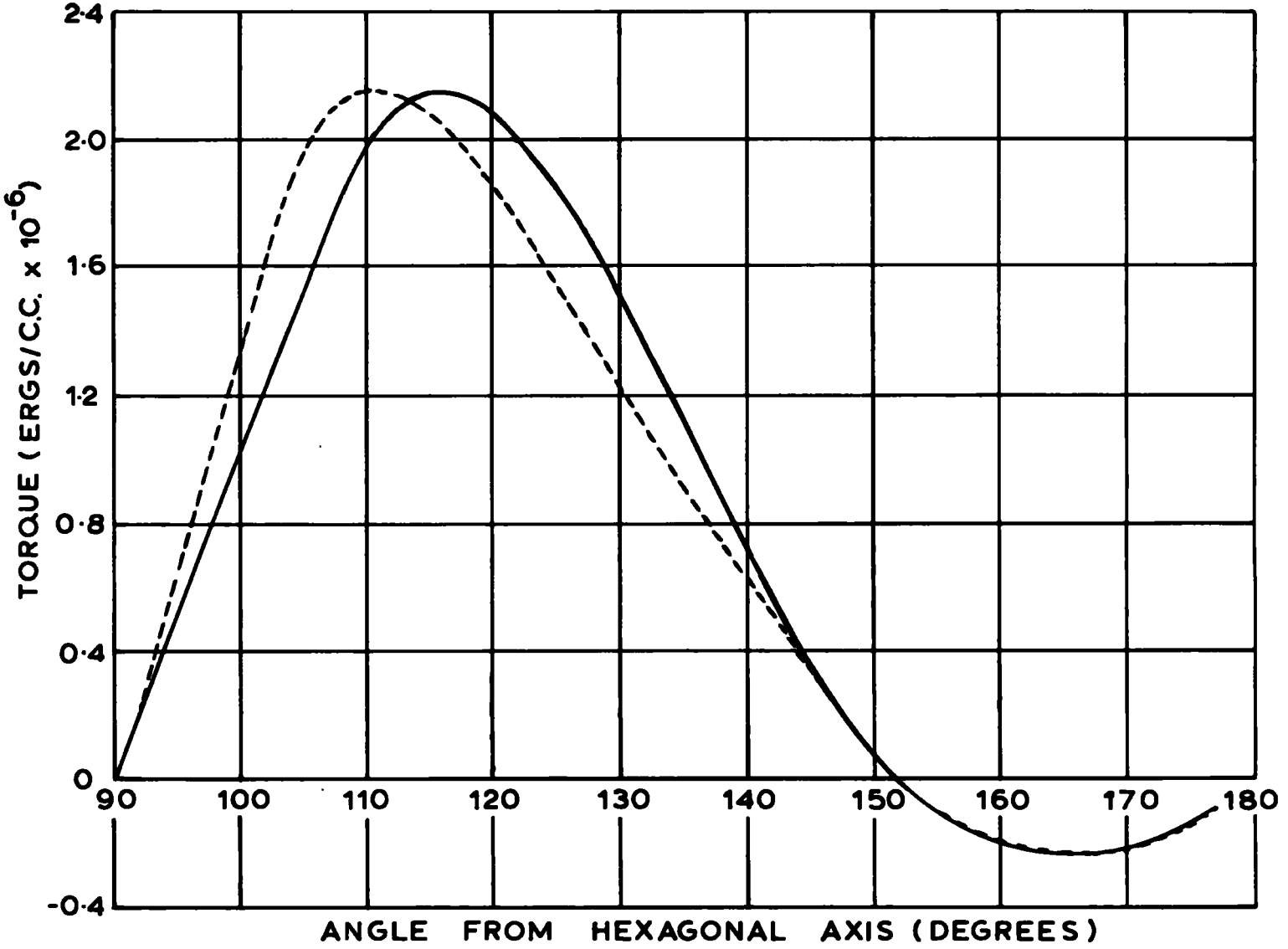

FIG. 5.6 TORQUE CURVE AT 20°K

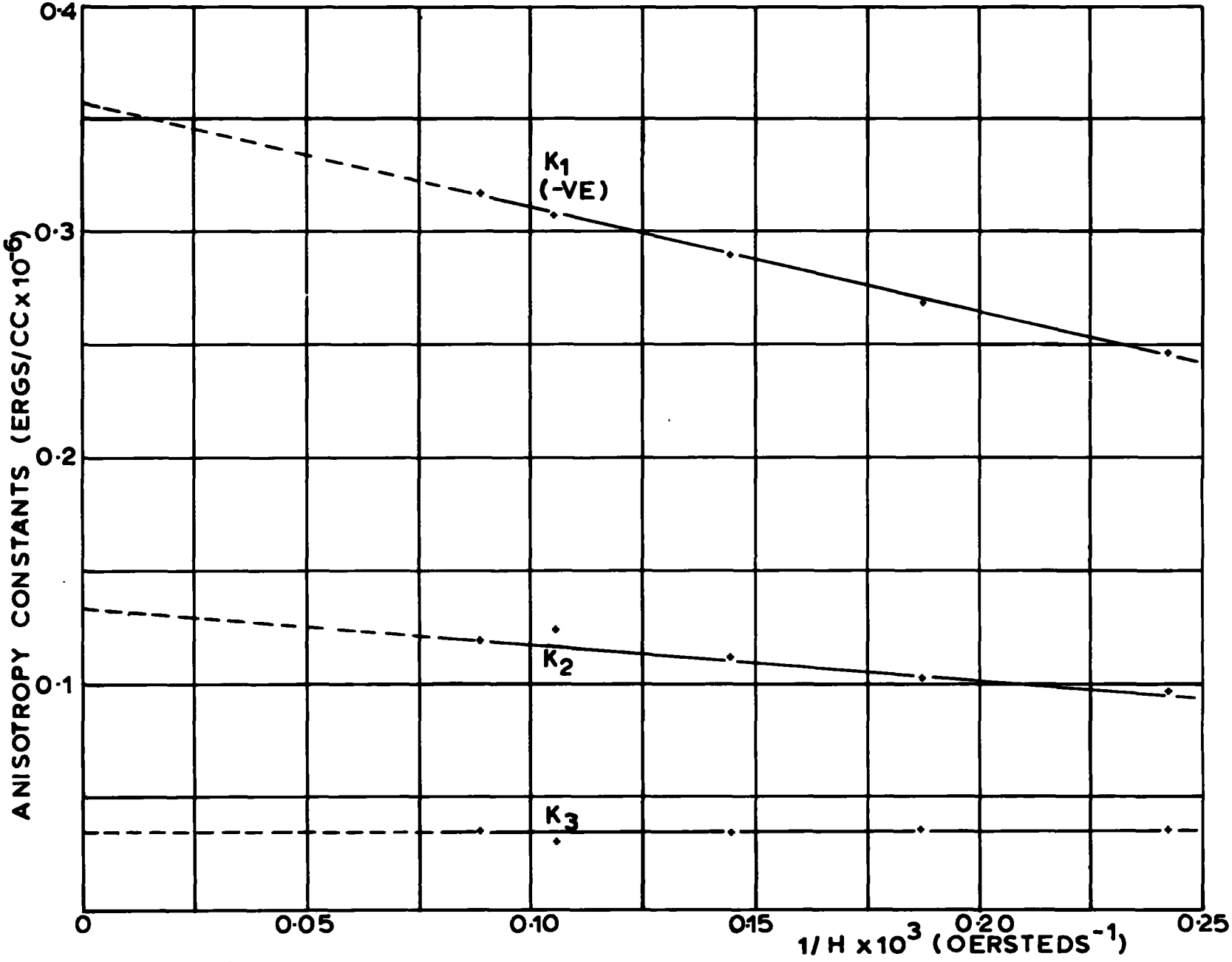

FIG. 5.7 EXTRAPOLATION TO $H = \infty$

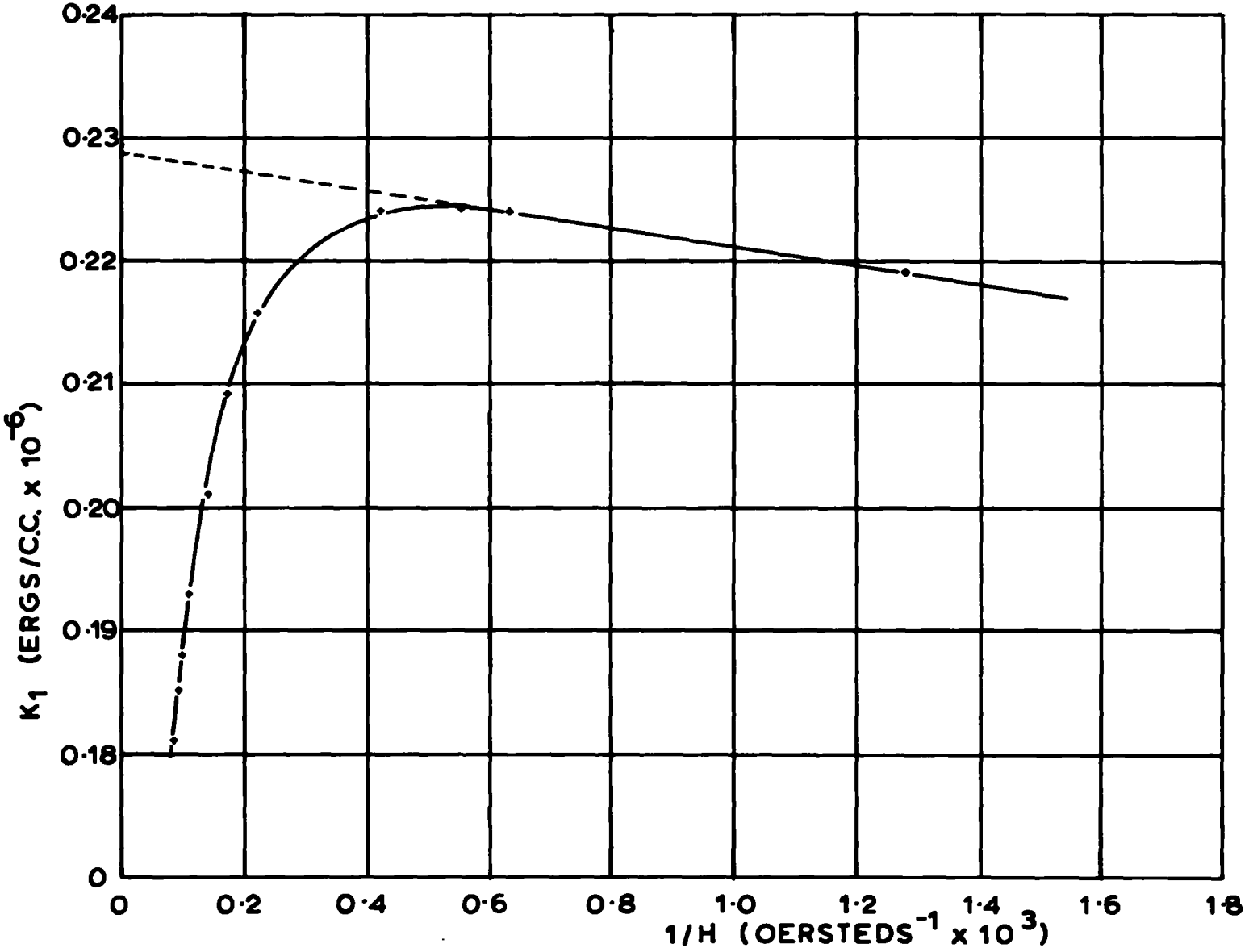

FIG. 5.8 THE PARAMAGNETIC EFFECT (T = 262°K)

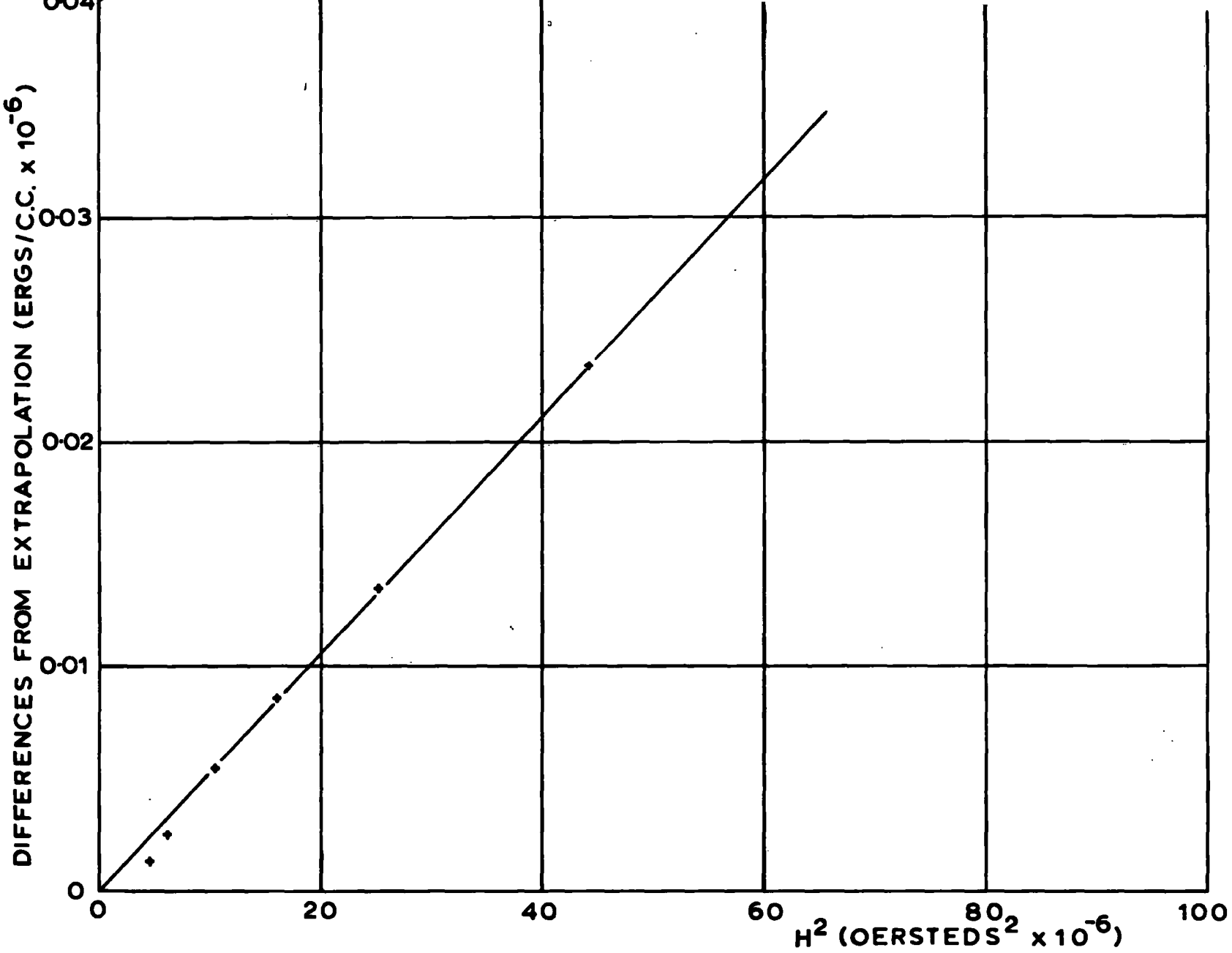

FIG. 5.9 VERIFICATION OF PARAMAGNETIC EFFECT

plotted in Fig. 5.7.

A combination of uncertainties in the shape of the specimen, orientation measurement of temperature and possible errors associated with the calibration of the torque magnetometer, gives a total uncertainty of not more than ±5% for the overall experiment. Maximum corrections, applied to the results (obtained from measurements with a field of 12,500 oersteds) to refer them to $H = \infty$, nowhere exceeded 5%.

The results, as shown in Fig. 5.1, have also been corrected for a paramagnetic component in the experimentally recorded value of K_1. The values of K_2 and K_3 may be shown to be unaffected, since for a paramagnetic substance the energy is given by:-

$$Ep. = \text{const.} - CH^2 \bar{\chi} \sin^2\theta$$

where C = constant, and $\bar{\chi}$ = the difference in the susceptibilities parallel and perpendicular to the reference direction.

For the ferromagnetic case:-

$$E_k = K_o + K_1 \sin^2\theta + K_2 \sin^4\theta + \text{--------}$$

Thus, it can be seen that the K_1 observed will be a combination of K_1 and a paramagnetic contribution which is proportional to H^2.

The effect of the paramagnetic component is shown adequately in the K_1 versus $1/H$ curve given in Fig. 5.8. To verify that the effect is actually proportional to H^2, differences between the straight line extrapolation and the experimental curve were plotted against H^2. In Fig. 5.9. it is seen that a linear

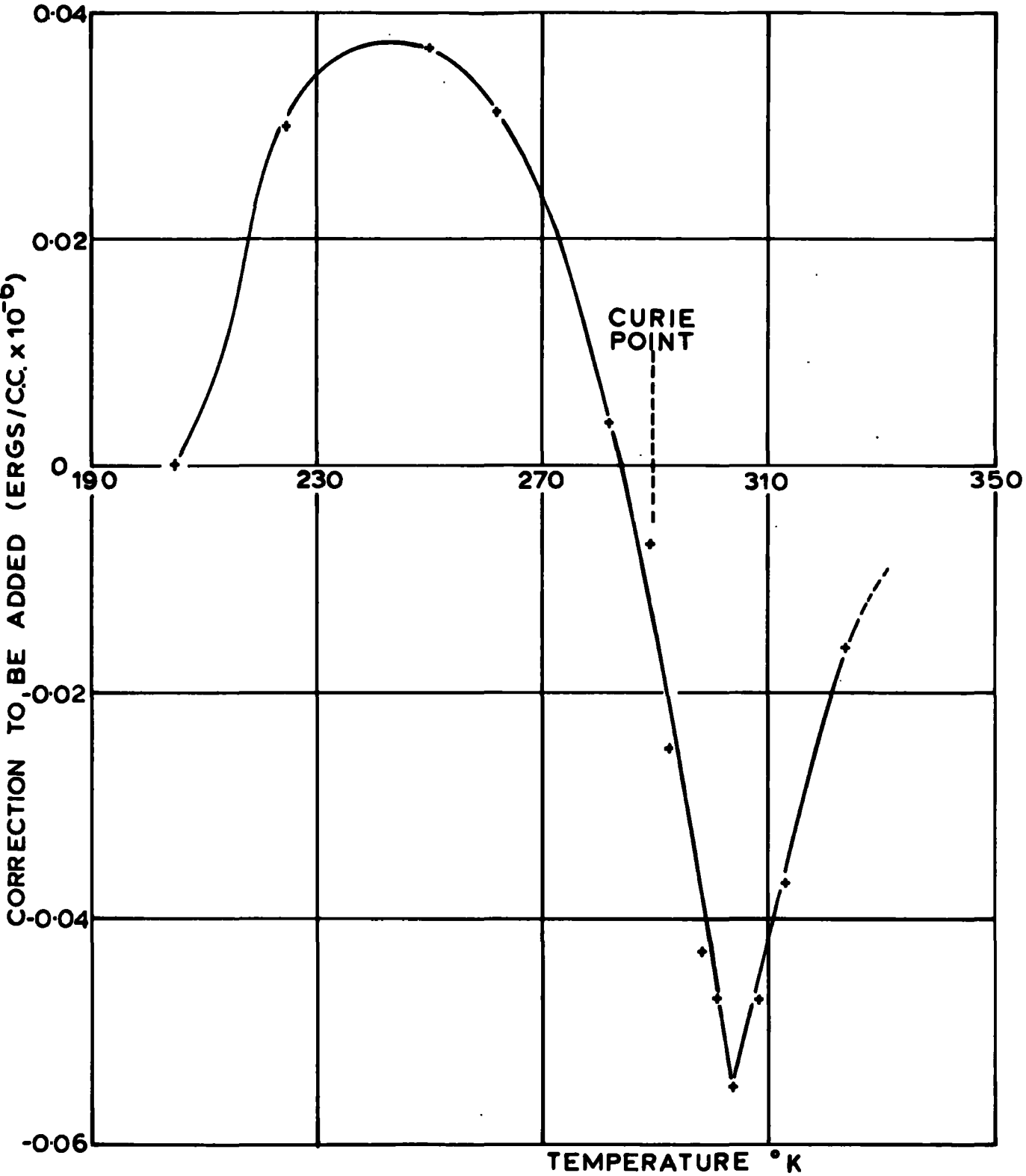

FIG. 5.10 THE TEMPERATURE DEPENDENCE OF THE PARAMAGNETIC COMPONENT

relationship does in fact exist, verifying that the effect is paramagnetic. The point off the curve at $H^2 = 10^8$ (oersteds)^2 is due to an approach to saturation of the paramagnetic component.

Hence, the paramagnetic component of the observed K_1 could be simply calculated:-

$$(K_1)_{H_1} = (K_1 + C \dot{\chi} H_1^2)$$

$$(K_1)_{H_2} = (K_1 + C \bar{\chi} H_2^2)$$

where H_1, H_2 represent two different field strengths

Thus $(K_1)_{H_1} - (K_1)_{H_2} = C \bar{\chi} (H_1^2 - H_2^2)$

$$C \bar{\chi} = \frac{(K_1)_{H_1} - (K_1)_{H_2}}{H_1^2 - H_2^2}$$

Values of the paramagnetic correction were therefore obtained by observing the torque curve at two different fields, and applying the treatment described above. The paramagnetic effect was found to exist down to a temperature of 205°K where it was considered to be zero since the K_1 versus $1/H$ graph became linear. The paramagnetic component of K_1 (observed) is shown plotted in Fig. 5.10. and it is seen that there is a change of sign associated with the Curie point.

5.2. Discussion.

As can be seen from the results shown in Fig. 5.1a, the

most striking fact about the magnetocrystalline anisotropy of gadolinium is that, for the greater part of its ferromagnetic range, the sign of K_1 is negative, indicating that the easy direction of magnetization lies in the basal plane. This is contrary to a suggestion by Birss (1960) who indicates that the easy direction lies along the hexagonal axis.

Behrendt et al (1958) have studied the magnetic properties of dysprosium, another rare earth metal with a hexagonal close-packed structure and having a ferromagnetic Curie - temperature of 85°K. They have found that it too has easy directions in the basal plane with the hexagonal axis extremely 'hard'. Perhaps this bears some significance since both are members of the same group of elements and have a similar crystal structure, although dysprosium exhibits a non - integral number of spins per atom (equivalent to 10.61 μB) indicating that the 4f shell in this case is not so tightly bound.

K_3 becomes measureable at a temperature of $\sim 240°K$. The presence of K_3 indicates that anisotropy will exist in the basal plane. The crystal disc used in the present experiment contains one of the three equivalent hexagonal axes and the K_3 measured in this case may be referred to one of these. If gadolinium bears any further similarity to dysprosium, it is to be expected that six-fold anisotropy will be present in the basal plane.

Above 235°K the sign of K_1 is positive and the crystals exhibits a uniaxial character similar to cobalt. The change

in sign of K_1 causes the crystal to become isotropic at a temperature of $\sim 227^{\circ}K$, when $(K_1 + K_2 + K_3) = 0$ and in this region measured values of torque were very small.

The fact that K_1 undergoes a change of sign immediately prohibits any comparison with the treatment of Zener, where

$$K_1 (T) \propto \left[\frac{I_{s(T)}}{I_{s(o)}}\right]^{\frac{n(n+1)}{2}}$$

since this must necessarily be of uniform sign and thus this treatment is totally inadequate in the case of gadolinium. There is possibly a fit for K_2 and K_3 but the process cannot really be of any relevance when K_1 does not conform.

An interesting observation connected with the change of sign of K_1 is the apparent correlation with the thermal expansion curve of Birss (Fig 1.4). The negative peak of the expansion anomaly occurs at the position of the positive K_1 maximum $\sim 280^{\circ}K$ and then the K_1 changes sign at $\sim 235^{\circ}K$, the approximate temperature at which the anomaly changes sign also.

It is unfortunate that no measurements were possible in the temperature range from $77^{\circ}K$ to $20^{\circ}K$, as obviously there is an anomaly existing in the curves for K_1, K_2 and K_3. The measurements at $77^{\circ}K$ and $90^{\circ}K$ were repeatable to better than 1%, including a measurement made at $77^{\circ}K$ with the 300 turn counter torque coil. The measurement at $20^{\circ}K$ was not repeated, but the given values of K_1, K_2 and K_3 are the extrapolation of six readings at different fields taken over a period of

1.1/4 hours. No doubt existed concerning the temperature and the measurements were consistent. In Fig 5.1b, the curves have been extended by a smooth dotted line to include the measurement at $20^{\circ}K$, but the possibility of an actual anomaly existing in this range cannot be ruled out.

5.3. Suggestions for Further Work.

Further investigations of the magnetocrystalline anisotropy would be desirable. Particularly it would seem important to carry out measurements in the temperature range from $77^{\circ}K$ to $4.2^{\circ}K$ to resolve the present doubt existing about the form of variation in this region.

The question of the possible anisotropy existing in the basal plane should also be a point for further investigation. The crystal specimen used in this experiment is not suitably orientated for this purpose and another oblate spheroid would be required, which contained the basal plane.

ACKNOWLEDGMENTS.

The author wishes to express his sincere thanks to Dr. W.D. Corner, F. Inst. P. who was always at hand to give help and guidance throughout the project.

The author is also grateful to Prof. G.D. Rochester, F.R.S. for the research facilities made available and to the Physics Dept. Workshop staff, especially Mr. D. Jobling, for technical assistance.

The author is also indebted to Mr. F. Venmore and the General Workshop for the construction of the electromagnet.

The author also wishes to express his gratitude to Dr. J.C. Chaston (Johnson, Matthey and Co. Ltd.) for providing the single crystal piece of Gadolinium.

Further thanks are due to my fellow research student, J.J. Mason, B.Sc., for many stimulating discussions and interesting suggestions.

Finally thanks are due to D.S.I.R. for a Research Studentship from 1958 to 1961.

W.C.R.
October, 1961.

REFERENCES.

Ampere (1823) - Mem. de l'Institut 6, 175.

Bannister, J.R., Legvold, S. and Spedding, F.H. (1954) - Phys. Rev., 94, 1140.

Behrendt, D.R., Legvold, S. and Spedding, F.H. (1958) - Phys. Rev., 109, 1544.

Birss, R.R., (1960) - Proc. Roy. Soc., 255A, 398.

Bloch, F., Gentile, G. (1931) - Z. Physik, 70, 395.

Bozorth, R.M. (1954) - Phys. Rev., 96, 311.

Brooks, H. (1940) - Phys. Rev., 58, 909.

Cørner, W.D., Hutchinson, F. (1960) - Proc. Phys. Soc., 75, 781.

Croft, G.T., Donahoe, F.J., and Love, W.F. (1955) - Rev. Sci. Inst., 26, 360.

Davis, M., Calverly, A. and Lever, R.F. (1956) - J. Appl. Phys., 27, 195.

Elliot, J.F., Legvold, S. and Spedding, F.H. (1953) - Phys. Rev., 91, 28.

Farmer, M.H., Glaysher, G.H. (1953) - J. Sci. Inst., 30, 9.

Fletcher, G.C. (1954) - Proc. Phys. Soc., A67, 565.

Griffel, M., Skochdopole, R.E. and Spedding, F.H. (1954) - Phys. Rev., 93, 675.

Guillaud, C. (1943) - Thesis, Strasbourg.

Harrison, F.W. (1955) - J. Sci. Inst., 33, 5.

Heisenberg, W. (1928) - Z. Physik, 49, 619.

Hudson, R.P. (1949) - J. Sci. Inst., 26, 401.

Hunt, G.H. (1954) - Thesis, University of Durham.

Hutchinson, F. (1958) - Thesis, University of Durham.

Keffer, F. (1955) - Phys. Rev., 100, 1692.

Kip, A.F., Arnold, R.D. (1949) - Phys. Rev., 75, 1556.

Kittel, C. (1948) - Phys. Rev., 73, 155.

" " (1949) - Rev. Mod. Phys., 21, 541.

Legvold, S., Spedding, F.H., Barson, F. and Elliot J.F. (1953) Rev. Mod. Phys., 25, 129.

Mahajani, G. (1929) - Trans. Roy. Soc. (London) 228A, 63.

Mckeehan, L.W. (1934) - Rev. Sci. Inst., 5, 265.

" " (1937) - Phys. Rev., 52, 18.

Myers, H.P. and Sucksmith, W. (1951) - Proc. Roy. Soc., A207, 427.

Nosov, A.V. and Bykov, D.V. (1956) - D.S.I.R. Translation - Working Metals, by Electro - Sparking.

Pearson, R.F. and Guildford, L., (1957) - Mullard Report No. MRL/2159.

Pearson, R.F. (1959) - Mullard Report No. MRL/290.

Penoyer, R.F. (1956) - Proc. A.I.E.E. Conference on Magnetism P.365.

Powell, F.C. (1930) - Proc. Roy. Soc. (London), 130A, 167.

Slater, J.C. (1930) - Phys. Rev., 36, 57.

Spedding, F.H. (1959) - Private Communication.

Stoner, E.C. (1933) - Phil. Mag., (7). 15, 1018.

Tarasov, L.P. (1939) - Phys. Rev., 56, 1231.

Trombe, F. (1937) - Annales de Physique, 7, 385.

Van Vleck, J.H. (1937) - Phys. Rev., 52, 1178.

Weber, W. (1854) - Pogg. Ann. 87, 145.

Weiss, P. (1907) - J. Phys. (4), 6, 661.

Williams, H.J. (1937) - Rev. Sci. Inst., 8, 56.

Zener, C. (1954) - Phys. Rev., 96, 1335.

APPENDIX ONE.

Chemical Analysis of Gadolinium Single Crystal.

Element.	
Tantalum	approx. 0.1%
Copper	100 p.p.m.
Iron	80 "
Silicon	50 "
Aluminium	5 "
Calcium	5 "
Silver	2 "
Magnesium	1 "
Sodium	1 "

The following elements were not detectable:-

As, Au, B, Ba, Be, Bi, Cd, Co, Cr, Cs, Ga, Ge, Hf, Hg, In, Ir, K, Li, Mo, Nb, Ni, Os, P, Pb, Pd, Pt, Rb, Re, Rh, Ru, Sb, Se, Sn, Sr, Te, Ti, Tl, V, W, Zn, Zr.

Compound.	
Tb_4O_7	0.05%, if any.
Eu_2O_3	0.05%, if any.

Other rare earths not detectable.